DEFENCE S&T TECHNICAL BULLETIN

VOL. 7 NUM. 1 YEAR 2014 ISSN 1985-6571

CONTENTS

STRIDE

SCIENCE & TECHNOLOGY RESEARCH INSTITUTE FOR DEFENCE

AIMS AND SCOPE

The Defence S&T Technical Bulletin is the official technical bulletin of the Science & Technology Research Institute for Defence (STRIDE). The bulletin, which is indexed in, among others, Scopus, Index Corpenicus, ProQuest and EBSCO, contains manuscripts on research findings in various fields of defence science & technology. The primary purpose of this bulletin is to act as a channel for the publication of defence-based research work undertaken by researchers both within and outside the country.

WRITING FOR THE DEFENCE S&T TECHNICAL BULLETIN

Contributions to the bulletin should be based on original research in areas related to defence science & technology. All contributions should be in English.

PUBLICATION

The editors' decision with regard to publication of any item is final. A manusript is accepted on the understanding that it is an original piece of work which has not been accepted for publication elsewhere.

PRESENTATION OF MANUSCRIPTS

The format of the manuscript is as follows:

a) Page size A4
b) MS Word format
c) Single space
d) Justified
e) In Times New Roman ,11-point font
f) Should not exceed 20 pages, including references
g) Texts in charts and tables should be in 10-point font.

Please e-mail the manuscript to:

1) Dr. Zalini bt Yunus (zalini.yunus@stride.gov.my)
2) Dr. Mahdi bin Che Isa (mahdi.cheisa@stride.gov.my)
3) Dr. Dinesh Sathyamoorthy (dinesh.sathyamoorthy@stride.gov.my)

The next edition of the bulletin is expected to be published in November 2014. The due date for submissions is 10 September 2014. **It is strongly iterated that authors are solely responsible for taking the necessary steps to ensure that the submitted manuscripts do not contain confidential or sensitive material.**

The template of the manuscript is as follows:

TITLE OF MANUSCRIPT

Name(s) of author(s)

Affiliation(s)

E-mail:

ABSTRACT

Contents of abstract.

Keywords: *Keyword 1; keyword 2; keyword 3; keyword 4; keyword 5.*

1. TOPIC 1

Paragraph 1.

Paragraph 2.

1.1 Sub Topic 1

Paragraph 1.

Paragraph 2.

2. TOPIC 2

Paragraph 1.

Paragraph 2.

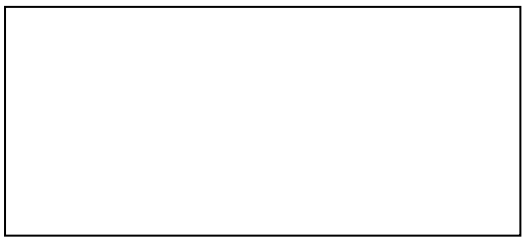

Figure 1: Title of figure.

Table 1: Title of table.

Content	Content	Content
Content	Content	Content
Content	Content	Content
Content	Content	Content

Equation 1 (1)
Equation 2 (2)

REFERENCES

Long lists of notes of bibliographical references are generally not required. The method of citing references in the text is 'name date' style, e.g. 'Hanis (1993) claimed that...', or '…including the lack of interoperability (Bohara *et al.*, 2003)'. End references should be in alphabetical order. The following reference style is to be adhered to:

Books

Serra, J. (1982). *Image Analysis and Mathematical Morphology*. Academic Press, London.

Book Chapters

Goodchild, M.F. & Quattrochi, D.A. (1997). Scale, multiscaling, remote sensing and GIS. *In* Quattrochi, D.A. and Goodchild, M.F. (Eds.), *Scale in Remote Sensing and GIS*. Lewis Publishers, Boca Raton, Florida, pp. 1-11.

Journals / Serials

Jang, B.K. & Chin, R.T. (1990). Analysis of thinning algorithms using mathematical morphology. *IEEE T. Pattern Anal.*, **12**: 541-550.

Online Sources

GTOPO30 (1996). *GTOPO30: Global 30 Arc Second Elevation Data Set*. Available online at: http://edcwww.cr.usgs.gov/landdaac/gtopo30/gtopo30.html (Last access date: 1 June 2009)

Unpublished Materials (e.g. theses, reports and documents)

Wood, J. (1996). *The Geomorphological Characterization of Digital Elevation Models*. PhD Thesis, Department of Geography, University of Leicester, Leicester.

STUDY ON TROPICAL WEATHERING EFFECTS ON EPOXY COMPOSITE MATERIALS FROM AN ALUDRA TUAV

Chan Keng Sam*, Nor Azlan Sarjo, Wan Fadilah Wan Abdullah, Syed Roslee Sayd Bakar, Mohd Sal Salsidu & Zainol Abidin Awang Sa

Mechanical & Aerospace Technology Division (BTJA), Science & Technology Research Institute for Defence (STRIDE), Malaysia

*Email: chan.kengsam@stride.gov.my

ABSTRACT

This paper is aimed at studying the changes in physical and mechanical properties of epoxy composite materials, from an ALUDRA tactical unmanned aerial vehicle (TUAV), caused by the combined effects of high heat, humidity and ultraviolet (UV) radiation in tropical environments. Two types of composite samples, carbon (CF) and glass (GF) fibre reinforced composites, were exposed to natural outdoor and laboratory accelerated weathering. Surface morphology and tensile property analyses were used to evaluate the resulting characteristics of the samples after specific durations of exposure. The results obtained established that the degradation of the composite samples was mainly due to extensive erosion of the epoxy matrix by the weather elements. The ultimate tensile strength (UTS) of the GF samples reduced gradually over the exposure duration, but the change in UTS of the CF samples was unanticipated. It was determined that exposure duration of 500 h in laboratory accelerated weathering is approximately equivalent to 10 months of exposure in in the actual tropical environment.

Keywords: *Carbon (CF) and glass (GF) fibre reinforced composites; natural outdoor and laboratory accelerated tropical weathering; surface morphology; ultimate tensile strength (UTS); composite aging.*

1. INTRODUCTION

Composite materials are increasingly being utilised in modern aviation, automobile and marine industries. More and more advanced structures are being created using composite materials, taking advantages of their inherent light weight, and enhanced strength and flexibility over traditional materials, such as aluminium and magnesium alloys (Salah *et al.,* 2005). Despite these advantages, there are concerns over the durability and long term behaviour of composite materials when exposed to various climatic environments. Composite materials, composed of organic resin matrix reinforced with carbon (CF) or glass (GF) fibres, are sensitive to weather elements, which leads to environmental aging. Tropical weather elements, including high heat, humidity and solar radiation, may cause significant material degradation after the composite material is exposed for a prolonged period of time (Chin *et al*., 1997; Bhavesh *et al*., 2002; Shenghu *et al*., 2007).

Generally, composite aging is primarily resin related. Moisture diffusion into the resin leads to changes in thermophysical and mechanical characteristics (Zhou & Lucas, 1999; Zamri *et al*., 2012). The resin is then broken down by heat and ultraviolet (UV) radiation, and oxidises and changes based on the surrounding. Resin dominated properties are significantly affected and hence, the entire composite structure is also affected (Renard *et al*., 1993; Perreux & Suri, 1997). A consequence of environmental aging is the reduction of mechanical properties, such as stiffness and strength (Sachin *et al*., 2000; Moe & Kin, 2002; Ismail *et al*., 2007; Kashtalyan & Soutis, 2013).

This paper is aimed at studying the changes in physical and mechanical properties of epoxy composite materials, from an ALUDRA tactical unmanned aerial vehicle (TUAV), caused by the combined

effects of high heat, humidity and ultraviolet (UV) radiation in tropical environments. This study involved the collection and analysis of data from two types of composite specimens, CF and GF reinforced composites, which were subjected to natural outdoor and laboratory accelerated weathering. Surface morphology and tensile property analyses were used to evaluate the changes in physical and mechanical properties of the specimens after specific durations of exposure. The accelerated test approach was validated through comparison of the surface morphologies and mechanical properties of the samples of the same material exposed in natural outdoor.

2. EXPERIMENTAL PROCEDURE

2.1 Sample Exposure

The composite samples used for this study were provided from the manufacturer of the ALUDRA TUAV. Both materials, manufactured locally with propriety formulation, are used for the fabrication of the main body of the TUAV, which is currently under trials for military and tactical applications. Two sets of CF and GF composite samples with thickness of 1.2 mm, sectioned to a size of 300 x 300 mm, were exposed to natural outdoor and laboratory accelerated weathering. Only one side of the samples was exposed to the weathering. The samples were examined and tested after specific durations of exposure.

2.1.1 Natural Outdoor Weathering

The samples were placed on exposure racks in an outdoor exposure station for two years. The station, comprising of the exposure racks and an environmental monitoring station, was located at about 2.58°N, 101.5°E, 82.3 m (STRIDE, Kajang, Selangor). The design of the exposure racks and method of sample exposure were in accordance with the requirements of ASTM (2005a). The exposure racks had south-facing walls at an angle of 5°, in accordance with ASTM (2005b).

The relative humidity (RH) at the station, recorded by the environmental monitoring station, was within a range of 47-99%, with minimum and maximum RH normally occurring at 1400-1500 and 0500-0600 respectively (Figure 1(a)). The temperature at station was within a range of 22-37 °C, with minimum and maximum temperatures normally occurring at 0600-0700 and 1400-1500 respectively (Figure 1(b)).

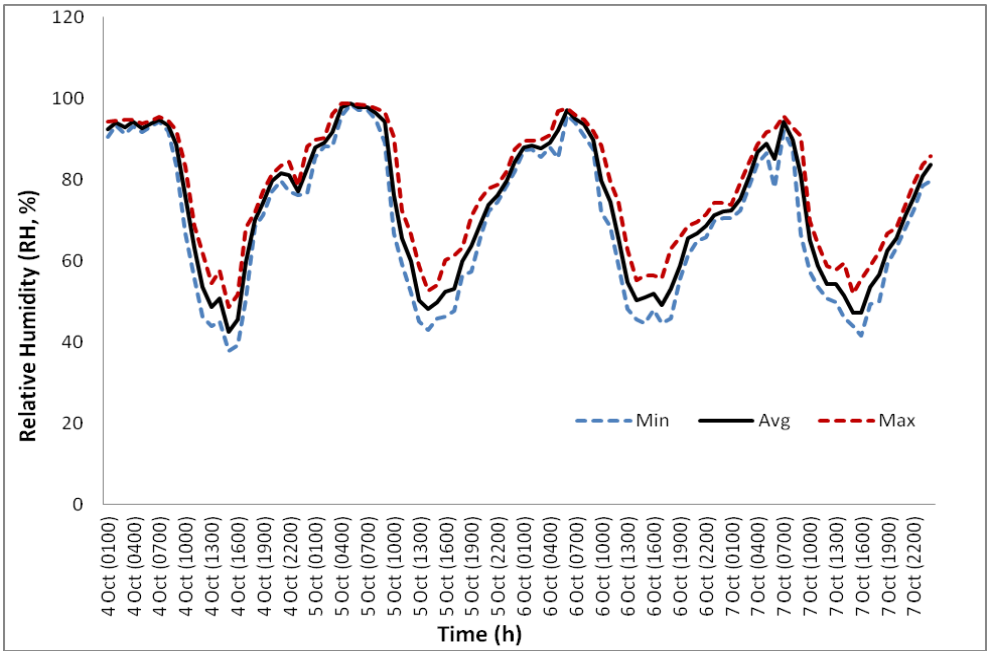

(a)

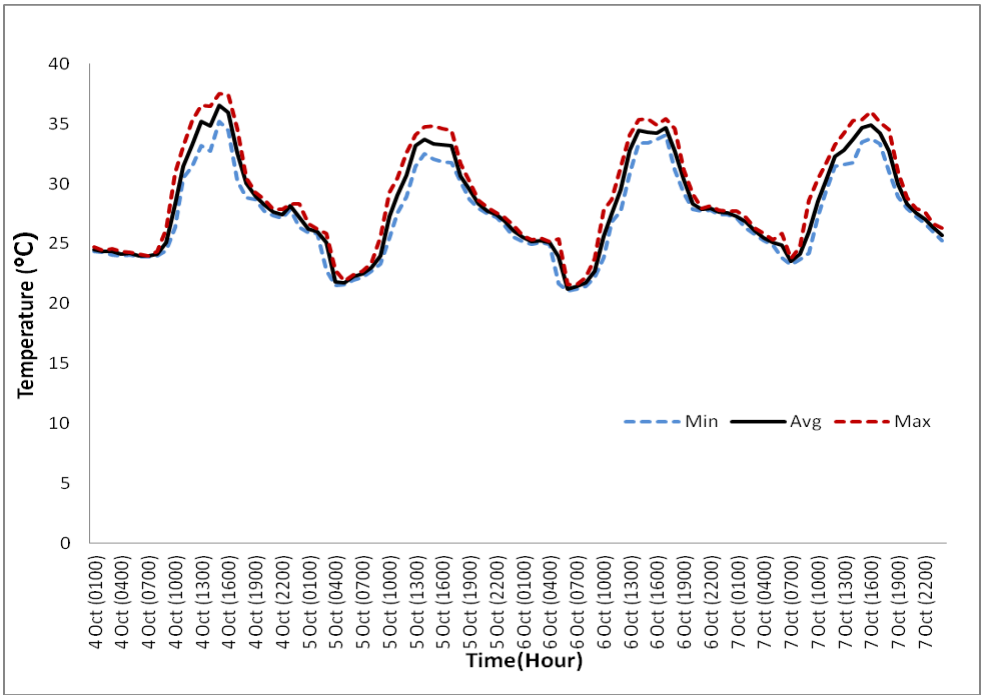

(b)

Figure 1: (a) Relative humidity (RH) and (b) temperature at the outdoor exposure station during the period of the test in October 2013.

The samples were subjected to cyclic exposure conditions as shown in Table 1 for 750 h. The exposure conditions were adapted from ASTM (2005c) with modifications to relative humidity and air temperature to simulate local tropical weather conditions.

Table 1: Test cycle for the laboratory accelerated weathering process.

Step no.	Cycle description	Duration (min)	Relative humidity (%)	Uninsulated black panel temperature (°C)	Air temperature (°C)	Typical irradiance (W/m^2)
1	Light	40	75 ± 5	70 ± 2	40 ± 2	0.55 ± 0.02
2	Light and water spray	20	n/a	48 ± 2	40 ± 2	0.55 ± 0.02
3	Light	60	75 ± 5	70 ± 2	40 ± 2	0.55 ± 0.02
4	Dark and water spray	20	n/a	n/a	38 ± 2	n/a
5	Dark	40	95 ± 5	n/a	38 ± 2	n/a

n/a: Not applicable

2.2 Surface Morphology Analysis

A LEO VPSEM 1430 scanning electron microscope, (SEM) was used to perform surface morphology analysis on the samples after specific exposure durations. This analysis assessed the physical and texture changes on the surfaces of the samples caused by the weather elements. The findings were used to correlate with the changes in mechanical properties.

2.3 Tensile Property Analysis

An INSTRON 4484 tensile testing machine with hydraulic grip at constant cross-speed of 2 mm/min was used to perform tensile property analysis on the samples at room temperature. The mechanical properties of the samples after specific exposure durations were evaluated in accordance with the requirements of ASTM (2008). The samples were cut longitudinally into rectangular shape and placed in the grip of the tensile machine at a specified grip separation and pulled until failure. The stress-strain diagrams generated were used to determine the tensile moduli of the samples.

3. RESULTS AND DISCUSSION

3.1 Surface Morphology Analysis

3.1.1 CF Composite Samples

Figure 2 shows the SEM micrographs of the CF composite samples prior to exposure to natural outdoor weathering and after specific exposure durations. As shown in Figure 2(a), the sample surface prior to exposure was an epoxy layer characterised by a wave pattern, with some imperfections and no CF exposed. After 10 months of natural weathering exposure, the CF was clearly exposed as the epoxy layer was extensively eroded by the weather elements, as shown in Figure 2(b). The epoxy layer was almost completely eroded after 16 months of exposure, as shown in Figure 2(c).

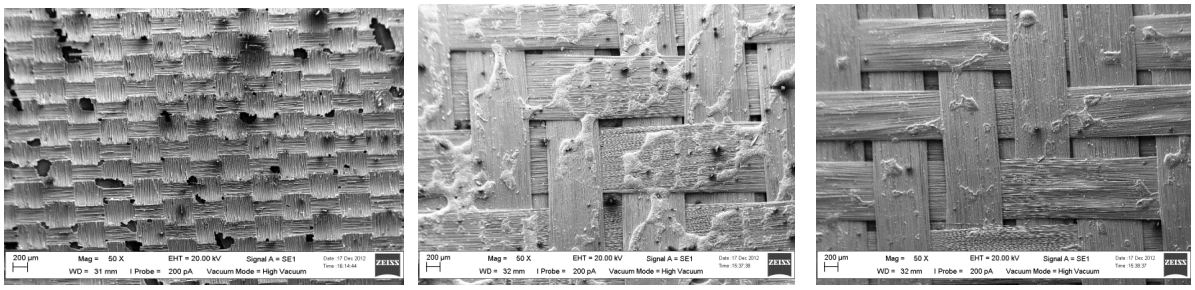

(a) **(b)** **(c)**

Figure 2: SEM micrographs (50x) for the CF composite samples exposed to natural outdoor weathering: (a) Prior to exposure (b) After 10 months (c) After 16 months.

Figure 3 shows the SEM micrographs of the CF composite samples prior to exposure to laboratory accelerated weathering and after specific exposure durations. After 500 h of exposure, the CF was partially exposed as some of the epoxy layer was eroded, as shown in Figure 3(b). The epoxy layer was further worn and gnarled after another 750 h of exposure, as shown in Figure 3(c).

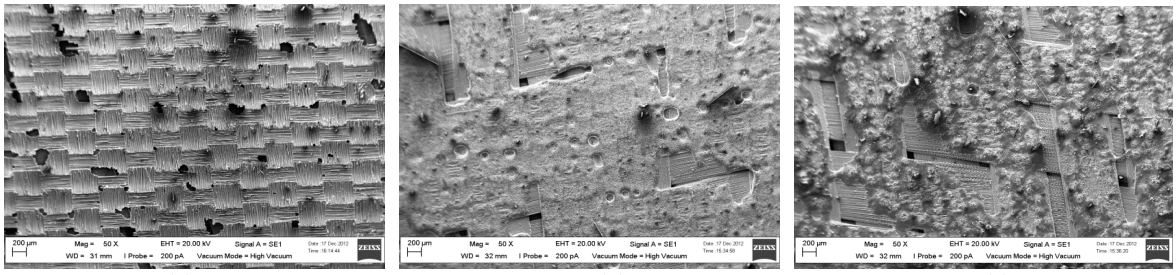

(a) **(b)** **(c)**

Figure 3: SEM micrographs (50x) for the CF composite samples exposed to laboratory accelerated weathering: (a) Prior to exposure (b) After 500 h (c) After 750 h.

3.1.2 GF Composite Samples

Figure 4 shows the SEM micrographs of the GF composite samples prior to exposure to natural outdoor weathering and after specific exposure durations. As shown in Figure 4(a), the sample surface prior to exposure was characterised by a relatively smooth epoxy layer, scattered with some imperfections and with no GF exposed. After 10 months of exposure, most of the epoxy layer was eroded, exposing the GF, as shown in Figure 4(b). After another 16 months of exposure, the epoxy layer was completely worn off, revealing only bare GF, as shown in Figure 4(c).

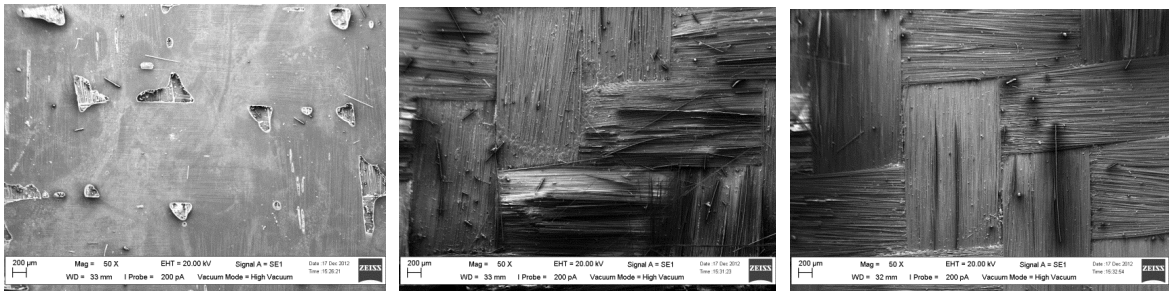

(a) **(b)** **(c)**

Figure 4: SEM micrographs (50x) for the GF composite samples exposed to natural outdoor weathering: (a) Prior to exposure (b) After 10 months (c) After 16 months.

Figure 5 shows the SEM micrographs of the GF composite samples prior to exposure to laboratory accelerated weathering and after specific exposure durations. After 500 h of exposure, the GF was clearly exposed as the epoxy layer was almost completely eroded, as shown in Figure 5(b). Erosion of the epoxy resin in the inter-laminar layer was observed after a further 750 h of exposure, as shown in Figure 5(c).

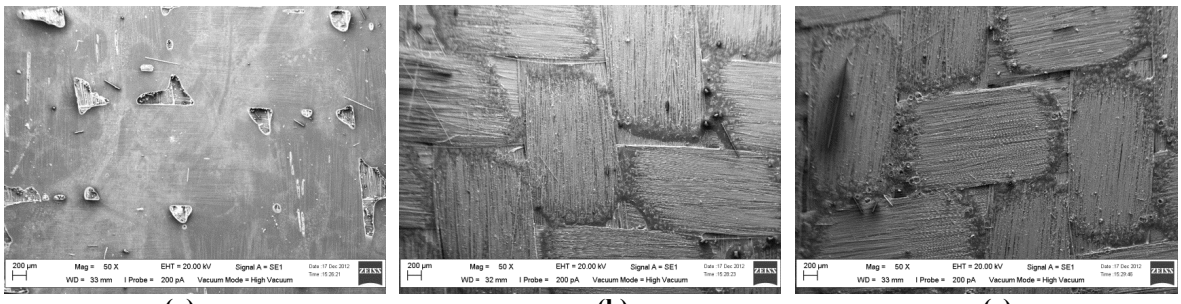

(a) **(b)** **(c)**

Figure 5: SEM micrographs (50x) for the GF composite samples exposed to laboratory accelerated weathering: (a) Prior to exposure (b) 500 h (c) 750 h.

3.2 Tensile Property Analysis

Figure 6 shows the changes in ultimate tensile strength (UTS) of the CF and GF composite samples as a function of time (exposure duration) after exposure to natural outdoor and laboratory accelerated weathering. The CF composite samples generally exhibited higher UTS than the GF composite samples throughout the exposure duration due to the greater strength possessed by CF as compared to GF (Hull & Clyne, 2003).

The behaviour depicted by the GF composite samples was expected, with their UTS reducing gradually due to degradation over the exposure duration. The epoxy matrix was steadily eroded by the weather elements when the samples were exposed to natural outdoor environments, leading to reduction in mechanical properties. It was noted there was a steep reduction in UTS during the initial 150 h exposure in the laboratory accelerated weathering environment, after which the reduction in

UTS was much slower. This was due to the extensive erosion of the epoxy matrix at the initial stage, leaving the GF as the predominant component, which was less affected by the weather elements at the later stage.

However, the behaviour of the CF composite samples was unanticipated. Their UTS decreased after the initial stage of exposure, as expected. Then, their UTS began to increase after 5 months of natural outdoor exposure and reached the maximum after 10 months. The CF composite samples exposed to laboratory accelerated weathering exhibited similar behaviour, with their UTS increasing after 150 h and reaching the maximum after 500 h of exposure. Further studies are required to investigate the reason for this unanticipated change.

The UTS results for both the GF and CF composite samples exhibited similar patterns over the exposure durations for natural outdoor and laboratory accelerated weathering. Exposure time of 500 h in laboratory accelerated weathering is approximately equivalent to 10 months of exposure in the actual tropical environment.

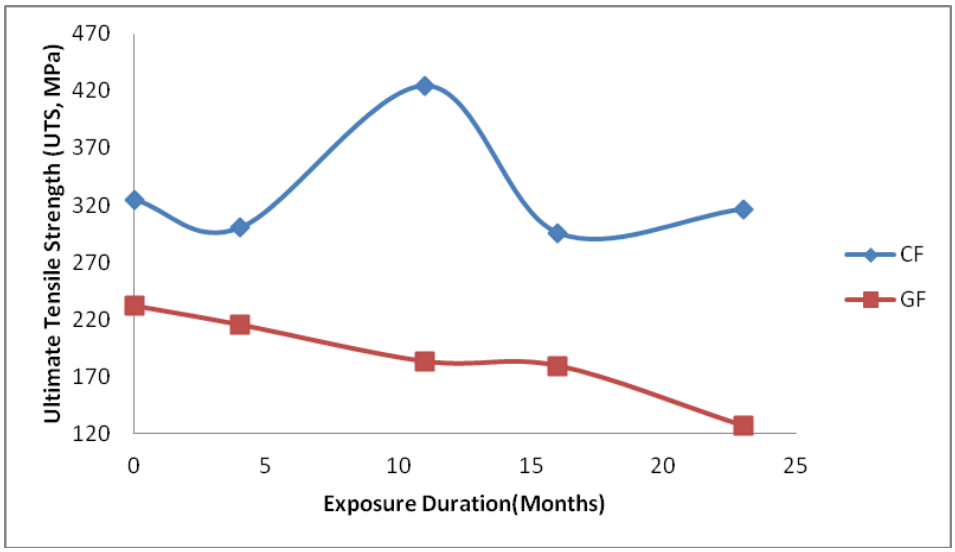

(a)

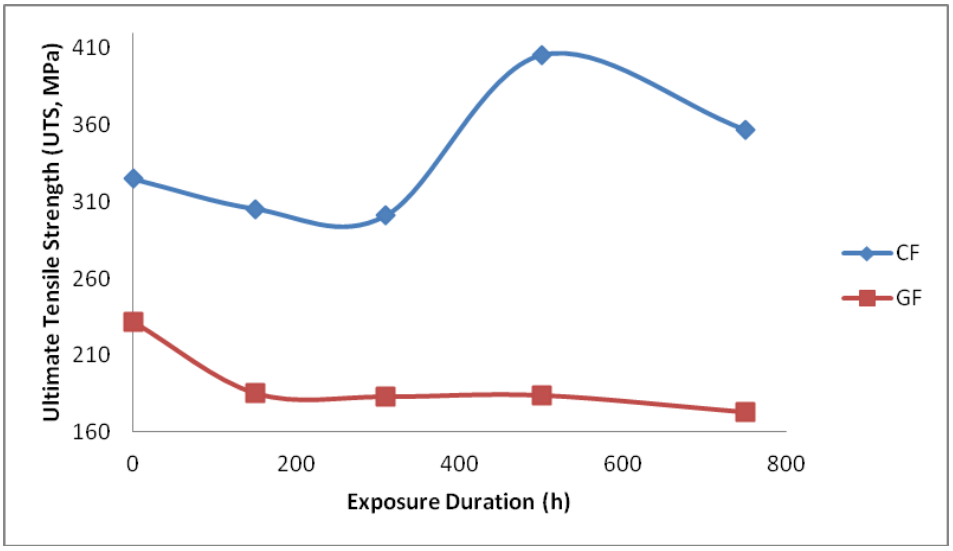

(b)

Figure 6: Changes in ultimate tensile strength (UTS) as a function of time for the CF and GF composite samples after exposure to (a) natural outdoor and (b) laboratory accelerated weathering.

4. CONCLUSION

The results of this study have established that the combined effects of tropical weather elements caused extensive erosion of the epoxy matrix on the composite samples, affecting their physical and mechanical properties. It was observed that the epoxy resin bonded better with CF than with GF due to the greater strength possessed by CF as compared to GF. Hence, the outer epoxy layers of the GF composite samples wore off much faster as compared to the CF composite samples under the same weathering conditions. The GF composite samples showed gradual reduction in UTS over the exposure duration, but this was not overly significant as UTS is fibre-dominated. However, the change in UTS of the CF samples was unanticipated, with further studies to be conducted to investigate the reason for this. It was determined that exposure duration of 500 h in laboratory accelerated weathering is approximately equivalent to 10 months of exposure in the actual tropical environment.

REFERENCES

ASTM (American Society for Testing and Materials) (2005a). *ASTM D1435-05: Standard Practice for Outdoor Weathering of Plastics*. American Society for Testing and Materials (ASTM), West Conshohocken, Pennsylvania.

ASTM (American Society for Testing and Materials) (2005b). *ASTM G7/G7M-05: Standard Practice for Atmospheric Environmental Exposure Testing of Non-metallic Materials*. American Society for Testing and Materials (ASTM), West Conshohocken, Pennsylvania.

ASTM (American Society for Testing and Materials) (2005c). *ASTM G155-05a: Standard Practice for Operating Xenon Arc Light Apparatus for Exposure of Non-metallic Materials*. American Society for Testing and Materials (ASTM), West Conshohocken, Pennsylvania.

ASTM (American Society for Testing and Materials) `(2008). *ASTM D3039/3039M-08: Standard Test Method of Tensile Properties of Polymer Matrix Composite Materials*. American Society for Testing and Materials (ASTM), West Conshohocken, Pennsylvania.

Bhavesh, G.K., Raman, P.S. & Tosho, N. (2002). Degradation of carbon fiber-reinforced epoxy composites by ultraviolet radiation and condensation. *J. Comp. Mat.*, **36**: 2713-2733.

Chin, J.W., Nguyen, T. & Aouadi, K. (1997). Effects of environmental exposure on fiber-reinforced plastic (FRP) materials used in construction. *J. Comp. Tech. Resear.*, **19**: 205-213.

Hull, D. & Clyne, T.W (2003). *An Introduction to Composite Material, 2nd Ed*. Cambridge University Press, Cambridge.

Ismail, I.N., Omar, S., Zainal Abidin, M.F. & Ahmad Marzuki, H.F. (2007). Thermo and mechanical properties of carbon fiber/epoxy composites under environment exposures. *3rd Thermal Analysis Conference 07*, 23-24 October 2007, UniKL, Malaysia.

Kashtalyan, M. &Soutis, C. (2013). Predicting residual stiffness of cracked composite laminates subjected to multi-axial in-plane loading. *J. Comp. Mat*., **47**: 2513-2524.

Moe, M.T. & Kin, L. (2002) Effects of environmental aging on the mechanical properties of bamboo-glass fiber reinforced pylomer matrix hybrid composite. *Compos. A*, **33**:43-52.

Perreux, D. & Suri, C. (1997) A study of the coupling between the phenomena of water absorption and damage in glass/epoxy composite pipes. *Comp. Sci Tech.*, **57**: 1403-1413.

Renard, J., Favre, J.-P. & Jeggy, T. (1993). Influence of transverse cracking on ply behavior: Introduction of a characteristic damage variable. *Comp. Sci. Tech.*, **46**: 29-37.

Sachin, K., Roberto, A., Lopez, A. & Rakesh, K.G., (2000) Environmental aging of fiber-reinforced polymer-wrapped concrete cylinders. *Mat. J.,* **97**:703-712

Salah, L., Tomblin, J. & Davies, C. (2005). Aging effects evaluation of a decommissioned Boeing CFRP 737-200 horizontal stabilizer (Phase II). *8th Joint FAA/DoD/NASA Aging Aircraft Conference*, Palm Springs, CA.

Shenghu, C., Zhishen, W. & Xin, W. (2009). Tensile properties of CRFP and hybrid FRP composites at elevated temperatures. *J. Comp. Mat.,* **43**: 315-330.

Zamri, M.H., Md Akil, H., Abu Bakar, A., Mohd Ishak, Z.A. & Leong, W.C. (2012). Effect of water absorption on pultruded jute/glass fibre reinforced unsaturated polyester hybrid composites. *J. Comp. Mat*., **46**: 51-60.

Zhou, J & Lucas, J. (1999). Hygothermal effects of epoxy resin. Part I: Nature of water in epoxy. *Polymer*, **40**: 5505-5512.

EVALUATION OF THE EFFECTIVENESS OF TITANIUM DIOXIDE (TiO_2) SELF-CLEANING COATING FOR INCREASED PROTECTION AGAINST CBRN INCIDENTS IN CRITICAL INFRASTRUCTURES

Alessandro Sassolini*, Andrea Malizia, Fabrizio D'Amico, Mariachiara Carestia, Daniele Di Giovanni, Orlando Cenciarelli, Carlo Bellecci & Pasquale Gaudio

Department of Industrial Engineering, Faculty of Engineering, University of Rome "Tor Vergata", Italy

*E-mail: alessandro.sassolini@gmail.com

ABSTRACT

Self-cleaning building materials is a form of passive safety technology that is used to provide increased resistance against chemical, biological, radiological and nuclear (CBRN) incidents. This paper is aimed at evaluating the effectiveness of a self-cleaning coating based on a dispersion in ethanol of titanium dioxide (TiO_2) powder at 0.5 gr/L distributed directly on stone materials. The parameters analysed in this study were stealthiness, performance against a toxic industrial chemical (TIC) and durability. It was found that the TiO_2 coating has low visibility, is able to partly remove TIC from the air and has high durability.

Keywords: *Titanium dioxide (TiO_2) self-cleaning coating; stone materials; stealthiness; toxic industrial chemical (TIC); durability.*

1. INTRODUCTION

The management of chemical, biological, radiological and nuclear (CBRN) safety of critical infrastructures requires a complex mixture of technologies and capabilities (Malizia *et al.*, 2010, 2011; 2012; Gallo *et al.*, 2012; Cenciarelli *et al.*, 2013a, b). In order to have an efficient CBRN emergency response system, it is necessary to arrange for the realisation and tuning of prediction models before the CBRN incident to be effective during and after the incident. In addition, the following decontamination procedures, and stand-on and stand-off detectors for chemical, biological and radiological agents are required (Bellecci *et al.*, 2010; Gaudio et *al.*, 2011; Pazienza *et al.*, 2013, 2014; Gaudio *et al.*, 2013a, b).

Our work highlights areas that we define as passive safety technologies, which can inherently provide increased resistance against a CBRN incident or speed up the return to full efficiency after the incident. When the protected infrastructures are not strictly of military use, such as offices and ministries, the level of decontamination that is needed is much higher than that of barracks or other facilities that can rely on the protection and training of personnel (Raber *et al.*, 2001). This paper focuses on one such passive safety technology; self-cleaning building materials.

The working principle of self-cleaning building materials is semiconductor photocatalysis, which increases the effectiveness of a photoreaction where a semiconductor acts as a catalyst and photon can originate from the sun or from a light source. The absorption of a photon of energy higher than the band gap of semiconductor activates these reactions. This results in the promotion of an electron from the valence band to the conduction band, with the concomitant generation of a hole in the valence band. In order to achieve an efficient catalysis, a new process involving electrons and holes at the semiconductor surface must be more efficient of the major deactivation process, which is the recombination between them (Figure 1). If the photocatalysis reaction is conducted in the presence of

oxygen, it results in a semiconductor-sensitised photo-mineralisation from organic compounds present in the environment (Chen & Mao, 2007):

$$\text{Organic pollutant} + O_2 \xrightarrow[h\nu \geq E_{bg}]{\text{Semiconductor}} H_2O + CO_2 + \text{mineral acids} \quad (1)$$

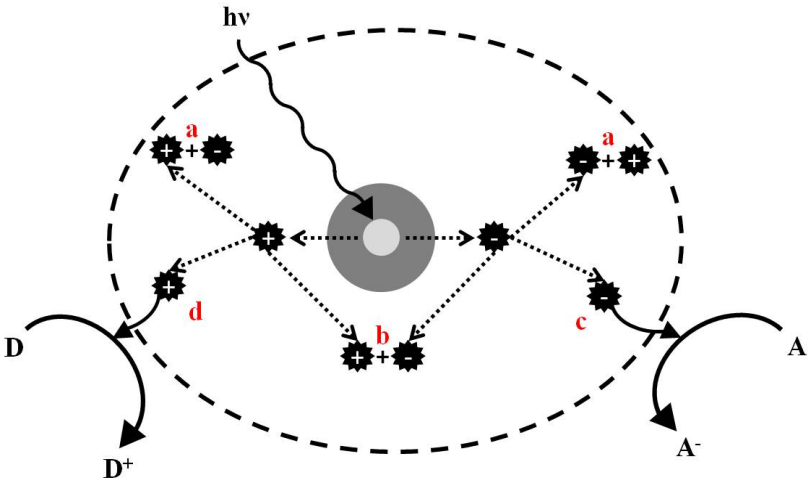

Figure 1: Formation and deactivation process of holes and electrons in the semiconductor particle. The dashed circle indicates the surface of the semiconductor. Reactions (a) and (b) are the electron-hole recombination at the surface and bulk respectively. Reactions (c) and (d) occur at the surface of the semiconductor particle. A indicates acceptor; A^-, reduced acceptor; D, donor; and D^+, oxidised donor. (Redrawn and adapted from Mills & Le Hunte (1997))

The use of photocatalyst materials in CBRN compounds is well documented, with many papers discussing the mineralisation of chemical warfare agents, and disinfection in water or on surfaces (Vorontosov *et al.*, 2004, 2005; Ming-Show *et al.*, 2006). Although the self-cleaning properties of photocatalyst materials were known since the 1960s, it is only in recent years they have begun to be used in a wide manner. The first application of self-cleaning concrete in Italy was in the *Dives in Misericordia* Church in Rome which was officially opened in 2003 (Pacheco-Torgal & Jalali, 2011). A number of experimental evidences have confirmed the ability of these coatings to oxidise organic molecules (Cassar *et al.*, 2004). It has also been demonstrated that these coatings have anti-microbial properties. Even if the mechanism is not completely clarified, according to several studies, it is believed that the metal oxides carry the positive charge while the microorganisms carry negative charge, causing electromagnetic attraction between microorganisms and the metal oxides, which leads to oxidisation and finally the death of microorganisms, such as algae (Linkous *et al.*, 2002) and bacteria (Zhang & Chen, 2009; Gupta *et al.*, 2013; Sikong *et al.*, 2010; Haghi *et al.*, 2012; Jain *et al.*, 2012). Generally, these materials are used in mortar or plaster. Many semiconductors have been tested as self-cleaning materials, but the most largely used is titanium dioxide (TiO_2) because of its efficiency, and low toxicity and cost.

There is another important mechanism that works well for TiO_2 self-cleaning coating, which is super-hydrophilicity. When a TiO_2 film is exposed to an ultraviolet (UV) irradiation, a very strong interaction develops between the photocatalytic surface and the water that is present in environment, which tends to spread on it in a flat manner rather than as a sphere. This effect can be explained by considering the high surface density of hydroxyl groups formed by UV light after the interaction between TiO_2 and water (Eshaghi et al., 2011). When the surface is rinsed with water, the contamination, such as oil, is washed away. Combining this effect with the degradation of organic matter, due to the photocatalysis process previously mentioned, it is possible to obtain a self-cleaning surface.

This paper is aimed at evaluating the effectiveness of a self-cleaning coating based on a dispersion in ethanol of micrometer size Degussa P25 TiO_2 powder at 0.5 gr/L distributed directly on stone materials. The parameters analysed were stealthiness, performance against a toxic industrial chemical (TIC) and durability.

2. METHODOLOGY

2.1 Stealthiness

In order to maintain stealthiness during the application, it is better that the coating is as less visible as possible. In our work, in order to evaluate this aspect, we made colorimetric measurements with a UV-Vis spectrophotometer (Jasco Inc.; the analysis was conducted according to the manufacturer's protocol) on some frequently used stone materials, such as travertine and brick, before and after the TiO_2 coating was applied. The variation of colour allowed for the evaluation of the visibility of the treatment.

2.2 Performance Against a TIC

The effectiveness of TiO_2 coating was evaluated by testing it against hydrogen sulphide, which is a TIC. This class of chemical compound can be considered as even more dangerous than chemical warfare agents due to its availability, as reported by DOL (2014).

The TiO_2 coating was spread on the travertine surface according to the following procedure:

1. A layer of TiO_2 was laid on a travertine plate, then cut with a microtome. The travertine plate was then transferred into a cuvette equipped with a cap that allows the passage of a teflon tube.
2. The bottom of the tube was inserted into the stopper of a flask containing an aqueous solution of thioacetamide (CH_3CSCH_3) acidified with hydrochloric acid (HCl). After sealing the flask, the mixture was heated at 60 °C in a thermostat. Thioacetamide is unstable under these conditions and reacts with water, resulting in the release of hydrogen sulphide.
3. The cuvette was radiated with UV from a xenon lamp for at least 8 h to simulate sunlight exposure.
4. At the end of the UV irradiation phase, a small sample of the exposed portion of the lamina was taken and analysed via Fourier transform infrared (FTIR) spectroscopy and ion chromatography techniques.

The whole procedure was repeated with a non-treated plate as a reference. Figure 2 shows the experimental setup.

2.3 Durability

In order to assess the durability of the coating, the effect of rain falling on TiO_2 treated stone materials with area of 2 cm^2 for two years was simulated in Rome, Italy (780 mm/year). It was calculated that 150 cm^3 of water would fall the plate from a height of 30 cm using a peristaltic pump (Figure 3). The persistence of the coatings of the stone material was evaluated by analysing the reflectance UV spectra.

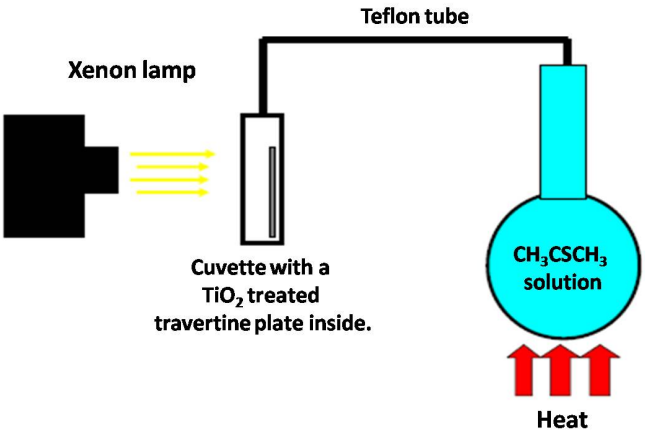

Figure 2: Experimental setup for evaluating the performance of TiO_2 coating against hydrogen sulphide.

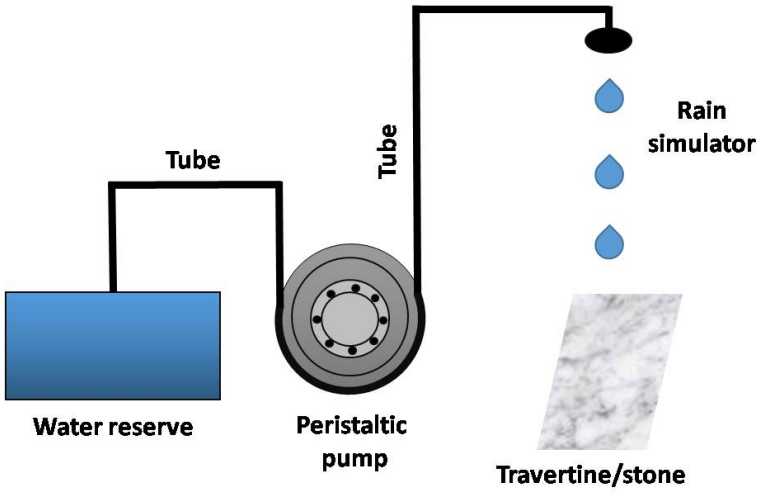

Figure 3: Experimental setup of the rain simulator.

3. RESULTS & DISCUSSION

3.1 Stealthiness

From the reflectance UV-Vis spectra, a quantitative measure of colour can be obtained. It is expressed as a point in a limited three-dimensional space, which are called chromatic coordinates. While translation of chromatic coordinates can be done in several ways, we choose the CIE*Lab* (CIE, International Commission on Illumination; *L*, lightness of colour; *a*, position between red / magenta and green; and *b*, position between yellow and blue) approach with coordinates *L.a.b*. This method, developed by the CIE in 1976, allows unambiguous encoding of the entire visible spectrum independently of any graphics technology. It is not important in this particular case how these values are defined, but it is important that the evaluation of the variation of colour correspond to the measurement of distance between the points representing the colour, which is known as the Pythagorean distance ΔE (CIE, 2014).

A value of $\Delta E = 2$ is considered as the limit of sensitivity of the human eye. This value is reported in Figure 4, which also shows the measures of variation of colour on 25 TiO_2 treated travertine plates, where these variations are averaging on the same order of magnitude. Similar results were obtained for bricks (data not shown). If the goal is to ensure complete invisibility of the coating, there is a large

amount of literature about the possibility to synthesise nano-sized particles of titanium (for example, Peng *et al.* (2005)). This particle size causes the absence of scattering of visible light and this coupled with the absence in TiO_2 bands absorbing visible light make negligible the hiding power opacity of the coating, without affecting the photocatalytic effectiveness of the coating itself, at least for the initial phase after the treatment.

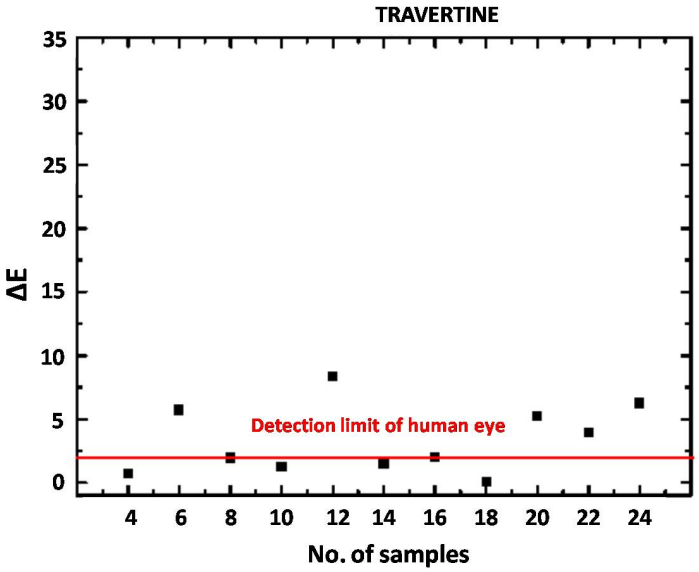

Figure 4: Variation *ΔE* for 25 TiO_2 treated travertine plates. The red bar is the human eye sensitivity.

3.2 Performance Against a TIC

Figure 5 shows the comparison between the FTIR spectra obtained from the TiO_2 treated and untreated plates after UV irradiation. There are intense bands assigned to carbonate, which is the most important component of travertine that is clearly identifiable and present in both spectra. There are also some identifiable bands, as reported in Table 1, that can be assigned to sulphate ions, which are not present in the reference sample of travertine without titanium. This corresponds to the expected reaction:

$$H_2S + O_2 + \text{Photocatalyst} \longrightarrow H_2SO_4 \quad (2)$$

where H_2S is hydrogen sulphide, O_2 is oxygen and H_2SO_4 is the reaction product, sulphuric acid. This finding infers that the TiO_2 coating is able to oxidise hydrogen sulphide by turning it into sulphur oxide and then removing it from the atmosphere.

3.3 Durability

Due to its strong 320 nm absorbance band (Table 1), TiO_2 was easily detected on carbonate (as shown by the difference between the black and red lines in Figure 6). It is observed that there is no difference between the UV spectra obtained before (red line) and after (green line) simulated rainfall. This indicates that even without any binder for the bonds to support, the photocatalyst has remarkable persistence on stone.

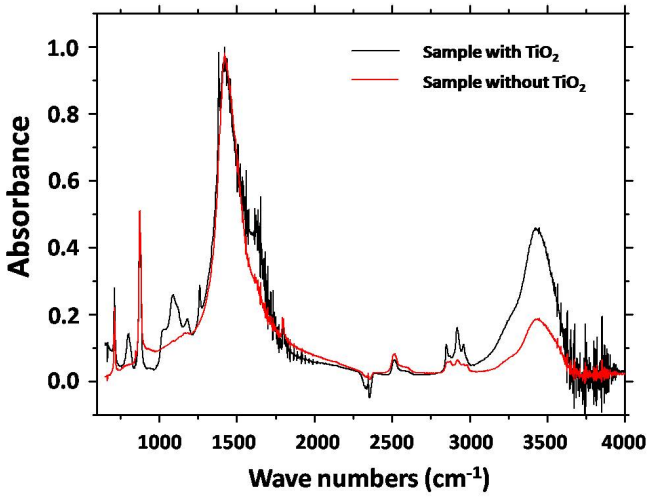

Figure 5: FTIR spectrum of travertine with and without TiO_2 after exposure to hydrogen sulphide acid and 8 ours of UV light.

Table 1: Intensities and attributions of absorption of the spectroscopic bands.

Band (cm^{-1})	Intensity of absorption	Attribution
1,090	Medium	Sulphate
1,117	Shoulder	
1,184	Weak	
1,470	Strong	Carbonate
3,500	Wide	Hydroxyl

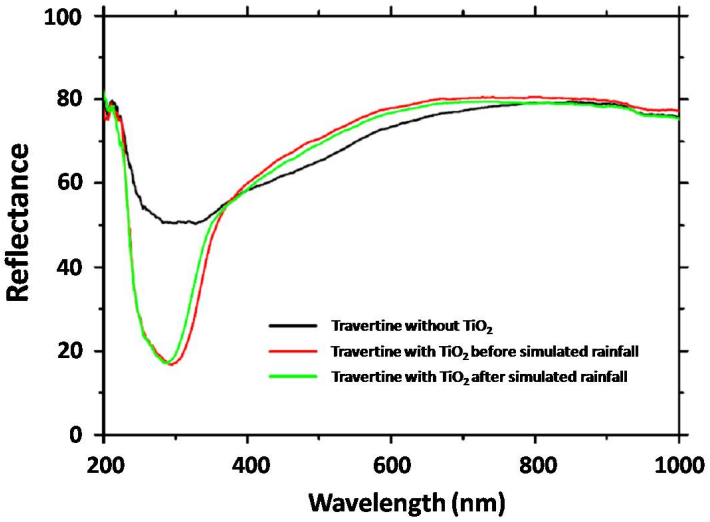

Figure 6: Reflectance UV spectra for travertine.

4. CONCLUSION

The effectiveness of TiO_2 self-cleaning protection to provide increased resistance against CBRN incidents was evaluated in this paper. It was found that the coating applied on common stone materials has low visibility, is able to partly remove TIC from the air and has high durability. It is necessary to underline that additional studies are required to properly evaluate the performance of self-cleaning coatings. While, in this study, the performance was evaluated for a maximum of several days after the treatment, for this kind of application, tests for over a number of years are necessary for more precise evaluation

ACKNOWLEDGEMENT

Special acknowledgment for the support received to realise this work goes to the Directive Board of International Master Courses in Protection Against CBRNe events (http://www.mastercbrn.com).

REFERENCES

Bellecci, C., Gaudio, P., Gelfusa, M., Malizia, A., Richetta, M., Serafini, C., & Ventura, P. (2010). Planetary boundary layer (PBL) monitoring by means of two laser radar systems: experimental results and comparison. *Proc. SPIE*, **7832**: 78320X.

Benedix, R., Dehn, F., Quaas, J., & Orgass, M. (2000). Application of titanium dioxide photocatalysis to create self-cleaning building materials. *Lacer*, **5**:157-168.

Cassar, L. (2004). Phocatalysis of cementitious materials: clean buildings and clear air. *MRS Bull.*, **29**:328-331.

Cenciarelli, O., Malizia, A., Marinelli, M., Pietropaoli, S., Gallo, R., D'Amico, F., Bellecci, C., Fiorito, R., Gucciardino, A. & Gaudio, P (2013). Evaluation of biohazard management of the Italian national fire brigade. *Defence S&T Tech. Bull.*, **6**:33-41.

Cenciarelli, O., Rea, S., Carestia, M., D'Amico, F., Malizia, A., Bellecci, C., Gaudio, P., Gucciardino, A. & Fiorito, R. . (2013). Bioweapons and Bioterrorism: A Review of History and Biological Agents. *Defence S&T Tech. Bull.*, **6**:111-129.

Chen, J., & Poon, C. S. (2009). Photocatalytic construction and building materials: from fundamentals to applications. *Build. Environ.*, **44**:1899-1906.

Chen, X., & Mao, S. S. (2007). Titanium dioxide nanomaterials: synthesis, properties, modifications, and applications. *Chem. Rev.*, **107**:2891-2959.

CIE (International Commission on Illumination) (2004). *CIE 15:2004 Colorimetry*. International Commission on Illumination (CIE), Vienna.

Department of Labor (DOL) (2014). *Toxic Industrial Chemical Guide OSHA*. https://www.osha.gov/SLTC/emergencypreparedness/guides/chemical.html (Last access date: 13 February 2014)

Eshaghi, A., Dashti, A., Eshaghi, A., & Mozaffarinia, R. (2011). Photo-induced superhydrophilicity of nanocomposite TiO_2-SiO_2 thin film. *Mat. Sci. Poland*, **29**: 22-28.

Gallo, R., De Angelis, P., Malizia, A., Conetta, F., Di Giovanni, D., Antonelli, L., Gallo, N., Fiduccia, A., D'Amico, F., Fiorito, R., Richetta, M., Bellecci, C. & Gaudio, P. (2013). Development of a georeferencing software for radiological diffusion in order to improve the safety and security of first responders. *Defence S&T Tech. Bull.*, **6**:21-32.

Gaudio, P., Gelfusa, M., Lupelli, I., Malizia, A., Moretti, A., Richetta, M., Serafini, C. & Bellecci, C. (2011). First open field measurements with a portable CO2 lidar/dial system for early forest fires detection. *Proc. SPIE*, **8182**: 818213.

Gaudio, P., Gelfusa, M., Malizia, A., Richetta, M., Antonucci, A., Ventura, P., Murari, A. & Vega, J. (2013). Design and development of a compact lidar/DIAL system for aerial surveillance of urban areas. *Proc. SPIE*, **8894**: 88940D.

Gaudio, P., Gelfusa, M., Malizia, A., Richetta, M., Serafini, C., Ventura, P., Bellecci, C., De Leo, L., Lo Feudo, T. & Murari, A. (2013). New frontiers of Forest Fire Protection: A portable Laser System (FfED). *WSEAS Tran. Environ. Dev.*, **9**: 195-205.

Gupta, K., Singh, R.P., Pandey, A. & Pandey, A. (2013). Photocatalytic antibacterial performance of TiO_2 and Ag-doped TiO_2 against *S. Aureus*, *P. aeruginosa* and *E. coli*. *Beilstein J. Nanotech.*, **4**:345-351.

Haghi, M., Hekmatafshar, M., Janipour, M.B., Seyyedgholizadeh, S., Faraz, M.K., Sayyadifar, F. & Ghaedi, M. (2012). Antibacterial effect of TiO_2 nanoparticles on pathogenic strain of *E. coli*. *Intl. J. Adv. Biotec. Res.*, **3**:621-624

International Commission of Illumination (CIE) (2014). *CIE Colorimetry - Part 4: 1976 L*a*b* Colour Space.* http://cie.co.at/index.php?i_ca_id=485 (Last access date: 13 February 2014)

Jain, N., Gupta, R., Rai, R.K., Ray, S.S. & Sharma, V. (2012). Anti-microbial activity of TiO_2 micro-particles in suspension on *E. coli* strains under UV irradiation. *J. Pharm. Biol. Sci.* **1**:21-30.

Kozlova, E. A., Smirniotis, P. G., & Vorontsov, A. V. (2004). Comparative study on photocatalytic oxidation of four organophosphorus simulants of chemical warfare agents in aqueous suspension of titanium dioxide. *J. Photoch. Photobio. A*, **162**:503-511.

Linkous, C. A., Carter, G. J., Locuson, D. B., Ouellette, A. J., Slattery, D. K., & Smitha, L. A. (2000). Photocatalytic inhibition of algae growth using TiO_2, WO_3, and cocatalyst modifications. *Environ. Sci. & Technol.*, **34**:4754-4758.

Malizia, A., Lupelli, I., D'Amico, F., Sassolini, A., Fiduccia, A., Quarta, A. M., Fiorito, R., Gucciardino, A., Richetta, M., Bellecci, C. & Gaudio, P. (2012). Comparison of Software for Rescue Operation Planning During an Accident in a Nuclear Power Plant. *Defence S&T Tech. Bull.*, **1**:36-45.

Malizia, A., Quaranta, R. & Mugavero, R. (2010). CBRN events in the subway system of Rome: Technical-managerial solutions for risk reduction. *Defence S&T Tech. Bull.*, **3**:140-157.

Malizia, A., Quaranta, R., Mugavero, R., Carcano, R., & Franceschi, G. (2011). Proposal of the prototype RoSyD-CBRN, a robotic system for remote detection of CBRN agents. *Defence S&T Tech. Bull.*, **4**:64-76.

Mills, A., & Le Hunte, S. (1997). An overview of semiconductor photocatalysis. *J. Photochem. Photobiol. A*, **108**:1-35.

Pacheco-Torgal, F., & Jalali, S. (2011). Nanotechnology: advantages and drawbacks in the field of construction and building materials. *Constr. and Build. Mater.*, **25**:582-590.

Parkin, I. P., & Palgrave, R. G. (2005). Self-cleaning coatings. *J. Mater. Chem.*, **15**:1689-1695.

Pazienza, M., Britti, M.S., Carestia, M., Cenciarelli, O., D'Amico, F., Malizia, A., Bellecci, C., Gaudio, P., Gucciardino, A., Bellino, M., Lancia, C., Tamburrini, A. & Fiorito, R. (2013). Application of Real-Time PCR to Identify Residual Bio-Decontamination of Confined Environments after Hydrogen Peroxide Vapor Treatment: Preliminary Results. *J. Microb. Biochem. Technol.*, **6**:24-28.

Pazienza, M., Britti, M.S., Carestia, M., Cenciarelli, O., D'Amico, F., Malizia, A., Bellecci, C., Fiorito, R., Gucciardino, A., Bellino, M., Lancia, C., Tamburrini, A. & Gaudio, P. (2014). Use of Particle Counter System for the Optimization of Sampling, Identification and Decontamination Procedures for Biological Aerosols Dispersion in Confined Environment. *J. Microb. Biochem. Technol.*, **6**: 43-48.

Peng, T., Zhao, D., Dai, K., Shi, W., & Hirao, K. (2005). Synthesis of titanium dioxide nanoparticles with mesoporous anatase wall and high photocatalytic activity. *J. Phys. Chem. B*, **109**:4947-4952.

Raber, E., Jin, A., Noonan, K., McGuire, R., & Kirvel, R. D. (2001). Decontamination issues for chemical and biological warfare agents: how clean is clean enough? *Int. J. Environ. Heal. R.*, **11**:128-148.

Serpone, N., & Pelizzetti, E. (Eds.) (1989). *Photocatalysis: Fundamentals and Applications*. Wiley, New York.

Sikong, L., Kongreong, B., Kantachote, D. & Sutthisripok, W. (2010). Photocatalytic activity and antibacterial behavior of Fe^{3+}-Doped TiO_2/SnO_2 nanoparticles. *Energy Res. J.*, **1**:120.

Vorontsov, A. V., Kozlov, D. V., Smirniotis, P. G., & Parmon, V. N. (2005). TiO2 photocatalytic oxidation: I. Photocatalysts for liquid-phase and gas-phase processes and the photocatalytic degradation of chemical warfare agent simulants in a liquid phase. *Kinet. Catal.*, **46**:189-203.

Wong, M. S., Chu, W. C., Sun, D. S., Huang, H. S., Chen, J. H., Tsai, P. J., Lin, N. T., Yu, M. S., Hsu, S.F., Wang, S. L. & Chang, H. H. (2006). Visible-light-induced bactericidal activity of a

nitrogen-doped titanium photocatalyst against human pathogens. *Appl. Environ. Microbiol.*, **72**:6111-6116.

Zhang, H. & Chen, G. (2009). Potent antibacterial activities of Ag/TiO_2 nanocomposite powders synthesized by a one-pot sol-gel method. *Environ. Sci. Technol.*, **43**:2905-2910.

SIMULATION OF CAESIUM-137 (^{137}Cs) LOCAL DIFFUSION AS A CONSEQUENCE OF THE CHERNOBYL ACCIDENT USING HOTSPOT

Ilaria Cacciotti[1,2*], Pio Ciro Aspetti[1,3], Orlando Cenciarelli[1], Mariachiara Carestia[1], Daniele Di Giovanni[1], Andrea Malizia[1], Fabrizio D'Amico[1], Alessandro Sassolini[1], Carlo Bellecci[1] & Pasquale Gaudio[1]

[1]Department of Industrial Engineering, University of Rome "Tor Vergata", Italy
[2]Department of Enterprise Engineering, University of Rome "Tor Vergata", RU INSTM Rome-"Tor Vergata", Italy
[3]BMD SpA, Italy

[*]Email: ilaria.cacciotti@uniroma2.it

ABSTRACT

The accident at the Chernobyl nuclear reactor in 1986 is considered as the most severe event that has ever occurred in the nuclear power industry, due to the considerable amounts of radioactive material released into the environment. The main purpose of this work is to simulate the dynamics of the local diffusion of caesium-137 (^{137}Cs) in the area strictly close to the Chernobyl reactor. Among the released radionuclides, we selected ^{137}Cs as it was responsible for most of the radiation exposure received by the general population. In order to simulate its local dispersion, HotSpot was used, being a user friendly freeware, and allowing to obtain data in terms of total effective dose equivalent (TEDE) and ground deposition. Two scenarios were simulated (General Fire and General Explosion) using boundary conditions selected from literature data. The obtained output data for the ground depositions were compared with the real ones, demonstrating that HotSpot allows for the simulation of radionuclide local release and diffusion due to the Chernobyl accident, even if only at a low scale. In fact, the relative proportions for the ground depositions values were respected and the measured TEDE values were in good agreement with the literature data.

Keywords: *Chernobyl accident; local caesium-137 (^{137}Cs) diffusion; HotSpot; total effective dose equivalent (TEDE); ground deposition.*

1. INTRODUCTION

On 26 April 1986, the most serious accident in the history of the nuclear industry occurred at the Chernobyl nuclear power plant in Ukraine, about 20 km south of the border with Belarus. This event can be considered one of the most significant nuclear accidents within the chemical biological, radiological & nuclear (CBRN) events (Bellecci *et al*., 2010; Malizia *et al*., 2010, 2011, 2012; Cenciarelli *et al*., 2013a, b; Gallo *et al*., 2013; Gaudio *et al*., 2011; Gaudio *et al*., 2013a, b; Pazienza *et al*., 2013, 2014).

Two explosions, which destroyed the core of Unit 4 and the roof of the reactor building, caused a dispersion of hot and highly radioactive debris, including fuel, core components, structural items and graphite into the air, and, at the same time, exposed the destroyed core to the atmosphere (IAEA, 2006). The plume of smoke, which contained radioactive fission products and debris, rose up to about 1 km into the air. Moreover, its duration was unexpectedly long, lasting over than ten days and presenting variable release rates. Both these factors (duration and altitude) were mainly ascribed to the graphite fire which was difficult to extinguish until Day 10, when the releases abruptly dropped and the intense release of radioactive materials stopped. The situation was further complicated by the meteorological conditions and the frequent changes of wind direction during the release period, leading to a non-uniform local contamination, either from the point of view of fallout density and radionuclide composition (IAEA, 2006).

For all these reasons, the area affected by the radioactive plume and the consequent deposition of radioactive substances on the ground were extremely large, surrounding the whole Northern hemisphere, even if significant contamination outside the former Soviet Union only involved a part of Europe. In 1988, the United Nations Scientific Committee on the Effects of Atomic Radiation (UNSCEAR) provided more precise data based not only on the Soviet deposition, but also on the worldwide one (UNSCEAR, 1988; Bergichev, 1990). On the basis of later analyses related to the core debris and the deposited material within the reactor building, it was estimated that the total release of radioactive substances was about 14 EBq, including 1.8 EBq of iodine-131 (^{131}I), 0.085 EBq of caesium-137 (^{137}Cs) and other caesium radioisotopes, 0.01 EBq of strontium-90 (^{90}Sr), and 0.003 EBq of plutonium radioisotopes. Noble gases contributed about 50% of the total release of radioactivity (IAEA, 2006). The release fraction of ^{137}Cs was 20 to 40% of the core inventory (i.e., 85±26 PBq) considering an average release fraction from fuel of 47% with subsequent retention of the remainder within the reactor building (IAEA, 1986; Bedyaev *et al*., 1991; Buzulukov & Dobrynin, 1993), whereas for ^{131}I, the most accurate estimate was 50 to 60% of the core inventory (i.e., 3,200 PBq).

Among the released radionuclides, the attention was mostly focused on ^{137}Cs, being considered as a particularly dangerous fission product, due to its intermediate half-life and its properties in terms of high-energy radioactivity and chemical reactivity. Its half-life of about 30 years is long enough to yield contaminated areas dangerous to humans for a generation or more , and it is short enough to ensure that even relatively small quantities of release causes dangerous doses of radiation (its specific radioactivity is 3.2×10^{12} Bq/g) (Bunting, 1975; Unterweger *et al*., 1992; NEA-OECD, 2002). In addition, ^{137}Cs undergoes high-energy beta decay (Parekh *et al*., 2008) and, being an alkali metal, is much more chemically reactive than many of the transition metal fission products. It also readily reacts with oxygen and water (Holleman & Wiberg, 2001).

As consequence of Chernobyl explosion, cesium radioactivity followed to ground deposition of fallout particles was over $1{,}5 \times 10^6$ Bq/m^2 within a 30 km radius, whereas it reached 5×10^6 Bq/m^2 in the northeast Belarus (NEA-OECD, 2002), and was only 8×10^4 Bq/m^2 in southern Sweden, several hundred km northwest (and upwind) of the disaster (Devell, 1986). In 2002, 16 years after the Chernobyl disaster (about one half of the ^{137}Cs half-life), a 4,000 km^2 area was still too contaminated to be unpopulated for several more years of the remaining half-life of the released ^{137}Cs (NEA-OECD, 2002).

It would be very interesting to make simulations of the dynamics of the local diffusion of ^{137}Cs in the area strictly close to the Chernobyl reactor in order to improve our knowledge about nuclear safety and security. In this work, HotSpot (Homann & Aluzzi, 2013) was used to achieve this purpose. This software presents many advantages, since it is a user friendly freeware and allows simulation of a wide range of scenarios, considering many concomitant factors. Indeed, in the case of severe nuclear accidents, the released radioactive materials, both in the form of gases and particulates, disperse downwind as a plume, and their concentrations in the air and, after the fallout, on the soil depend on several factors, such as the amount of released radionuclide and the height of emission point. Other factors, such as wind speed, atmospheric stability, and physical and chemical forms of the released material influence the radioactivity in the environment (IAEA, 2001).

2. HOTSPOT

HotSpot Health Physics aims to provide emergency response personnel and emergency planners with a fast, field-portable set of software tools for evaluating incidents involving radioactive material. The software is also used for safety analysis of facilities handling radioactive materials. The atmospheric dispersion models used by HotSpot software are a first-order approximation of the radiation effects associated with the short-term (less than a few hours) atmospheric discharge of radioactive materials. In fact, they are designed for near-surface releases, short-range (less than 10 km) dispersion, and short-term (less than 24 h) emission in unobstructed terrains and simple meteorological conditions. HotSpot estimates the dispersal of radioactive

material using the Gaussian model, since the adequacy of this model for making initial dispersion estimates or worst-case safety analyses has been tested and verified for many years (Homann & Aluzzi, 2013).

The HotSpot codes are continuously updated to incorporate the most current and approved radiological dose conversion data and methodologies. These codes are based on the well established Gaussian plume model (GPM), widely used for an initial emergency assessment or safety analysis planning of a radionuclide release. The main advantages of GPM are short computation time, extensive validation and worldwide acceptance. Virtual source terms are used to model the initial 3D distribution of material associated with an explosive or fire release, resuspension, or user-input geometry (Homann & Aluzzi, 2013). For evaluation of radiological scenarios, HotSpot uses the methods of radiation dosimetry recommended by the International Commission on Radiological Protection (ICRP) (ICRP, 2005) and US Environmental Protection Agency's (EPA) Federal Guidance Reports No. 11, 12 and 13 (EPA, 1988, 1993, 1999).

3. METHODOLOGY

For the simulation of the radionuclide dispersion during the Chernobyl accident, two different scenarios were applied (General Fire and General Explosion), taking into account that this event was characterised by two explosions and the graphite fire. Among the several involved radionuclides, we decided to study the dispersion of ^{137}Cs, since it was the main radionuclide responsible of exposure to the population. Moreover, another main purpose of this work was to evaluate its dispersion within the first hour from the beginning of the accident, according to the features of the software. All the parameters used were identified from literature data (Apsimon, 1985; IAEA, 2006). The selected boundary conditions are summarised in Table 1.

For the source term, the following values were selected: material at risk (MAR), 25 PBq (amount released on the first day (i.e., 26 April 1986)); damage ratio (DR), 1.00; leakpath factor, 1.00; airborne fraction (ARF), 1.00; and respirable fraction (RF), 1.00; and deposition velocity, 0.15 cm/s (Apsimon, 1985; IAEA, 2006). Specifically, in the case of the General Fire scenario, the cloud top was set as 900 m , since it was reported that the plume rose up to about 1 km into the air during the first hours (the software does not allow for the selection of a cloud top value higher than 900 m). For the General Explosion scenario, all the parameters were maintained unaltered, adding for high explosive a value of 10 t (22,000 lb), since the nuclear excursion released 40 bil. J of energy, which is the equivalent of about 10 t of trinitrotoluene (TNT) (Pakhomov & Dubasov, 2010).

Finally, the boundary conditions were selected, in terms of total effective dose equivalent (TEDE) and ground deposition (soil radioactivity value in kBq/m^2). For TEDE, the inner, middle and outer parameters were set up as 5 Sv (threshold for immediate deterministic effects), 20 mSv (maximum dose for first responders) and 1 mSv (operational level for evacuation) respectively (ICRP, 1996). Values of 2,000, 1,000 and 350 kBq/m^2 were chosen for the ground deposition inner, middle and outer parameters respectively on the basis of literature data, considering the area close to the Chernobyl district. In fact, four main ^{137}Cs contamination ranges (i.e., 37-185 kBq/m^2, 185-555 kBq/m^2, 555-1,480 kBq/m^2 and > 1,480 kBq/m^2) were reported and identified (IAEA, 2006) and, thus, in this simulation the three highest contamination level ranges were considered, employing the average values.

4. RESULTS & DISCUSSION

The HotSpot outputs for the General Fire and General Explosion scenarios are reported in Table 2. Figures 1 and 2 show the graphical representations of the results for both the simulated scenarios, in terms of ground deposition isoconcentration and TEDE isodose respectively, in a Cartesian system with the *x*-axis oriented in the main wind direction.

Table 1: Boundary conditions for the General Fire and General Explosion scenarios.

	Parameter	Value
Source term characteristics	Source material	^{137}Cs 30.0 y
	Material at risk (Bq)	25.0×10^{15}
	Deposition velocity (cm/s)	0.15
	Damage ratio	1.0
	Leakpath factor	1.0
	Airborne fraction (ARF)	1.0
	Respirable fraction (RF)	1.0
General Fire scenario		
Fuel fire information	Physical height of the fire (m)	10.0
	Release radius (m)	30.0
	Cloud top (m)	900.0
	Effective release height (m)	309.0
	Wind speed (*height*=10 m) (m/s)	10.0
	Distance coordinates	All distances are on the plume centreline
General Explosion scenario		
Explosive	High explosive (lb)	2.2×10^4
Meteorological conditions	10 m wind speed (m/s)	10.0
	Wind direction	175.0° (wind from south)
	Stability class	A
	Atmospheric stability (actual stability)	very unstable
	Non-respirable deposition velocity (cm/s)	8.0
	Receptor height	1.5 m
	Inversion layer height	None
	Sample time (min)	10.0
	Wind ref. Height (m)	10.0
	Breathing rate (m^3/s)	3.3×10^{-4}
TEDE (Sv)	Inner contour dose	5.0
	Middle contour dose	20.0×10^{-3}
	Outer contour dose	1.0×10^{-3}
Deposition (kBq/m^2)	Inner	2000.0
	Middle	1000.0
	Outer	350.0

The ground deposition contour plots highlight the maximum distances of deposition curves from the zero point (hotspot) downwind. Comparing the obtained areas (3.4, 8.6 and 29.0 km^2 for the General Fire scenario; 2.4, 6.8 and 25.0 km^2 for the General Explosion scenario), it was evident that they were remarkably lower with respect to the real ones (600, 900 and 3,200 km^2) (IAEA, 2006), as expected. HotSpot allows for the simulation of radionuclide atmospheric dispersion, providing reliable and significant data for up to only about 10 km from the reactor site. However, it is interesting to note that the ratios between the considered areas were comparable for the General Fire and General Explosion scenarios with respect to the real data, as reported in Table 3. This experimental evidence suggests, and further validates, that the HotSpot code is able to simulate the ^{137}Cs release due to Chernobyl accident at a low scale.

The measured TEDE values showed that the selected conditions were not able to induce a deterministic hazard, since the related threshold (i.e., 5 Sv) was not overcome. However, the simulation revealed the presence of areas with TEDE values higher than 20 mSv up to maximum distances between around 4.3 and 7.7 km, on the basis of the considered scenarios, suggesting the need of an immediate area evacuation. Moreover, considering the outer area, which measured approximately 216-244 km^2, it could be inferred that a maximum distance of around 45-50 km from hot spot would impart a TEDE of at least 1 mSv, even if it has to be taken into account that the HotSpot data can be considered as reliable for only within 10 km.

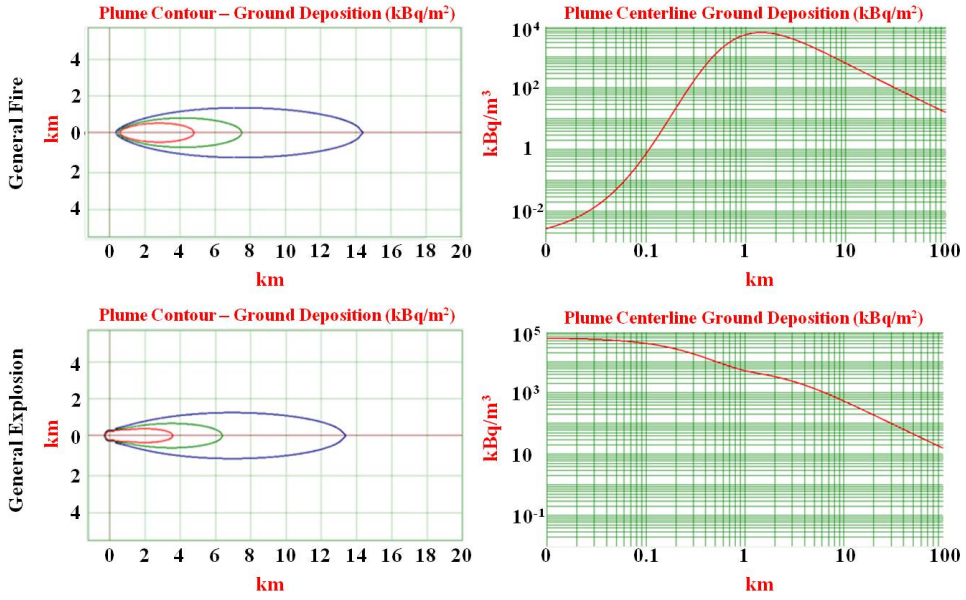

Figure 1: Ground deposition isoconcentration as a function of distance.

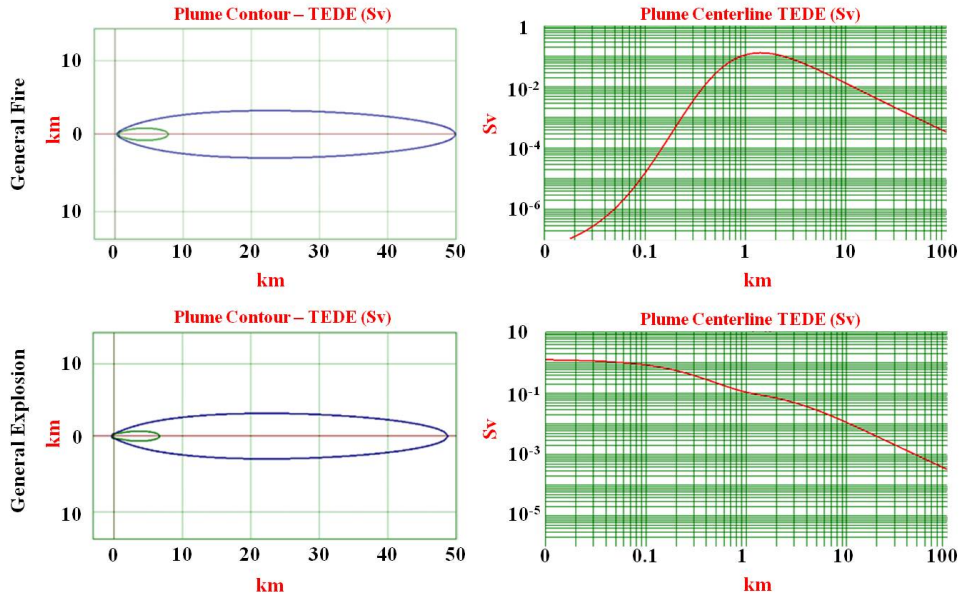

Figure 2: TEDE isodose as a function of the distance.

The output data obtained from General Fire scenario simulation fitted well with the data from the literature, since it was reported that the average effective doses were around 100 mSv for the liquidators (highly exposed), 50 mSv for the residents in strictly controlled zones (SCZs, where radioactive caesium contamination exceeded 555 kBq/m^2) and 30 mSv for the evacuees. In fact, a maximum TEDE value of 131 mSv was detected at 1.4 km from the release point, whereas TEDE values in the range 30-55 mSv were revealed between 4 and 8 km (that could be considered the SCZs in this low scale simulation). Moreover, in the case of General Explosion setup, remarkably higher maximum effective dose values (i.e. 1.3 Sv) were detected at around 0.01 km (very close to the release point), corroborating the very high values revealed in the area were strictly close to the reactor. In Table 4, the measured distances for the maximum TEDE values for the deterministic effects threshold and for several well-known Operational Intervention Levels (OILs) are reported for all the considered scenarios.

Table 2: HotSpot outputs for the General Fire (GF) and General Explosion (GE) scenarios.

Distance (km)	TEDE (Sv)		Respirable time-integrated air concentration ((Bq-sec)/m^3)		Ground surface deposition (kBq/m^2)		Ground shine dose rate (Sv/h)		Time (h:min)	
	GF	GE	GF	GE	GF	GE	GF	GE	GF	GE
0.03	2.80E-07	1.20E+00	8.9E+03	3.70E+10	1.3E-02	5.50E+04	2.6E-09	1.1E-02	<00:01	<00:01
0.1	1.50E-05	8.50E-01	4.9E+05	2.70E+10	7.3E-01	4.00E+04	1.5E-07	8.1E-03	<00:01	<00:01
0.2	4.80E-04	5.60E-01	1.5E+07	1.80E+10	2.2E+01	2.70E+04	4.5E-06	5.3E-03	<00:01	<00:01
0.3	3.50E-03	3.90E-01	1.1E+08	1.20E+10	1.7E+02	1.80E+04	3.3E-05	3.7E-03	<00:01	<00:01
0.4	1.20E-02	2.90E-01	3.8E+08	9.00E+09	5.7E+02	1.40E+04	1.1E-04	2.7E-03	<00:01	<00:01
0.5	2.70E-02	2.20E-01	8.5E+08	7.00E+09	1.3E+03	1.10E+04	2.5E-04	2.1E-03	<00:01	<00:01
0.6	4.60E-02	1.80E-01	1.4E+09	5.70E+09	2.2E+03	8.60E+03	4.3E-04	1.7E-03	<00:01	<00:01
0.7	6.60E-02	1.50E-01	2.1E+09	4.80E+09	3.1E+03	7.30E+03	6.2E-04	1.5E-03	<00:01	<00:01
0.8	8.50E-02	1.30E-01	2.7E+09	4.20E+09	4.0E+03	6.30E+03	8.0E-04	1.3E-03	00:01	<00:01
0.9	1.00E-01	1.20E-01	3.2E+09	3.80E+09	4.7E+03	5.70E+03	9.5E-04	1.1E-03	00:01	00:01
1	1.10E-01	1.10E-01	3.6E+09	3.50E+09	5.3E+03	5.20E+03	1.1E-03	1.0E-03	00:01	00:01
2	1.20E-01	7.10E-02	3.7E+09	2.20E+09	5.5E+03	3.30E+03	1.1E-03	6.7E-04	00:02	00:02
4	5.50E-02	3.70E-02	1.7E+09	1.20E+09	2.6E+03	1.80E+03	5.2E-04	3.5E-04	00:05	00:04
6	3.00E-02	2.30E-02	9.5E+08	7.20E+08	1.4E+03	1.10E+03	2.8E-04	2.2E-04	00:07	00:07
8	1.90E-02	1.60E-02	6.0E+08	4.90E+08	9.0E+02	7.40E+02	1.8E-04	1.5E-04	00:10	00:09
10	1.30E-02	1.10E-02	4.2E+08	3.60E+08	6.3E+02	5.30E+02	1.3E-04	1.1E-04	00:13	00:12
20	4.30E-03	4.00E-03	1.4E+08	1.30E+08	2.0E+02	1.90E+02	4.1E-05	3.7E-05	00:26	00:24
40	1.40E-03	1.40E-03	4.5E+07	4.30E+07	6.7E+01	6.40E+01	1.3E-05	1.3E-05	00:52	00:49
60	7.50E-04	7.30E-04	2.4E+07	2.30E+07	3.5E+01	3.40E+01	7.1E-06	6.9E-06	01:18	01:13
80	4.80E-04	4.70E-04	1.5E+07	1.50E+07	2.3E+01	2.20E+01	4.5E-06	4.4E-06	01:44	01:38

Table 3: Comparison between real and simulated ground deposition areas.

		Ground deposition (kBq/m^2)			Relative Proportions
		Inner (2,000)	Middle (1,000)	Outer (350)	
Area (km^2)	HotSpot ground deposition (General Fire)	3.4	8.6	29.0	0.12:0.30:1.00
	HotSpot ground deposition (General Explosion)	2.4	6.8	25.0	0.10:0.27:1.00
	Ukraine areas contaminated (IAEA, 2006)	600.0	900.0	3,200.0	0.19:0.28:1.00

The defined OILs, in terms of avertable doses by implementing protective measures, are (ICRP, 1996): OIL1, dose rate in radioactive plume = 1.0 mSv/h, evacuation or substantial sheltering in the affected 22.5° angular sector and the two adjacent sectors; OIL2, dose rate in radioactive plume = 0.1 mSv/h, thyroid blocking agent administration and sheltering with windows closed; OIL3, environmental dose rate in deposition = 1 mSv/h, evacuation and substantial sheltering in the affected sector; OIL4, environmental dose rate in deposition = 0.2 mSv/h, population relocation from the affected sector; and OIL5, environmental dose rate in deposition = 1 μSv/h, immediate restriction of food and milk consumption (potentially contaminated) from the affected sector until samples are analysed.

Table 4: Measured distances (km) for the maximum TEDE values, deterministic effects threshold and for several well-known Operational Intervention Levels (OILs).

Parameters		General Fire	General Explosion
Maximum TEDE value (Sv)		0.131	1.3
Maximum dose distance (km)		1.4	0.01
Deterministic effects threshold exceeding area		No exceeding	No exceeding
Exceeding area (km^2)	OIL1	50.0	49.0
	OIL2	-	-
	OIL3	1.0-2.0	1.0
	OIL4	10.0	6.0
	OIL5	-	-

Finally, HotSpot allows for the display of contours for both ground deposition and TEDE at the release location in Google Earth, inserting the Chernobyl reactor geographical coordinate (i.e., 51.38955 N, 30.09915 E). In Figure 3 the georeferencing of TEDE isodoses and ground deposition isoconcentrations are shown, indicating the areas affected by ^{137}Cs dispersion.

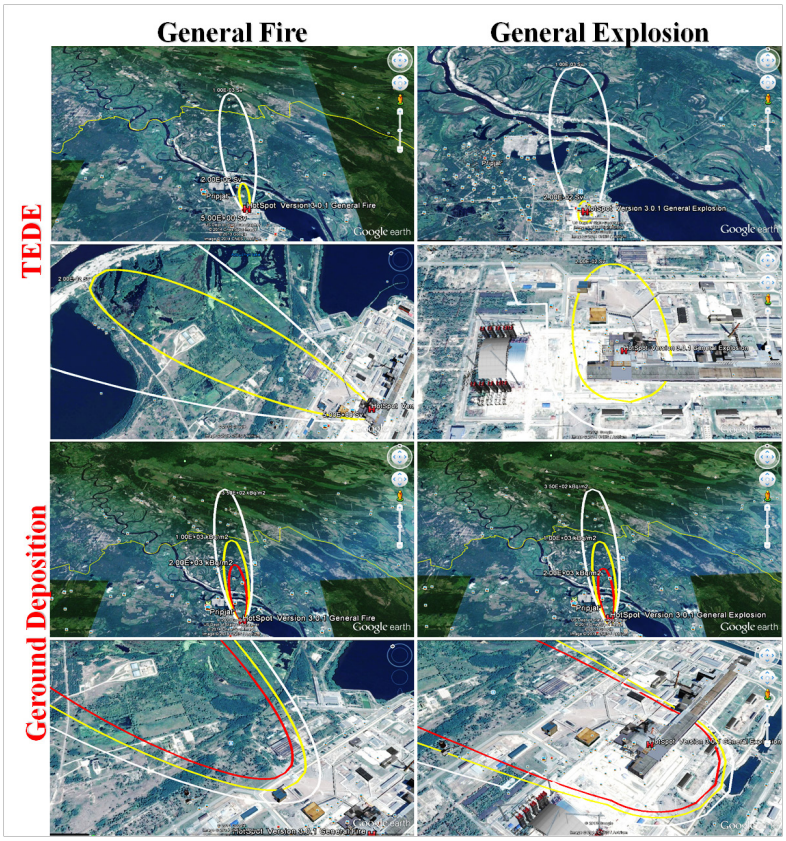

Figure 3: Georeferencing of TEDE and ground deposition data.

5. CONCLUSION

The ^{137}Cs air dispersion as a consequence of Chernobyl accident was simulated using HotSpot. Through comparison of the obtained output data for the ground depositions with the real ones, it was found that the relative proportions for the ground depositions values were respected and the measured TEDE values were in

good agreement with the literature data. Thus, it is possible to conclude that HotSpot code allows for the simulation of radionuclide local release and diffusion. Nevertheless, its limitations is that it is only designed for near-surface releases, short-range (less than 10 km) dispersion and short-term (less than 24 h) release durations in unobstructed terrains and simple meteorological conditions.

ACKNOWLEDGMENT

Special acknowledgment for the support received to develop this work goes to the Directive Board of International Master Courses in Protection Against CBRNe Events (http://www.mastercbrn.com).

REFERENCES

Apsimon, H.M., Goddard, A.J.H., Wrigley, J. & Crompton, S. (1985). Long-range atmospheric dispersion of radioisotopes-ii, application of the MESOS model. *Atmos. Environ.*, **19**:113-125.

Bedyaev, S.T., Borovoi, A.A., & Demin, V.F. (1991). The Chernobyl source term. *Proc. Seminar on Comparative Assessment of the Enviromental Impact of Radionuclides Released during Three Major Nuclear Accidents: Kyshtym, Windscale, Chernobyl*, EVR-13574, CEC, pp. 71-91.

Bellecci, C., Gaudio, P., Gelfusa, M., Malizia, A., Richetta, M., Serafini, C. & Ventura, P. (2010). Planetary boundary layer (PBL) monitoring by means of two laser radar systems: experimental results and comparison. *Proc. SPIE*, **7832**: 78320X.

Bergichev, S.N. (1990). Radioactive releases due to the Chernobyl accident. *In* Rogers, J.T. (Ed.), *Fission Product Transport Processes in Reactor Accidents*. JT Rogers, editor, Hemisphere Publishing, London.

Bunting, R. L. (1975). Nuclear data sheets for A= 137. *Nucl. Data Sheet.*, **15**: 335-369.

Buzulukov, Y.P. & Dobrynin, Y.L. (1993). Release of radionuclides during the Chernobyl accident. *Chernobyl Pap.*, **1**:3-21.

Cenciarelli, O., Malizia, A., Marinelli, M., Pietropaoli, S., Gallo, R., D'Amico, F., Bellecci, C., Fiorito, R., Gucciardino, A. & Gaudio, P. (2013a). Evaluation of biohazard management of the Italian national fire brigade. *Defence S&T Tech. Bull.*, **6**:33-41.

Cenciarelli, O., Rea, S., Carestia, M., D'Amico, F., Malizia, A., Bellecci, C., Gaudio, P., Gucciardino, A. & Fiorito, R. (2013b). Bioweapons and bioterrorism: A review of history and biological agents. *Defence S&T Tech. Bull.*, **6**: 111-129.

Devell, L., Tovedal, H., Bergström, U., Appelgren, A., Chyssler, J. & Andersson, L. (1986). Initial observations of fallout from the reactor accident at Chernobyl. *Nature*, **321**:192-193.

EPA (Environmental Protection Agency) (1988). *Federal Guidance Report No. 11: Limiting Values Radionuclide Intake and Air Concentration, and Dose Conversion Factors for Inhalation, Submersion, and Ingestion*. Environmental Protection Agency (EPA), Washington DC, USA.

EPA (Environmental Protection Agency) (1993). *Federal Guidance Report No. 12: External Exposure to Radionuclides in Air, Water, and Soil*. Environmental Protection Agency (EPA), Washington DC, USA.

EPA (Environmental Protection Agency) (1999). *Federal Guidance Report No. 13: Cancer Risk Coefficients for Environmental Exposure to Radionuclides*. Environmental Protection Agency (EPA), Washington DC, USA.

Gallo, R., De Angelis, P., Malizia, A., Conetta, F., Di Giovanni, D., Antonelli, L., Gallo, N., Fiduccia, A., D'Amico, F., Fiorito, R., Richetta, M., Bellecci, C. & Gaudio, P. (2013). Development of a georeferencing software for radiological diffusion in order to improve the safety and security of first responders. *Defence S&T Tech. Bull.*, **6**: 21-32.

Gaudio, P., Gelfusa, M., Lupelli, I., Malizia, A., Moretti, A., Richetta, M., Serafini, C. & Bellecci, C. (2011). First open field measurements with a portable CO_2 lidar/dial system for early forest fires detection. *Proc. SPIE*, **8182**: 818213.

Gaudio, P., Gelfusa, M., Malizia, A., Richetta, M., Antonucci, A., Ventura, P., Murari, A. & Vega, J. (2013a). Design and development of a compact lidar/DIAL system for aerial surveillance of urban areas. *Proc. SPIE*, **8894**: 88940D.

Gaudio, P., Gelfusa, M., Malizia, A., Richetta, M., Serafini, C., Ventura, P., Bellecci, C., De Leo, L., Lo Feudo, T. & Murari, A. (2013b). New frontiers of Forest Fire Protection: A portable Laser System (FfED). *WSEAS Tran. Environ. Dev.*, **9**: 195-205.

Holleman, A.F. & Wiberg, E. (2001). *Inorganic Chemistry*. Academic Press, London, UK.

Homann, S.G. & Aluzzi, F. (2013). *HotSpot Health Physics Codes Version 3.0 User's Guide*. National Atmospheric Release Advisory Center Lawrence Livermore National Laboratory, Livermore, California, USA.

IAEA (International Atomic Energy Agency) (1986). *Summary Report on the Post-Accident Review Meeting on the Chernobyl Accident.* Safety Series No. 75-INSAG-1*,* International Atomic Energy Agency (IAEA), Vienna, Austria.

IAEA (International Atomic Energy Agency) (2001). *Generic Models for use in assessing the impact of discharges of radioactive substances to the environment.* Safety Series No. 9*,* International Atomic Energy Agency (IAEA), Vienna, Austria.

IAEA (International Atomic Energy Agency) (2006). *Environmental consequences of the Chernobyl accident and their remediation: twenty years of experience / report of the Chernobyl, Forum Expert Group "Environment",* International Atomic Energy Agency (IAEA) International Atomic Energy Agency (IAEA) International Atomic Energy Agency (IAEA), Vienna, Austria.

International Commission on Radiological Protection (ICRP) (1996). *Basic Anatomical & Physiological Data for use in Radiological Protection: The Skeleton*. ICRP publication 70, ICRP, Elsevier, United Kingdom.

International Commission on Radiological Protection (ICRP) (2005). *Basis for Dosimetric Quantities Used in Radiological Protection*. ICRP, Ottawa, Canada.

Malizia, A., Quaranta, R. & Mugavero, R. (2010). CBRN events in the subway system of Rome: Technical-managerial solutions for risk reduction. *Defence S&T Tech. Bull.*, **3**:140-157.

Malizia, A., Quaranta, R., Mugavero, R., Carcano, R., & Franceschi, G. (2011). Proposal of the prototype RoSyD-CBRN, a robotic system for remote detection of CBRN agents. *Defence S&T Tech. Bull.*, **4**:64-76.

Malizia, A., Lupelli, I., D'Amico, F., Sassolini, A., Fiduccia, A., Quarta, A. M., Fiorito, R., Gucciardino, A., Richetta, M., Bellecci, C. & Gaudio, P. (2012). Comparison of software for rescue operation planning during an accident in a nuclear power plant. *Defence S&T Tech. Bull.*, **1**:36-45.

NEA-OECD (Nuclear Energy Agency of the Organization for Economic Cooperation and Development) (2002). *Chernobyl: Assessment of Radiological and Health Impacts*. Available online at: http://www.oecd-nea.org/rp/chernobyl (Last access: 15 February 2014).

Pakhomov, S.A. & Dubasov, Y.V. (2010). Estimation of explosion energy yield at Chernobyl NPP accident. *Pure Appl. Geophys.*, **167**:575-580.

Parekh, N.R., Poskitt, J.M., Dodd, B.A., Potter, E.D., Sanchez A. (2008). Soil microorganisms determine the sorption of radionuclides within organic soil systems. *J. Environ. Radioactiv.*, **99**: 841–852.

Pazienza, M., Britti, M.S., Carestia, M., Cenciarelli, O., D'Amico, F., Malizia, A., Bellecci, C., Gaudio, P., Gucciardino, A., Bellino, M., Lancia, C., Tamburrini, A. & Fiorito, R. (2013). Application of real-time PCR to identify residual bio-decontamination of confined environments after hydrogen peroxide vapor treatment: Preliminary Results. *J. Microb. Biochem. Technol.*, **6**: 24-28.

Pazienza, M., Britti, M.S., Carestia, M., Cenciarelli, O., D'Amico, F., Malizia, A., Bellecci, C., Fiorito, R., Gucciardino, A., Bellino, M., Lancia, C., Tamburrini, A. & Gaudio, P. (2014). Use of particle counter system for the optimization of sampling, identification and decontamination procedures for biological aerosols dispersion in confined environment. *J. Microb. Biochem. Technol.*, **6**: 43-48.

UNSCEAR (United Nations Scientific Committee on the Effects of Atomic Radiation) (1988). *Sources, Effects and Risks of Ionizing Radiation.* Report to the United Nations, United Nations Scientific Committee on the Effects of Atomic Radiation (UNESCAR), New York, USA.

Unterweger, M. P., Hoppes, D. D. & Schima, F. J. (1992). New and revised half-life measurements results. *Nucl. Instrum. Meth. A*, **312**:349-352.

FAILURE ANALYSIS OF A DIESEL MAIN ENGINE'S VALVE STEMS

Nik Hassanuddin Nik Yusoff*, Hasril Nain, Mahdi Che Isa & Irwan Mohd Nor

Marine Materials Research Group, Maritime Technology Division (BTM), Science & Technology Research Institute for Defence (STRIDE), Ministry of Defence, Malaysia

*Email: nhassanuddin.nyusoff@stride.gov.my

ABSTRACT

Several components of a Stork Wartsila 12V 28SW diesel main engine failed dramatically after 1,400 h of service. Upon inspection of the components, it was found that the valve stems of cylinder liner no. 2 were extremely damaged. Investigation of the valve stems was conducted through visual examination, chemical analysis and fractography. Various fracture mechanisms, such as fatigue fracture, ductile tensile overload and very high cycle fatigue (VHCF) were observed. It was determined that the damages sustained by the engine were a result of fatigue failure due to high usage of the valve stems. After long use and exposure to the high temperatures, the fatigue strength of the valve decreased and hence, fatigue failures of the materials occurred at stresses lower than the conventional fatigue limit.

Keywords: *Failure analysis; cylinder liner valve stems; fractography; ductile tensile overload; very high cycle fatigue (VHCF).*

1. INTRODUCTION

Stork-Wartsila 12V 28SW is a diesel main engine commonly used on ships. This engine can run up to 1,000 rpm (Wartsila, 2008). Figure 1 shows the layout of the components in the engine. It was reported that a Stork-Wartsila engine failed after 1,400 h of its engine service life. Before the failure, the ship was operated at 900 rpm for 1 h. The data collected on the engine temperature and lubricant pressure did not show any abnormal conditions of the engine. The ship was reported to have completed its scheduled maintenance but some of the components were not replaced as they were still in good physical condition.

The Science & Technology Research Institute for Defence (STRIDE), Malaysia was requested by the equipment owner to conduct an analysis of the engine's components in order to determine the root cause of the failure. The ensuing failure investigation was noteworthy due to the extent of the damage to the engine components and the variety of fracture mechanisms encountered. In this paper, the observations and conclusions of the failure analysis are provided as a case study, and recommendations are offered to help avoid similar failures in the future.

2. EXPERIMENTAL PROCEDURE

The investigation of the failure was carried out using several experimental tests, including visual examination, chemical composition analysis and fractography. Chemical composition analysis was carried out by using a Bruker S4 Pioneer wavelength dispersive X-ray flourensence (XRF) spectrometer with carbon and sulfur determinator. The fracture surfaces were inspected visually, then micro- and macroscopically using a Zeiss Axioplan light microscope. Throughout this process, care

was taken to avoid damage to the fracture surfaces. The fracture surfaces were ultrasonically cleaned and examined using a LEO VP 1480 scanning electron microscope (SEM).

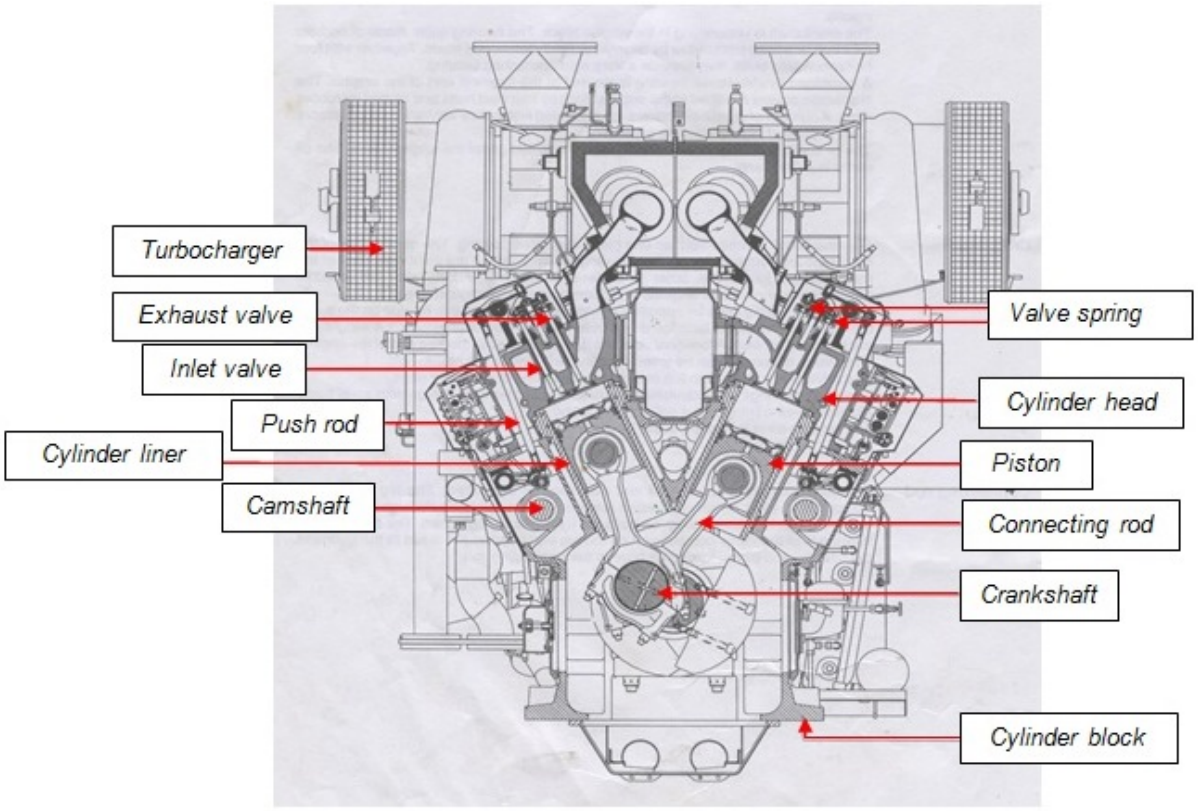

Figure 1: Layout of components of a Stork-Wartsila 12V 28SW engine. (Source: Wartsila (2008))

3. RESULTS

3.1 Visual Inspection

When cylinder liner no. 2 was disassembled, extensive damage to its piston was found. The piston crown was broken, separated from the piston skirt and stacked on the cylinder liner as shown in Figure 2. Figure 3 shows the valve heads that were found on the piston crown. It is clear that the recovered valve heads had experienced significant impact damage.

Figure 2: The separated piston crown and skirt.

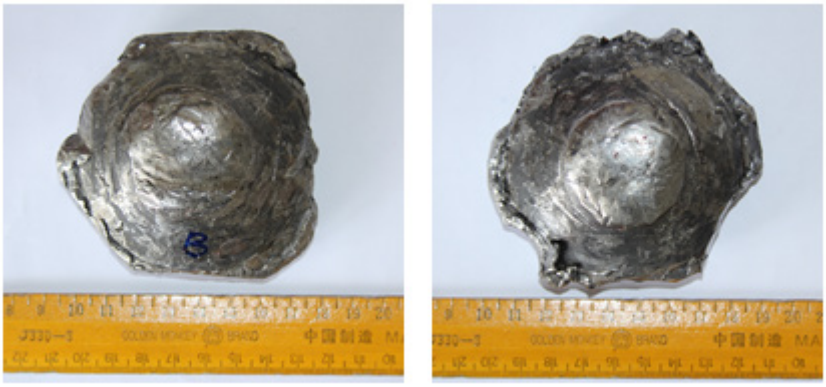

Figure 3: Two valve heads found on the piston crown.

The underside of cylinder head no. 2 also showed serious impact damage as shown in Figure 4. The valve stems were still in their guides, with three of the valve heads, nos. 1 to 3, fractured from their stems, while the remaining valve head (valve no. 4) was still attached to the stem. There was no damage to any of the valve springs that would otherwise have affected proper valve closure.

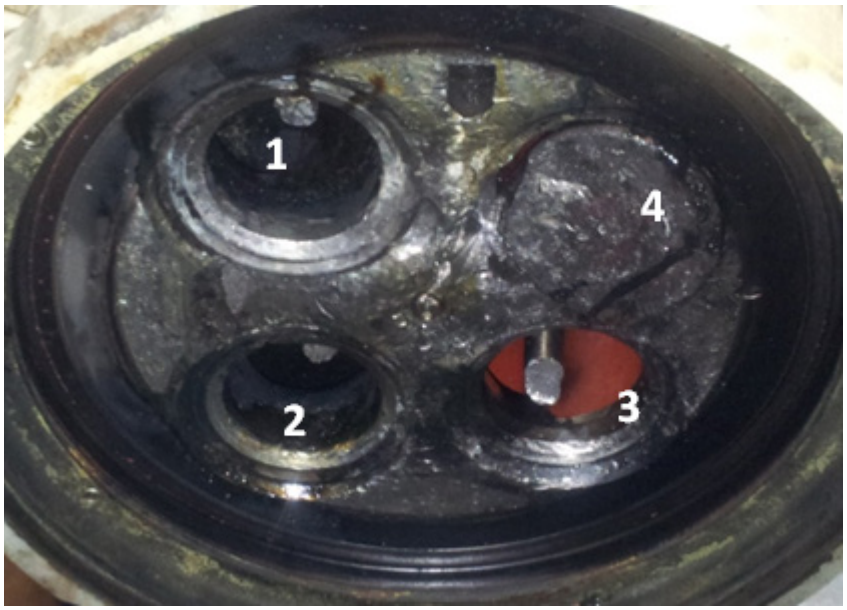

Figure 4: The underside of the cylinder head no. 2.

3.2 Chemical Composition Analysis

From the results of the composition examination of the valve material, as shown in Table 1, the composition of the base alloys was found to be X45CrSi93, which is commonly used as a valve (ASM, 1990).

Table 1: Chemical composition of the valve stem and head materials.

Sample	Composition (%)							
	Cr	Si	C	Cu	Mn	Zn	Ni	Fe
Valve stem	8.9	2.6	0.48	0.27	0.2	0.1	0.1	Bal
Valve head	8.9	2.9	0.49	0.28	0.2	0.1	0.1	Bal

3.3 Fractography

The fracture surfaces of the three valve stems shown in Figure 4 were analysed visually and via SEM. The fracture surface of valve stem no. 1, as shown in Figure 5, was undamaged after the fracture. The presence of beach marks can be seen clearly in Figure 6. From the beach marks' orientation, the location of the crack initiation point can be determined. It is strongly believed that the crack started at the point due to surface defects of the valve stem. The red arrows in Figure 5 show the surface cracks that occurred on the valve stem resulting from the bending moment to the areas.

Figure 5: The fracture surface of valve stem no. 1.

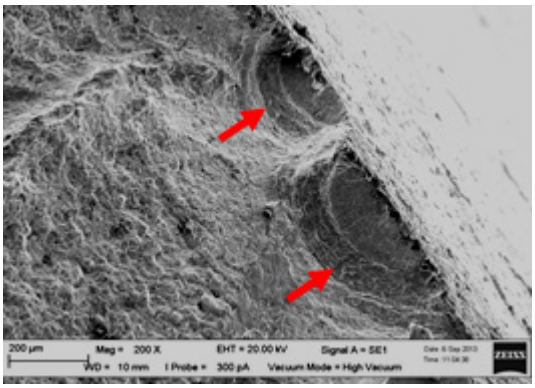

Figure 6: The fatigue region observed using SEM.

The fracture surface of valve stem no. 2, as shown in Figure 7, was also undamaged after the fracture. As observed using high magnification SEM (Figure 8(a)), the central region of the fracture surface was highly topographical, which is consistent with ductile tensile overload. The surface consists of dense dislocated walls and almost free channels. The presence of the slip bands and dimple marks describe the overload that happened. As shown in Figure 8(b), a considerable amount of secondary cracking was visible even under low magnification.

The fracture surface of valve stem no. 3, as shown in Figure 9, consists of two areas. The smooth and burnished area shows the progress of the fatigue crack up to the moment of final rupture, and the final granular area due to fast fracture. The crack origin can be clearly seen at the surface of the valve stem. The surface defects due to impact initiated the crack leading to the failure.

Figure 7: The fracture surface of valve stem no. 2.

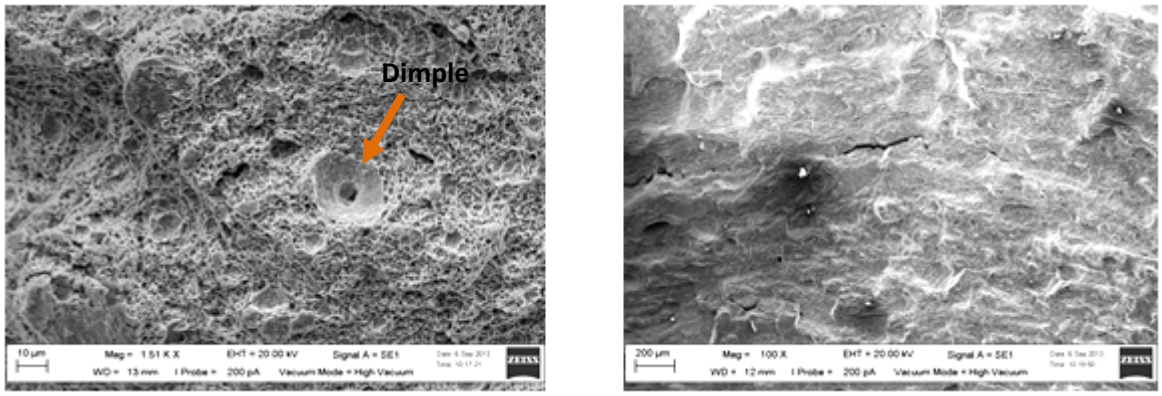

(a) **(b)**

Figure 8: SEM images of the fracture surface: (a) The central region (b) Secondary crack.

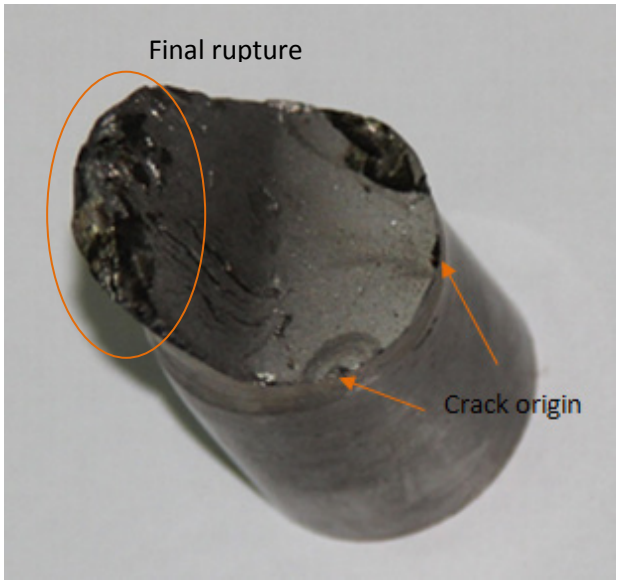

Figure 9: The fracture surface of valve stem no. 3.

4. DISCUSSION

The failure of the cylinder no. 2 was the event that alerted the operators of the main engine to the wider damage. The observations of this failure analysis suggest that the broken piston and bending of the pushing rod were merely a secondary consequence of the fracture of the three valve stems. Therefore, in order to understand the wider failure, it is necessary to examine what caused the fracture of the valve stems in the first place.

The X45CrSi93 base alloys are ferritic-martensitic, force shaped and annealed valve steel (ASM, 1990). The chemical compositions of valve stem and head material are similar, indicating that the valve is monometallic. There were no signs of the materials decarburisation from high temperature exposure (Vardar & Ekerim, 2010).

Examination of the fracture surface of the valve stems showed that valve stem no. 1 failed due to fatigue, which was initiated by the surface defect. The crack on the surface results from the bending load that can be seen in Figure 5. The fracture surface of the valve stem no. 3 also originated from the surface defect which was caused by impact. The presence of the defects act as stress raisers, where the applied stress concentrates until it exceeds the local strength of the materials and produces a crack (Fonte & de Freitas 2009; Muhammad *et al*., 2010).

The fracture surface of the valve stem no. 2 shows the presence of persistent slip bands at the centre region of the fracture surface. The slip bands have a well-defined dislocation structure characterised by a length which separates the walls of dislocation dipoles (Brown, 2000), and form where plastic deformation is concentrated (Pyttel *et al*., 2011). This structure leads to the initiation of fatigue cracks through the intersection of the external surface of the material. Through this, they cause stress concentrations and generate intrusions, which follow the interface between the slip bands and matrix within which it is embedded (Brown, 2000).

Normally, the presence of persistent slip bands is related to very high cycle fatigue (VHCF). Lei *et al*. (2013) described VHCF as a fatigue that occurs to the material due high frequency of use, usually more than 10^7 cycles. This fatigue is usually initiated from subsurface cracks due to microscopic defects (inclusions, pores) but sometimes these failures cannot be retraced to microstructural inhomogeneities. They are referred to as non-defect or matrix failures (Pyttel *et al*., 2011). In this case, the failure of the valve stem no. 2 is believed to have initiated from the subsurface defect, which is proved by the presence of the persistent slip bands. After long use and exposure to the high temperatures, the fatigue strength of the valve decreased (Kwon & Han 2004). As a result, fatigue failures of the materials may occur at stresses lower than the conventional fatigue limit (Sun *et al*., 2013). The decrease of the fatigue strength is widely discuss through the stress-cycle (S-N) curve by the researchers (Marines, 2003; Sonsino, 2007; Pyttel *et al*., 2011).

5. CONCLUSION

Based on the evidence found from the fracture surfaces of the valve stems from cylinder liner no. 2, it was determined that fatigue failure had occurred. The initial cause of the fatigue was from an internal crack in valve stem no. 2 due to high usage of the component. The highly used valves had reduced fatigue strength, resulting in fatigue failure at stresses lower than the conventional fatigue limit.

REFERENCES

American Society for Metals (ASM) (1990). *ASM Metals Handbook, Volume 1:Properties and Selection*. American Society for Metals (ASM), Russell Township, Ohio.

Brown, L. (2000). Dislocation plasticity in persistent slip bands. *Mater. Sci. Eng. A*, **285**: 35–42.
Fonte, M. & de Freitas, M. (2009). Marine main engine crankshaft failure analysis: A case study. *Eng. Fail. Anal.*, **16**: 1940–1947.
Kwon, O.G. & Han, M.S. (2004). Failure analysis of the exhaust valve stem from a Waukesha P9390 GSI gas engine. *Eng. Fail. Anal.*, **11**: 439–447.
Lei, Z., Xie, J., Chengqi, S., Liu, X. & Hong,Y. (2013). Effects of microstructure on very-high-cycle fatigue crack initiation and life scatter for a high strength steel. *13th Int. Conf. Fracture*, 16-21 June 2013, Beijing, pp. 1–8.
Marines, I. (2003). An understanding of very high cycle fatigue of metals. *Int. J. Fatigue*, **25**: 1101–1107.
Muhammad, M.M., Isa, M.C.& Din Yati, S. (2010). Failure analysis of a diesel engine rocker arm. *Defence S&T Tech. Bull.*, **3**:78–84.
Pyttel, B., Schwerdt, D. & Berger, C. (2011). Very high cycle fatigue – Is there a fatigue limit? *Int. J. Fatigue*, **33**: 49–58.
Sonsino, C. (2007). Course of SN-curves especially in the high-cycle fatigue regime with regard to component design and safety. *Int. J. Fatigue*, **29**: 2246–2258.
Sun, C., Lei, Z., Xie, J. & Hong, Y. (2013). Effects of inclusion size and stress ratio on fatigue strength for high-strength steels with fish-eye mode failure. *Int. J. Fatigue*, **48**: 19–27.
Wartsila (2008). *Wartsila 38 - Project Guide*. Wartsila Ship Power Technology, Drunen, Netherlands.
Vardar, N. & Ekerim, A. (2010). Investigation of exhaust valve failure in heavy-duty diesel engine. *Gazi Uni. J. Sci.*, **23**: 493–499.

FAILURE ANALYSIS OF A MAIN WHEEL BRAKE ASSEMBLY OF A ROYAL MALAYSIAN ARMED FORCES (RMAF) AIRCRAFT

Syed Roslee Sayd Bakar* & Mohd Yazid Ahmad

Mechanical & Aerospace Technology Division (BTJA), Science Technology Research Institute for Defence, (STRIDE), Selangor, Malaysia

*Email: syroslee.sybakar@stride.gov.my

ABSTRACT

This paper presents the failure analysis of a broken main wheel brake assembly of a Royal Malaysian Armed Forces (RMAF) aircraft. The analyses performed included visual and macroscopic observations, together with fractographic and chemical composition analyses. Based on the analyses conducted, shrinkage porosities and intergranular crack propagation along the dendrite boundaries were revealed. Scanning electron microscope (SEM) analysis found a number of voids in between the dendrite arms as evidence of shrinkage porosities that lead to material separation and crack propagation before the component fractured. It was concluded that service life and environmental factors caused the crack to initiate from the porosities, which propagated intergranularly and created connections between each other. This activity weakened the structure of the composition and hence, the fracture occurred once the crack propagation exceeded its critical limit.

Keywords: *Failure analysis*; *aluminium cast; shrinkage porosity; dendritic microstructure; hardness test.*

1. INTRODUCTION

Metallurgical failure analysis is a scientific process in which a failed component is analysed to determine the cause of failure. It also suggests corrective actions to prevent such failures from occurring in the future (Findlay & Harrison, 2002). The failure analysis process usually involves visual examination, photo-documentation, and macroscopic and microscopic examinations, supported by hardness test and chemical composition analysis (Craig, 2010). According to McMullan (2006), modern equipment with skilled and experienced specialists is essential in evaluating and interpreting the final results. Without proper equipment, such as scanning electron microscope coupled with energy dispersive X-ray (SEM-EDX), failures cannot not be easily determined (Danilatos, 1990; McCoy, 2004). Metallurgical failure analysis is also supported by several mechanical evaluations conducted on the failed component to verify the compliance of its mechanical properties with the specifications and technical requirements (Li *et al*., 2013).

This paper presents the failure analysis of a broken main wheel brake assembly obtained from the starboard side of a Royal Malaysian Armed Forces (RMAF) aircraft. The brake housing assembly was installed on the aircraft in February 2007, with a total number of 1,543 landings recorded until the date of failure (2010). Prior to the incident, the related aircraft parts, including the main brake assembly, brake wear, wheel clearance, brake system pipeline, hoses, self-sealing couplings, valves and brake fluid level, had gone through scheduled visual inspection with the reported status as in good condition.

2. MACROSCOPIC AND MICROSCOPIC EXAMINATIONS

Visual examination of the received failed brake housing assembly found that it was broken into two pieces, as shown in Figure 1. The crack was believed to have initiated from the centre nut holes (dotted circle), and

propagated towards the left and right sides (arrows). An abraded mark can also be seen at the lower side of the assembly. The close-up view of the fracture surface (Figure 2) revealed a black abraded mark at the edge of fracture surface adjacent to the brake pad.

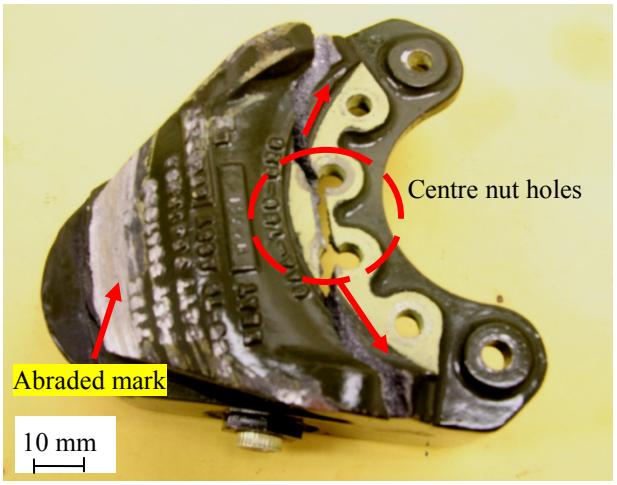

Figure 1: Broken brake assembly of the RMAF aircraft.

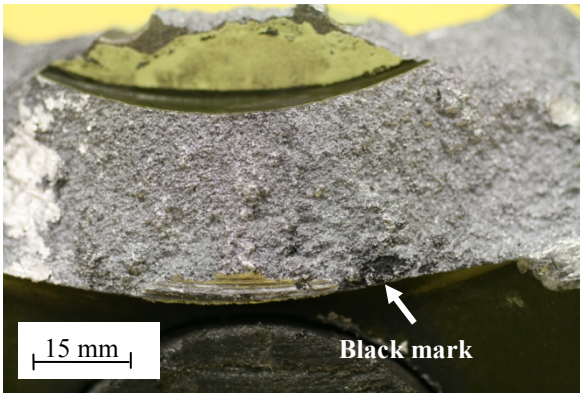

Figure 2: A black mark found on the fracture surface.

Examination of the fracture surface was carried out using a stereomicroscope at 3x and 5x magnification. Further examination of the black mark region revealed a pattern of semi-circle lines (dotted lines) adjacent to the suggested crack initiation point as indicated by the arrow shown in Figure 3. The rest of the fracture surface was difficult to examine at the macroscopic level and hence, further analysis using SEM was required to determine the mode of the failure.

The failed brake assembly was sectioned at the black mark region using a diamond blade cutter and was prepared for metallographic examination. The sample was then mounted with Bakelite powder, before undergoing grinding, polishing and etching processes with Keller's reagent for about 20 s to reveal its microstructures. Typical aluminium cast microstructures and shrinkages porosities (voids) were revealed adjacent to the fracture origin as shown in Figures 4 and 5. Both figures also show an intergranular crack propagation along the dendrite boundaries, which was connected to porosities in the microstructure.

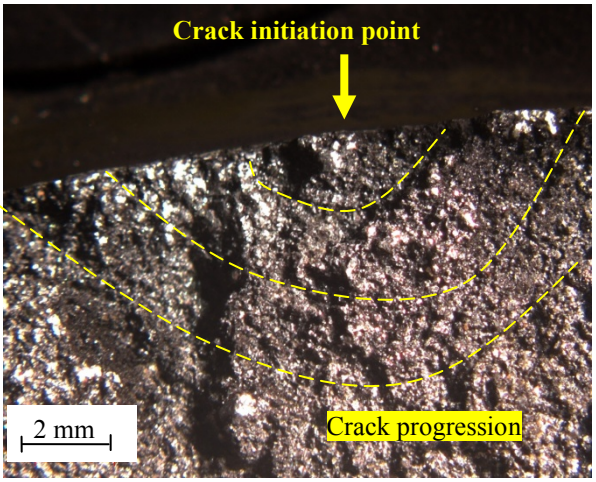

Figure 3: The arrow indicates the initiation point of failure, while the semi-circles (dotted lines) indicate fatigue failure mode.

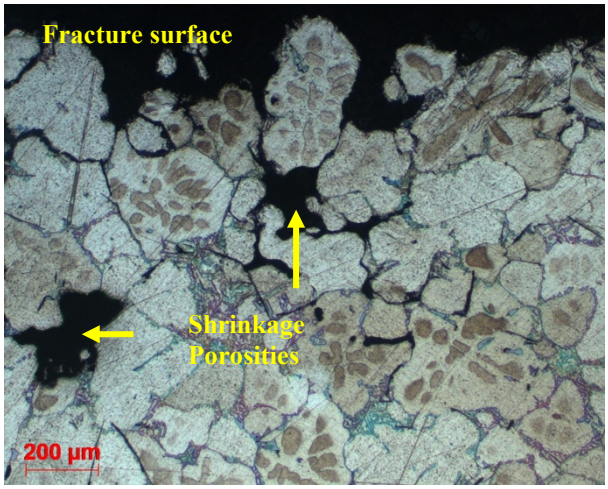

Figure 4: Dendritic microstructure and shrinkage porosities of the fractured brake assembly adjacent to the fracture surface.

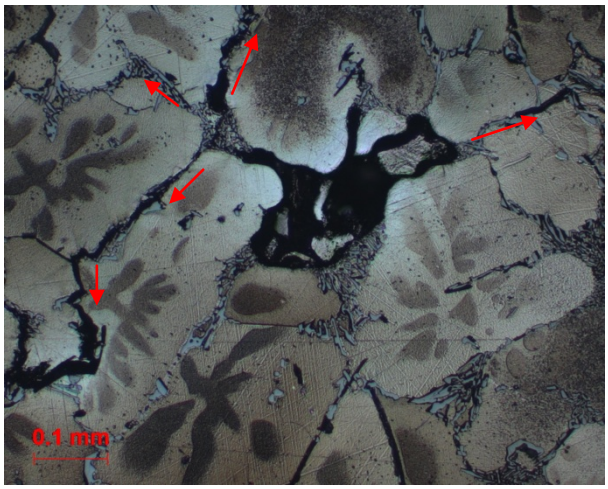

Figure 5: Intergranular crack propagation (arrows) along the dendritic microstructure initiated from the shrinkage porosity of the fractured brake assembly.

3. FRACTOGRAPHIC AND CHEMICAL COMPOSITION ANALYSES

SEM was used to examine the black mark region of the fracture surface. A numbers of shrinkage porosities were found in between the dendrite arms, with the nearest distance of porosities measured from the coating layer being approximately 250 µm, as shown in Figures 6 and 7. A Rockwell 2000 hardness tester was used to measure the hardness of the brake assembly, with the average hardness result obtained being 85.30 HRB.

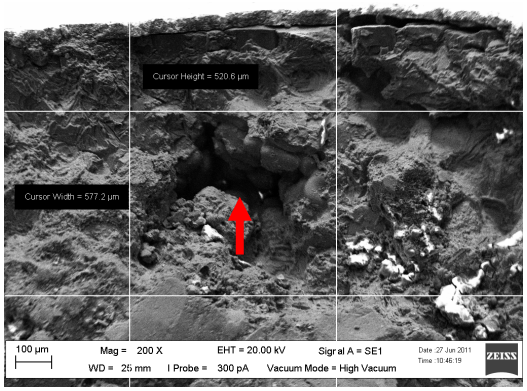

Figure 6: SEM image showing the suspected fractured origin void, located approximately 250 µm from the component's external surface.

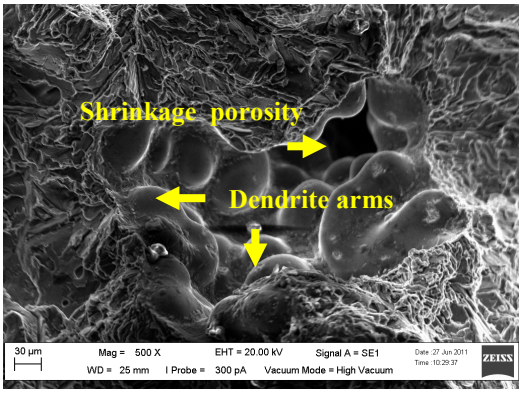

Figure 7: SEM image showing the separated shrinkage porosity on the fracture surface in between of the dendrite arms spacing.

A Shimadzu 720 energy dispersive X-ray fluorescence spectrometer (EDS) was used to analyse the material of the brake housing. The brake housing was sectioned into a portion with size of approximately 10 x 10 mm with 15 mm thickness and was then placed in the sample chamber for elemental detection. The results obtained are shown in Table 1.

Table 1: Results of chemical composition analysis of the failed brake housing.

Chemical Composition (wt.%)	
Silicon (Si)	4.5
Iron (Fe)	0.4
Copper (Cu)	2.0
Sulphur (S)	0.8
Titanium (Ti)	0.4
Tantalum (Ta)	0.2
Aluminium (Al)	Balance

4. DISCUSSION

From the visual examination conducted, it was found that the failed brake assembly had fractured into two pieces across the centre nut holes, which was predicted as the weakest point of the structure due to the component's configuration and design. The chemical composition analysis results showed that the brake assembly was made of cast aluminium alloy with silicon as the major alloying element, which has good castability and corrosion resistance, light weight, and high strength (Ramasamy, 2002; Degarmo *et al*., 2003). Based on the results obtained, the brake assembly was believed to be made of silicon grade cast aluminium alloy, with the nearest grade being A443. The results of the hardness test showed typical hardness for aluminium casting (Anirudh & Deepak, 2012).

Microscopic examination using SEM showed that the brake housing failed due to metal defect. The black mark found on the fracture surface indicated that the component was already defected (micro-cracks) near the surface. The dust produced from the brake pad and dirt from the environment was found accumulated in the crack. The microstructure of the brake housing revealed a dendritic microstructure of typical cast material (Nowotnik *et al*., 2007). The shrinkage porosities found in between the dendrite arms were a typical defect in the metal casting during the solidification process (Peter & Robert, 1986; Donald & Pradeep, 2006). Due to high usage, environment and porosity factors under normal loading conditions, a crack started to develop from the porosities near the surface and propagated intergranularly, connecting one void to another void, and thus, weakening the microstructure, resulting in the failure.

5. CONCLUSION

It was believed that the failure of the main wheel brake assembly happened during the normal landing process due to aircraft loading when the crack propagation exceeded the critical limit. In order to avoid / prevent recurrences of the incident, it is recommended that nondestructive inspection (NDI) should be performed instead of visual inspection for the affected component, including hidden parts in the assembly.

ACKNOWLEDGEMENT

The authors would like to thank the Science and Technology Research Institute for Defence (STRIDE) for providing research facilities and are thankful to the supporting technical staff of the Structural Mechanics Branch for their assistance and cooperation in completing this work. The authors also acknowledge the RMAF for providing materials, information, support and useful discussions.

REFERENCES

Anirudh, B. & Deepak, B. (2012). Mechanical properties of silicon based aluminium alloy 22.92. *VSRD Int. J. Mech. Automob. Prod. Eng.*, **2**: 313-319.

Danilatos, G.D. (1990). Theory of the gaseous detector device in the ESEM. *Adv. Electron. Physics*, **78**: 1–10.

Degarmo, E.P., Black, J.T. & Kohser, R.A. (2003). *Material Processes Manufacturing, 9th Ed*. Wiley, New York.

Donald, R. A. & Pradeep, P. P. (2006). *The Science and Engineering of Materials, 5th Ed*. Thomson, New York.

Findlay, S.J. & Harrison, N.D. (2002). Why aircraft fail. *Mater. Today,* **5**: 18-25.

Jack, A.C. (1993). *Failure of Materials in Mechanical Design: Analysis, Prediction, Prevention, 2nd Ed*. John Wiley & Sons, New York.

McCoy, R. A. (2004). SEM fractography and failure analysis of nonmetallic materials. *J. Failure Anal. Prevention,* **4**: 58-64.

Li, Y.D., Liu, C.B., Xu, N., Wu, X.F., Guo, W.M. & Shi, J.B. (2013). A failure study of the railway rail serviced for heavy cargo trains. *Case Stud. Eng. Failure Anal.*, **1**:4: 243–248.

McMullan, D. (2006). Scanning electron microscopy 1928–1965. *Scanning,* **17**: 175-185.

Nowotnik, G.M., Sieniawski, J. & Wierzbinska, M. (2007). Analysis of intermetallic particles in AlSi1MgMn aluminium alloys. *J. Achieve. Mec. Met. Eng.,* **20**:1-2.

Peter, S.P. & Robert, P.W. (1986). *Metals Handbook. Vol. 11: Failure Analysis and Prevention*. ASM International, Materials Park, Ohio.

Ramasamy, S. (2002). Drawn arc aluminum stud welding for automotive applications. *J.Mater. Process. Tech.,* **54**: 44-46.

FATIGUE LIFE PREDICTION OF AA 7075-T6 UNDER SPECTRUM LOADING USING FINITE ELEMENT ANALYSIS (FEA) SIMULATION

Fadzli Ibrahim[1*], Masliza Mustafar[1], Shamsiah Kalil[1], Mohd Yazid Ahmad[1] & Mohd Norhasani Abdullah Sani[2]

[1]Mechanical and Aerospace Technology Division, Science and Technology Research Institute for Defence (STRIDE), Ministry of Defence, Malaysia
[2]Automated Design Xpress Sdn. Bhd. (ADeX)

[*]Email: fadzli.ibrahim@stride.gov.my

ABSTRACT

This paper presents a study on fatigue life prediction of an aluminium alloy (AA) 7075-T6 coupon using finite element analysis (FEA) simulation. The design part represented a wing lug component of a Royal Malaysian Air Force (RMAF) training aircraft. Linear static analysis indicated that the coupon material could withstand a maximum force of 70 kN with deformation of 1.22 mm before yielding. Then, by applying the most severe condition of real spectrum loading from the aircraft, fatigue analysis demonstrated that the coupon could survive until fatigue life of 3.0 x 10^7 cycles without considering any mean stress correction, and surface treatment or finishing. Finally, optimisation analysis proved that stress correction using the Gerber equation provided significantly better results than the Goodman equation. It was found that the material using polished surface finishing and nitrided surface treatment provided the best fatigue life result.

Keywords: *Fatigue life prediction; aluminium alloy (AA) 7075-T6; finite element analysis (FEA); linear static, fatigue life and optimisation analyses; mean stress correction, and surface finishing and treatment.*

1. INTRODUCTION

Fatigue life prediction has been one of the most important issues in failure analysis since the first half of the nineteenth century (Suresh, 2006). The investigation of fatigue life is essential for reliable life prediction of critical engineering components, such as aircraft and automotive parts. Over the past three decades, various models have been developed to correlate fatigue life and crack growth under variable loading conditions (Beden *et al*., 2010; Newman Jr *et al*., 2014).

Finite element analysis (FEA) is used as an additional tool to traditional methods for fatigue life prediction using mechanical dynamic machines. This method has become more significant in recent years as mathematical solutions can be obtained by using this method for even very complex stress problems (Roylance, 2001). The design is analysed for specific stresses in order to verify whether it can perform under the required specifications prior to construction or manufacturing. The solid bodies of the material are discretised using FEA into small and finite volumes known as finite elements, where elasticity principles can be easily applied. Its procedure requires a pre-processing operation that converts a computer aided design (CAD) model into a discretised form of mesh which contains various equations. The mesh is then computed by a solver, with the results obtained interpreted by a post-processing unit (Zienkiewicz *et al*., 2005; Rao, 2010).

This paper presents a study fatigue life prediction of an aluminium alloy (AA) 7075-T6 coupon using FEA simulation. This material is used in a wing lug component of a Royal Malaysian Air Force

(RMAF) training aircraft. AA 7075-T6 is widely used in the aerospace industry as it provides high yield strength and low density characteristics (Shigley & Mischke, 1989; Mac Donald, 2007; Zhao & Frankel, 2007). Furthermore, its high corrosion resistance is crucial for a number of aircraft and aerospace structure applications (Lee *et al*., 2000; Oskoiei & Ibrahim, 2011; Rafi *et al*., 2010; Zakaria *et al*., 2013). The properties of the material are shown in Table 1.

Table 1: Material properties of the AA 7075-T6.
(Source: Hibler, 2005)

Properties	Value
Modulus of elasticity	71.1 GPa
Poisson ratio	0.33
Maximum yield strength	565 MPa
Ultimate tensile strength	572 MPa

The objectives of this study are:

a) To determine the maximum forces that can be applied to the component before it yields
b) To determine the fatigue life of the component under the most severe spectrum loading
c) To determine the configuration of mean stress correction, and surface finish and treatment that produces the best fatigue life using optimisation function.

2. METHODOLOGY

This study contains two major parts, which are linear static analysis and fatigue life prediction. Using the standard dimensions, the design of the coupon is modelled in the UGS NX 6.0 CAD software. The model is then analysed using the MSC Patran-Nastran analysis software for static analysis, and MSC Fatigue for fatigue life and optimisation analyses.

MSC Patran is used in this study as a pre- / post- processing software since it is the most common software that provides meshing on solid modelling. It provides analysis setup tools that simplify the analysis of ready-made models for MSC Nastran, which is an FEA solver (Ibrahim & Toha, 2012; MSC, 2013). This solver is designed to simulate the stress and dynamic loadings of the model. The finalised model which has been applied with designated loadings will then be analysed using MSC Fatigue. This solver is used to analyse and simulate the fatigue life of the model, which is better known as fatigue life prediction analysis. It is also used to perform optimisation analysis. The combination of these modules gives satisfactorily precise results to estimate the performance of products (MSC, 2013).

2.1 Model Design

Figure 1 shows the model of the coupon designed using UGS NX 6.0. The coupon is designed based on the Metals Test Methods and Analytical Procedures (ASTM, 2009), with thickness of 10 mm. As this investigation is only focused on normal fatigue life prediction without considering any fatigue crack initiation and propagation, notches are not placed on the material, even though practical engineering structures contain some notches (Sun & Shang, 2010).

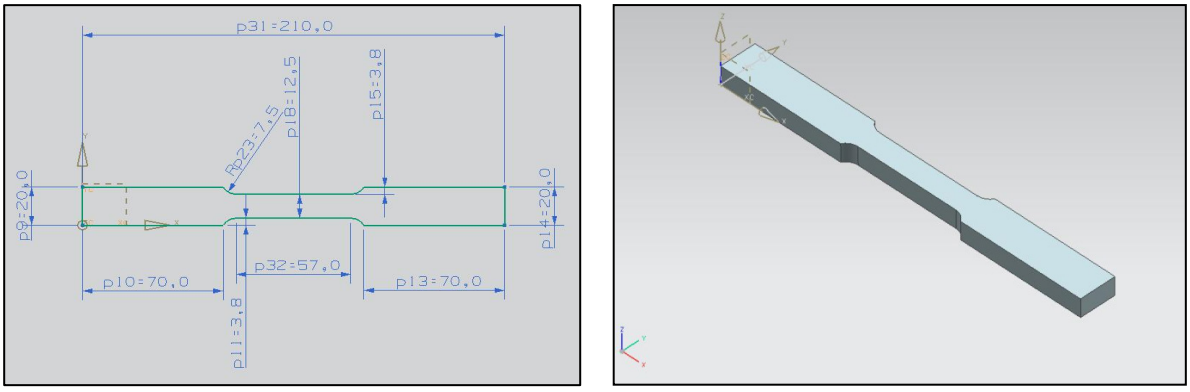

(a) (b)

Figure 1: Design of the coupon using UGS NX 6.0: (a) 2D drawing with the dimensions (b) 3D model.

2.2 FEA Simulation

The coupon is modelled as a linear elastic and isotropic material, and is identified as a solid element. The model is then exported into MSC Patran-Nastran for static analysis, and MSC Fatigue for fatigue life and optimisation analyses. Figure 2 shows that the mesh generated using the software and the boundary conditions determined as a replicate to the real situation that the structure experiences during its operation. Using the tetmesh configuration, the model generates 156 nodes and 372 elements. Then, one end of the model is fixed with constraints in all direction to simulate the clamp condition during testing, while the other end is applied with force which replicates a normal tensile test for static analysis.

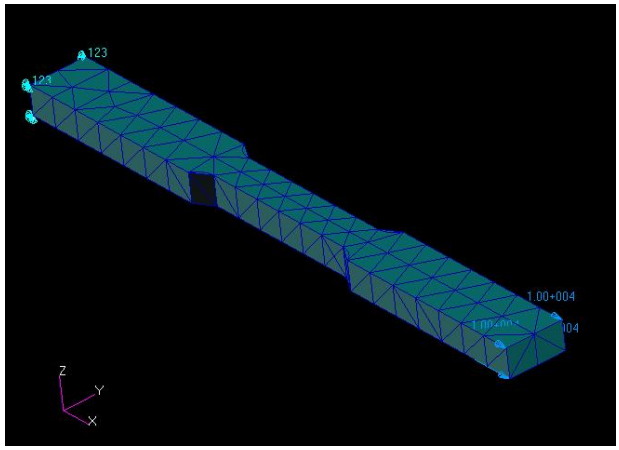

Figure 2: Boundary conditions and meshing configuration for the coupon.

2.2.1 Linear Static Analysis

Static analysis is performed in order to calculate the maximum load before the material starts to yield and break. The most suitable theory to be used for this ductile material is the distortion-energy theory, which is also known as the Von-Mises theory (Shigley & Mischke, 1989; Suresh, 2006). Von-Mises stress σ' is calculated as follows:

$$\sigma' = \sqrt{\left\{(\sigma_1 - \sigma_2)^2 + (\sigma_2 - \sigma_3)^2 + (\sigma_1 - \sigma_3)^2\right\}/2} \quad (1)$$

where σ_1, σ_2 and σ_3 are the principal stresses associated with the three principal directions, which are the x, y and z axes (Jafari *et al*., 2006).

2.2.2 Fatigue Life Analysis

Since the wing lug material of the aircraft experiences low-amplitude cyclic stress that induces primarily elastic deformation in a component designed for long life, it can be considered as having high cycle fatigue life. Hence, the best analysis method to be used is the stress-life approach, where the effects of stress concentrations, mean stresses and types of loading need to be considered. For the initial setup, mean stress correction, and surface finishing and treatment are not considered in determining the results.

Using the stress result from the static analysis as the input, fatigue life analysis was conducted using MSC Fatigue. This module requires three particular inputs; stress values of the coupon model from the linear static analysis, material properties of the coupon and the loading profile. For this study, the spectrum loading data is extracted from the flight data recorder (FDR) of the aircraft. This sensor records all the spectrum loading data of the aircraft during operation, which was later exported into MSC Fatigue. Figure 3 shows the spectrum loading data taken from a RMAF training aircraft for a period of 2,040 s (1 point per s). This data is considered as the most severe loading data for the aircraft's life and can be assumed to be similar for along the analysis life. Finally, with all three inputs complete, fatigue life analysis was conducted.

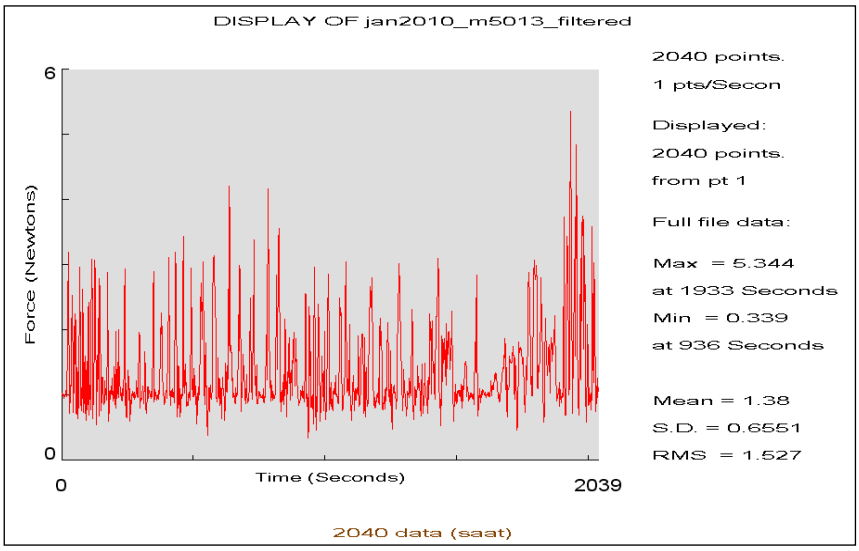

Figure 3: Real spectrum loading data from the aircraft.

2.2.3 Optimisation Analysis

After the fatigue life analysis was completed, MSC Fatigue's optimisation function is used to investigate the effects of mean stress correction, and surface finishing and treatment on fatigue life. This analysis is performed to scrutinise alternative configurations to extend the fatigue life of the material.

The two most common equations for mean stress correction are the Goodman (Equation 2) and Gerber (Equation 3) equations (Suresh, 2006):

$$\sigma_a = \sigma_{a|\sigma_m=0}\left\{1-\left(\sigma_m/\sigma_{TS}\right)\right\} \quad (2)$$

$$\sigma_a = \sigma_{a|\sigma_m=0}\left\{1-\left(\sigma_m/\sigma_{TS}\right)^2\right\} \quad (3)$$

where $\sigma_{a|\sigma m=0}$ is the stress amplitude (for a fixed life) for fully-reversed loading and σ_{TS} is the tensile strength of the material.

The manner in which a surface is prepared during the manufacturing process has important effect on fatigue life, with different types of material preparations giving different results of fatigue life. (Suresh, 2006). To this end, the solver offers different types of surface finishing and treatment for the optimisation analysis. The options given are based on common material preparations in real physical fatigue testing. The options given for surface finishing are polished, ground, machined (good, average and poor), hot rolled, forged, cast, and exposure to normal water and seawater. The options given for surface treatment are nitrided, cold rolled and shot peened.

3. RESULTS AND DISCUSSION

3.1 Linear Static Analysis

The results of the FEA simulation conducted on the material model show that the maximum force that the structure can withstand before yielding is 70 kN with maximum deformation of 1.22 mm, with the red portion in Figure 4 representing the area of maximum stress and deformation. As maximum deformation dramatically increases with increment of force (Suripa & Chaikittiratana, 2008), stress increment is always associated with a given strain increment (Mingzhou *et al*., 2002). In a situation where the load applied to the coupon is greater than these two important parameters, the structure would deform permanently or even break (Xu *et al*., 2007).

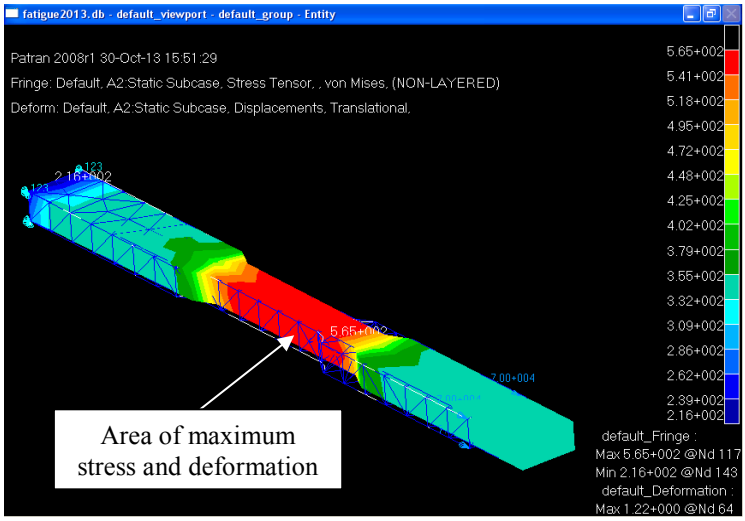

Figure 4: Stress analysis result for maximum stress and deformation at the yield point.

For simple verification, this maximum stress σ_{max} is computed as:

$$\sigma_{\max} = P / A \tag{4}$$

where P is the maximum force that is exerted during yielding (Equation 5) and A is model's area (which in this case is 125 mm).

$$\begin{aligned} P &= \sigma_{max} \text{ x } A \\ &= 565 \text{ x } 125 \\ &= 70.625 \text{ kN} \end{aligned} \tag{5}$$

Based on this calculation, the simulation's result of 70 kN is just less than 1% of the manually calculated force.

3.2 Fatigue Life Analysis

Fatigue life analysis is carried out in order to determine the maximum life of the structure before it fails and the location where it will fail. The result of the FEA simulation for fatigue life prediction is shown in Figure 5. The maximum fatigue life for the structure is 3.0 x 10^7 cycles and the area of failure is, as expected, at the mid-section of the coupon. The failure occurred at this section because it experienced the highest stress as compared to other sections. This failure result is for the analysis without any mean stress correction, or surface finishing and treatment. This indicates the general result of the failure mode for a very general configuration.

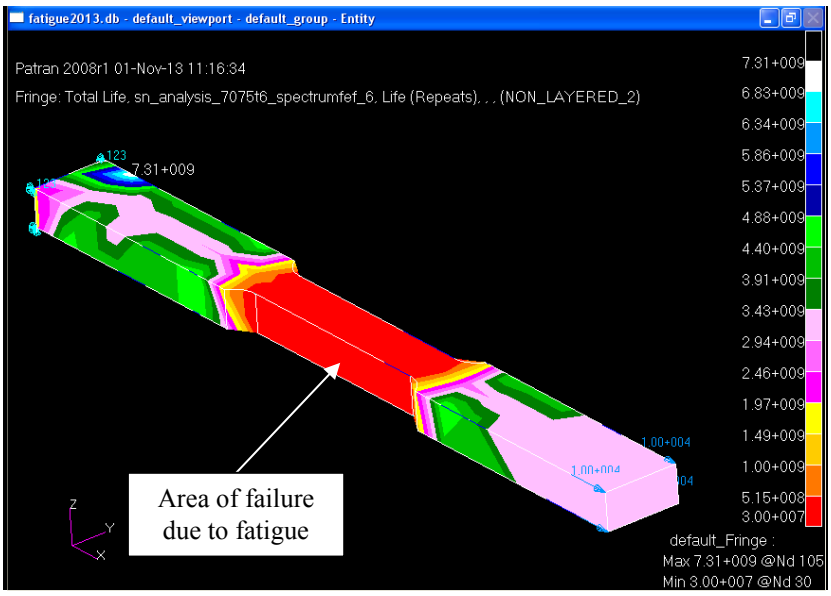

Figure 5: Location where the fatigue failure occurs when the maximum force is applied.

3.2 Optimisation Analysis

The results of the optimisation analysis are shown in Tables 2 to 4. Table 2 shows that the fatigue life of the material using the Gerber equation (Equation 3) is significantly better than using the Goodman equation (Equation 4), as the former provides larger stress amplitude (Suresh, 2006).

Table 2: Fatigue life of the material for different types of mean stress correction.

Mean stress correction	Fatigue life (cycles)
None	3.00×10^7
Gerber	5.12×10^6
Goodman	1.86×10^5

Table 3 shows the fatigue life for the coupon for various surface finishing methods. The results show that the best fatigue life occurred for the polished surface, which removes microscopic notches that can cause stress concentration. The worst fatigue life occurred for exposure to seawater, which has higher corrosion effect.

Table 3: Fatigue life of the material for different types of surface finishing methods.

Surface finish	Factor	Fatigue life (cycles)
Polished	1.0	3.00×10^7
Ground	0.9123	1.24×10^7
Good machined	0.8437	5.87×10^6
Average machined	0.7759	2.62×10^6
Poor machined	0.7228	1.33×10^6
Hot rolled	0.6231	4.15×10^5
Forged	0.4631	7.63×10^4
Cast	0.4472	6.49×10^4
Water	0.5038	1.15×10^5
Seawater	0.3516	20969

Table 4 shows the fatigue life of the material for different types of surface treatment. The material with nitrided surface treatment gave better fatigue life as compared to other surface treatments. This is because the nitriding process produces compressive stresses in the diffusion region that cause the material to be hardened (Suresh, 2006).

Table 4: Fatigue life of the material for different types of surface treatments.

Surface treatment	Factor	Fatigue life (cycles)
None	1.0	3.00×10^7
Nitrided	2.0	2.32×10^{10}
Cold rolled	1.5	1.47×10^9
Shot peened	1.15	1.15×10^8

4. CONCLUSION

This paper presented the fatigue analysis of AA 7075-T6 which is used in a wing lug component of a RMAF training aircraft via FEA simulation. Static analysis indicated that the coupon material could withstand a maximum force of 70 kN with 1.22 mm deformation before it yielded. Fatigue life analysis demonstrated that the coupon material can achieve fatigue life of 3.0 x 10^7 cycles without considering any mean stress correction, or surface treatment and finishing. Finally, optimisation analysis proved that stress correction using the Gerber equation provided significantly better results than the Goodman equation. It was found that the material using polished surface finishing and nitrided surface treatment provided the best fatigue life result.

The outcomes of the FEA simulations conducted in this study only identified the maximum force as well as the fatigue life cycle when the load is applied to the structure. This simulation results will benefit researchers by saving time and cost instead of physical testing on fabricated coupons using mechanical dynamic testing machines. Although these results are considerably correct by assuming that all the parameters given represent the real situation, further experimental investigations to validate the findings of the FEA simulations are required. This validation process between FEA simulations and laboratory coupon testing will give higher a confidence level in contributing to the decision on prediction of fatigue life of aircrafts.

REFERENCES

American Society for Testing and Materials (ASTM) (2009). *3.01: 66 - Metals Test Methods and Analytical Procedures*. American Society for Testing and Materials (ASTM), West Conshohocken, Pennsylvania.

Beden, S.M., Abdullah, S., Ariffin, A.K. & Al-Asady, N.A. (2010). Fatigue crack growth simulation of aluminium alloy under spectrum loadings. *Mater. Design*, **31**: 3449-3456.

Garino, C.G., Gabaldon, F. & Goicolea, J.M. (2006). Finite element simulation of the simple tension test metals. *Finite Elem. Anal. Des.,* **42**: 1187-1197

George, S.B., Henry, R.C. & John, A.V. (2002). *Materials Handbook, 15th Edition*. McGraw Hill Companies, New York.

Hibler, R.C., (2005). *Mechanic of Materials*. Prentice Hall, New York.

Ibrahim, F. & Toha, M.S. (2012). Finite element analysis (FEA) of a C130 towing bar. *Defence S&T Tech. Bull*., **5**: 159-166.

Jafari, A., Khanali, M., Mobli, H. & Rajabipour, A. (2006). Stress analysis of front axle of JD 955 combine harvester under static loading. *J. Agr. Soc. Sci.*, **2**: 133- 135.

Lee, W.S., Sue, W.C., Lin, C.F. & Wu, C.J. (2000). The strain rate and temperature dependence of the dynamic impact properties of 7075 aluminium alloy. *J. Mater. Process. Tech.,* **100**: 116–122.

Mac Donald, B.J., (2007). *Practical Stress Analysis with Finite Elements.* Glasnevin, Dublin.

Mingzhou, S., Qiang, G. & Bing, G. (2002). Finite element analysis of steel members under cyclic loading. *Finite Elem. Anal. Des.*, **39**: 43–54

MacNeal-Schwendler Corporation, MSC (2013). *Patran: Complete FEA Modeling Solution*. Available online at: http://www.mscsoftware.com/en-asean/product/patran (Last access date: 12 December 2013).

Newman Jr., J.C., Anagnostou, E.L. & Rusk, D. (2014). Fatigue and Crack-growth analyses on 7075-T651 aluminum alloy coupons under constant- and variable-amplitude loading. *Int. J. Fatigue,* In press.

Oskoiei, R.H. & Ibrahim, R.N. (2011). The effect of typical flight temperatures on the fatigue behaviour of Al 7075-T6 clamped plates. *Mater. Sci. Eng. A-Struct.,* **528**: 1527-1533.

Rafi, H.K., Ram, G.D.J., Phanikumar, G. & Rao, K.P. (2010). Microstructure and tensile properties of friction welded aluminium alloy AA7075-T6. *Mater. Design*, **31**: 2375–2380.

Rao, P.N. (2010). *CAD/CAM Principles and Applications 3rd Edition*. McGraw Hill, New Delhi.

Roylance, D. (2001). *Finite Element Analysis*. Massachusetts Institute of Technology, Cambridge.

Shigley, J.E. & Mischke, C.R. (1989). *Mechanical Engineering Design, 5th Ed.* McGraw Hill Companies, Singapore.

Sun, G.Q. & Shang, D.G. (2010). Prediction of fatigue lifetime under multiaxial cyclic loading using finite element analysis. *Mater. Design*, **31**: 126-133.

Suresh, S. (2006). *Fatigue of Materials 2nd Edition*. Cambridge University Press, New York.

Suripa, U. & Chaikittiratana, A. (2008). Finite element stress and strain analysis of a solid tyre. *J Achieve. Mater. Manuf. Eng.*, **31**: 576-579

Xu, C.G., Liu, G.H., Ren, G.S., Shen, Z., Ma, C.P. & Ren, W.W. (2007). Finite element analysis of axial feed bar rolling. *Acta Metall. Sinica,.* **20**: 463-468

Zakaria, K.A., Abdullah, S. & Ghazali, M.J. (2013). Comparative study of fatigue life behaviour of AA6061 and AA7075 alloys under spectrum loadings. *Mater. Design*, **49**: 48-57.

Zhao, Z. & Frankel, G.S. (2007). On the first breakdown in AA7075-T6. *Corros. Sci.*, **49**: 3064–3088

Zienkiewicz, O.C., Taylor, R.L. & Zhu, J.Z. (2005). *The Finite Element Method: Its Basis & Fundamentals*. Elsevier, Burlington.

ANALYSIS OF SPATIAL SIGNIFICANCE OF MOUNTAIN OBJECTS EXTRACTED FROM MULTISCALE DIGITAL ELEVATION MODELS

Dinesh Sathyamoorthy

Instrumentation & Electronics Technology Division (BTIE), Science & Technology Research Institute for Defence (STRIDE), Ministry of Defence, Malaysia

*E-mail: dinesh.sathyamoorthy@stride.gov.my

ABSTRACT

The derivation of spatial significance is an important aspect of geospatial analysis and hence, various methods have been proposed to compute the spatial significance of entities based on spatial distances with other entities within the cluster. This paper is aimed at studying the spatial significance of mountain objects extracted from multiscale digital elevation models (DEMs). At each scale, the value of spatial significance index SSI of a mountain object is the minimum number of morphological dilation iterations required to occupy all the other mountain objects in the terrain. The mountain object with the lowest value of SSI is the spatially most significant mountain object, indicating that it has the shortest distance to the other mountain objects. It is observed that as the area of the mountain objects reduce with increasing scale, the distances between the mountain objects increase, resulting in increasing values of SSI. The results obtained indicate that the strategic location of a mountain object at the centre of the terrain is more important than its size in determining its reach to other mountain objects and thus, its spatial significance.

Keywords: *Multiscale digital elevation models (DEMs); mountain objects; spatial significance; iterative morphological dilation;geometric proximity and size*.

1. INTRODUCTION

A spatially significant entity can be defined as an entity from which it is easy to reach all of its neighbouring entities (e.g., objects, hotspots, zones). A spatially significant entity has greater geometric proximity to the other entities, and should be at a strategic location and possess a relatively larger size (Anselin, 1992; Câmara & Carvalho, 2002; Chainey, 2010; Sagar *et al*., 2013). The derivation of spatial significance is an important aspect of geospatial analysis and hence, various methods have been proposed to compute the spatial significance of entities based on spatial distances with other entities within the cluster, including kernel density estimation (Silverman, 1986; Schölkopf & Smola, 2002; Feitosa *et al*., 2007), spatial proximity matrix (Ding & Fotheringham, 1992; de Aguiar, 2003), local indicators of spatial association (Anselin, 1995), vulnerable localities index (Chainey, 2008) and local clustering index (Baohua *et al*., 2012). These methods only consider the proximities of the entities, but not their geometric properties.

To this end, Sagar *et al.* (2013) proposed a mathematical morphological based algorithm to compute the spatial significance of entities. The algorithm employed iterative dilations between origin and destination entities to determine the dilation distance. The computed dilation distances are then used to determine the spatial significance index *SSI* of each entity. As the effects of the morphological operations have intuitive interpretations using geometric terms of shape, size and location, the computed values of *SSI* are affected by the entities' boundary points that are furthest out with respect to the other entities. The algorithm was demonstrated using a cluster of water bodies and states in India.

In this paper, the algorithm proposed in Sagar *et al.* (2013) is employed to study the spatial significance of mountain objects extracted from multiscale digital elevation models (DEMs). Scale

variations can constrain the detail with which information can be observed, represented and analysed. The term scale refers to a combination of both spatial extent, and spatial detail or resolution (Tate & Wood, 2001; Li, 2008; Goodchild, 2011; Drăguţ & Eisank, 2011). Changing the scale without first understanding the effects of such an action can result in the representation of patterns or processes that are different from those intended due to loss of detail, and variations in terrain parameters and landforms (Lam et al., 2004; Summerfeld, 2005; Goodchild, 2011; Drăguţ & Eisank, 2011). Hence, feature detection and characterisation often need to be performed at different scales of measurement. Wu *et al.* (2008), Wood (2009), Drăguţ *et al.* (2011) and Poulos *et al.* (2012) demonstrated that analysis of a location at multiple scales allows for a greater amount of information to be extracted from a digital elevation model (DEM) about the spatial characteristics of a feature.

2. COMPUTATION OF SPATIAL SIGNIFICANCE

Mathematical morphology is a branch of image processing that deals with the extraction of image components that are useful for representational and descriptional purposes. It has a well developed mathematical structure that is based on set theoretic concepts. The fundamental morphological operators are discussed in Matheron (1975), Serra (1982), Soille (2003), Najman and Talbot (2010) and Sagar (2013). Morphological operators generally require two inputs; the input image A, which can be in binary or grayscale form, and the kernel B, which is used to determine the precise effect of the operator. Each cell in A is compared with B by moving B so that its centre hits the cell. Depending on the type of morphological operator employed, the cell value is reset to the value or average value of one or more of its neighbours.

Dilation (Equation 1) sets the cell values within the kernel to the maximum value of the cell neighbourhood. Binary dilation gradually enlarges the boundaries of regions of foreground cells, resulting in areas of foreground cells growing in size, and holes within those regions becoming smaller. Dilation can be performed iteratively for n times as in Equation 2.

$$A \oplus B = \{a + b : a \in A, b \in B\} \tag{1}$$

$$A \oplus nB = (A \oplus B) \oplus B \ldots n \text{ iterations} \tag{2}$$

Let a cluster of entities A be consisted of N number of entities denoted as A_1, A_2, A_3, … , A_N. An entity is designated as spatially most significant if its distance to the other entities in the cluster is the shortest. The dilation distance d from an origin entity A_i and a destination entity A_j is minimum number of dilation iterations required for A_i to occupy A_j:

$$d(A_{ij}) = \min\left(n : A_j \subseteq \left(A_i \oplus nB\right)\right) \tag{3}$$

Similarly, the dilation distance from A_j to A_i is computed as follows:

$$d(A_{ji}) = \min\left(n : A_i \subseteq \left(A_j \oplus nB\right)\right) \tag{4}$$

If both A_i and A_j have the same size, shape and orientation, $d(A_{ij}) = d(A_{ji})$. If there is a shape-size dissimilarity between the two entities, $d(A_{ij}) \neq d(A_{ji})$. A smaller entity would require a greater number of dilation iterations to occupy a larger entity and hence, the larger entity would have a smaller dilation distance.

SSI determines the spatial significance on an entity based on the distance from the other entities in the cluster. The lower the value of *SSI* of an entity, the higher is its significance, indicating that it has shorter distance to the other entities. The entity with the lowest value of *SSI* is the spatially most

significant entity. The value of *SSI* for A_i is the minimum number of dilation iterations required for A_i to occupy all the other entities in the cluster, which would be the largest value of $d(A_{ij})$:

$$SSI(A_i) = \max_{\forall j}\left(\min\left(n : \left(A_j \subseteq \left(A_i \oplus nB\right)\right)\right)\right) \quad (5)$$

3. METHODOLOGY

3.1 Dataset

The DEM in Figure 1 shows the area of Great Basin, Nevada, U.S., which is bounded by latitude 38° 15' to 42° N and longitude 118° 30' to 115° 30'W. The DEM was resampled to 925 m in both *x* and *y* directions. It is a Global Digital Elevation Model (GTOPO30) and was downloaded from the USGS GTOPO30 website (GTOPO30, 1996). GTOPO30 DEMs are available at a global scale, providing a digital representation of the Earth's surface at a 30 arc-seconds sampling interval. The land data used to derive GTOPO30 DEMs are obtained from digital terrain elevation data (DTED), 1-degree DEMs for USA and the digital chart of the world (DCW). The accuracy of GTOPO30 DEMs varies by location according to the source data. The DTED and the 1-degree dataset have a vertical accuracy of ±30 m while the absolute accuracy of the DCW vector dataset is ±2,000 m horizontal error and ±650 m vertical error (Miliaresis & Argialas, 2002). Tensional forces on the terrain's crust and thins by normal faulting cause the formation of an array of tipped mountain blocks that are separated from broad plain basins, producing a basin-and-range physiography (Howell, 1995; Summerfield, 1996, 2000; Miliaresis & Argialas, 1999; Miliaresis, 2008).

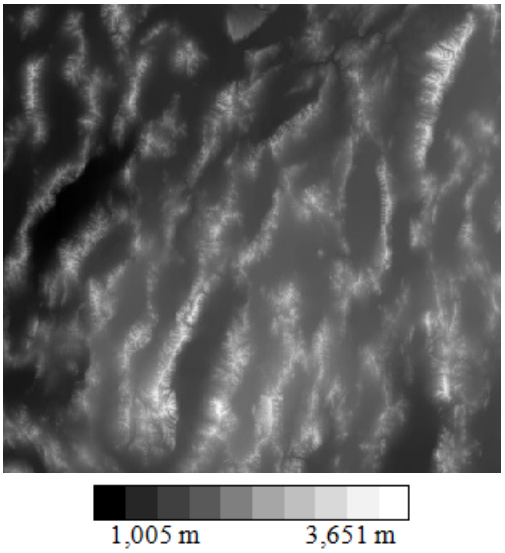

Figure 1: The GTOPO30 DEM of Great Basin. The scale is approximately 1:3,900,000.

3.2 Generation of Multiscale DEMs

In this paper, multiscaling is performed using the lifting scheme (Sweldens, 1996, 1997), which has proven to be a powerful multiscale analysis tool in image and signal processing (Claypoole & Baraniuk 2000, Starck 2002, Guo *et al*. 2008; Abdul-Rahman *et al.*, 2013), and has received recent attention in geospatial analysis (Hayat *et al*., 2008; Bernadin *et al*., 2008; Yang *et al*., 2009; Dinesh *et al.*, 2011; Ahmad Fadzil *et al*., 2011; Chiao *et al.*, 2013). This is due to its ability to preserve accurate surface profiles, in terms of waveform, shape and amplitude, without causing boundary destruction (Jiang *et al.*, 2001a,b; Nonomura *et al.*, 2010). It is used to decompose an original dataset into low and high frequency subsets using the following three steps:

Step 1: Split

The original dataset $x[n]$ is divided into two disjoint subsets, even $x_e[n]$ and odd $x_o[n]$ indexed points.

Step 2: Predict

The odd and even subsets are often highly correlated. As this correlation structure is typically local, one subset can be used to predict the other subset. In this case, the even indexed subset is used to compute a course approximation of the odd indexed subset using the prediction operator P (Equation 6). The predicted odd indexed subset is smoother than the original odd indexed subset, with the high frequency components removed. Hence, the difference between the two subsets gives the high frequency subset $d[n]$ (Equation 7). The even indexed subset is left unchanged to become the input for the next step in the transform.

$$P(x_o[n]) = \frac{1}{2}(x_e[n] + x_e[n+1]) \tag{6}$$

$$d[n] = x_o[n] - P(x_o[n]) \tag{7}$$

Step 3: Update

The update operator U (Equation 8) uses $d[n]$ to compute the difference between the original dataset and its coarse approximation, which consists of the low frequency components of the original dataset. This is then applied to the even indexed subset to obtain the low frequency subset $c[n]$ (Equation 9).

$$U(d[n]) = \frac{1}{4}(d[n-1] + d[n+1]) \tag{8}$$

$$c[n] = x_e[n] + U(d[n]) \tag{9}$$

The above three steps form a lifting stage. Using a DEM as the input, an iteration of the lifting stage generates the complete set of multiscale DEMs $c_s[n]$ and the elevation loss caused by the change of scale $d_s[n]$. At each iteration, $c_s[n]$ only contains half of the points of the input for the iteration, and hence, the resolution of the generated multiscale DEM is reduced by half. At each iteration, the cells of the DEM that are modified are curvatures regions, while the unmodified cells are planar regions. The iterations are repeated until all curvatures in the DEM are removed, leaving only planar regions. For varying DEMs, the number of iterations required would be dependent on the surface profile; a rougher surface profile would require more iterations, while a smoother surface profile would require fewer iterations.

Multiscale DEMs of the Great Basin terrain are generated by implementing the lifting scheme for scales s of 1 to 20. As shown in Figure 2, as the scale increases, the merging of small regions into the surrounding grey level regions increases, causing removal of fine detail in the DEM. As a result, the generated multiscale DEMs possess lower resolutions at higher degrees of scaling.

3.3 Mountain Extraction

Mountains are portions of a terrain that are sufficiently elevated above the surrounding land (greater than 300 up to 600 m) and have comparatively steep sides. In a mountain, two parts are distinctive (Neuendorf, 2005):

1) The summit, the highest point (the peak) or the highest ridges
2) The mountainside, the part of a mountain between the summit and the foot.

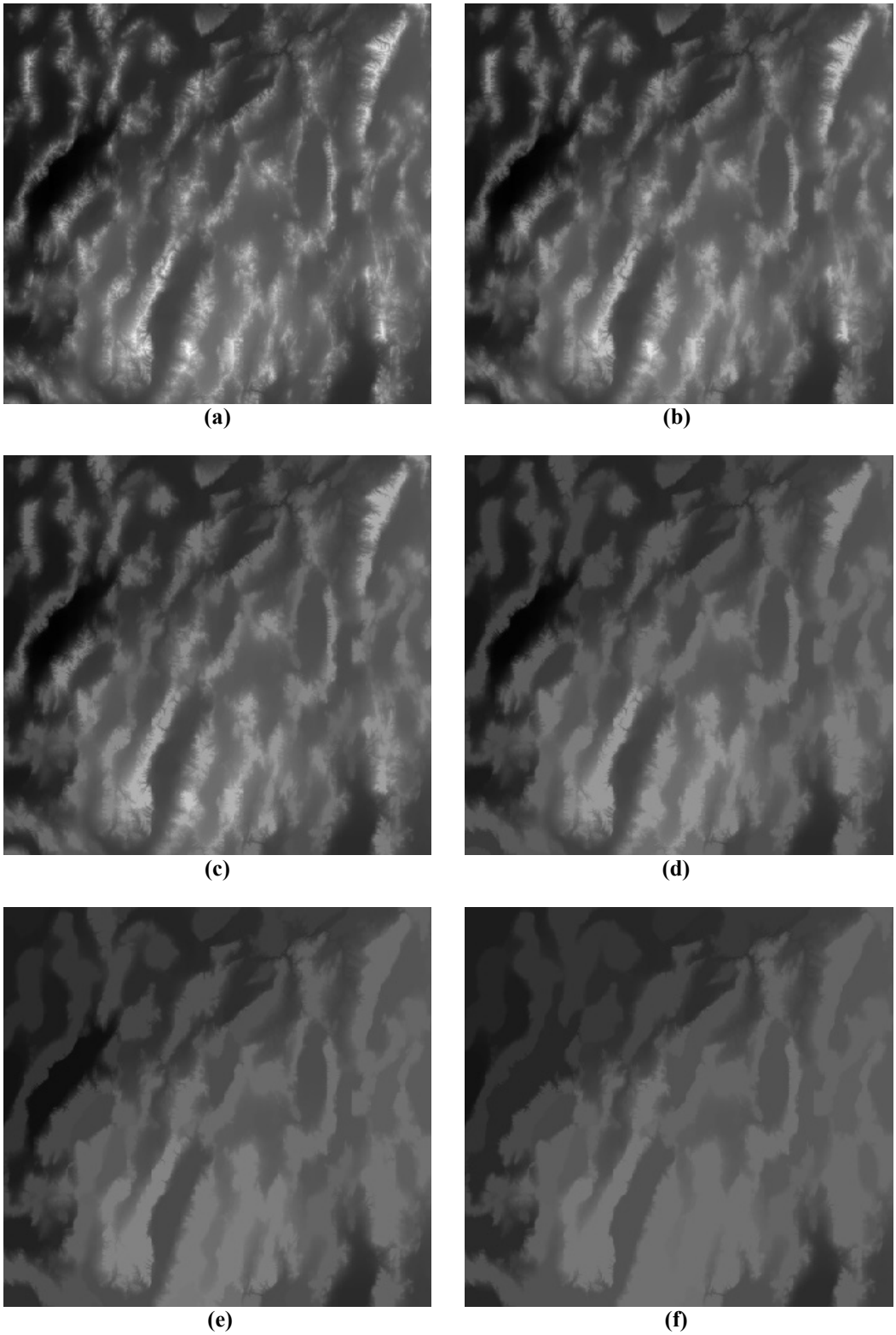

Figure 2: Multiscale DEMs generated using scales of (a) 1 (b) 3 (c) 5 (d) 10 (e) 15 (f) 20.

The mountains of the generated multiscale DEMs are extracted using the mathematical morphological based algorithm proposed in Dinesh (2006). First, ultimate erosion is performed on the DEM to extract the peaks of the DEM. Conditional dilation is performed on the extracted peaks to obtain the mountains of the DEM. As shown in Figure 3, the merge of small regions into the surrounding grey level regions and removal of fine detail in the DEM cause a reduction in the area of the extracted mountains.

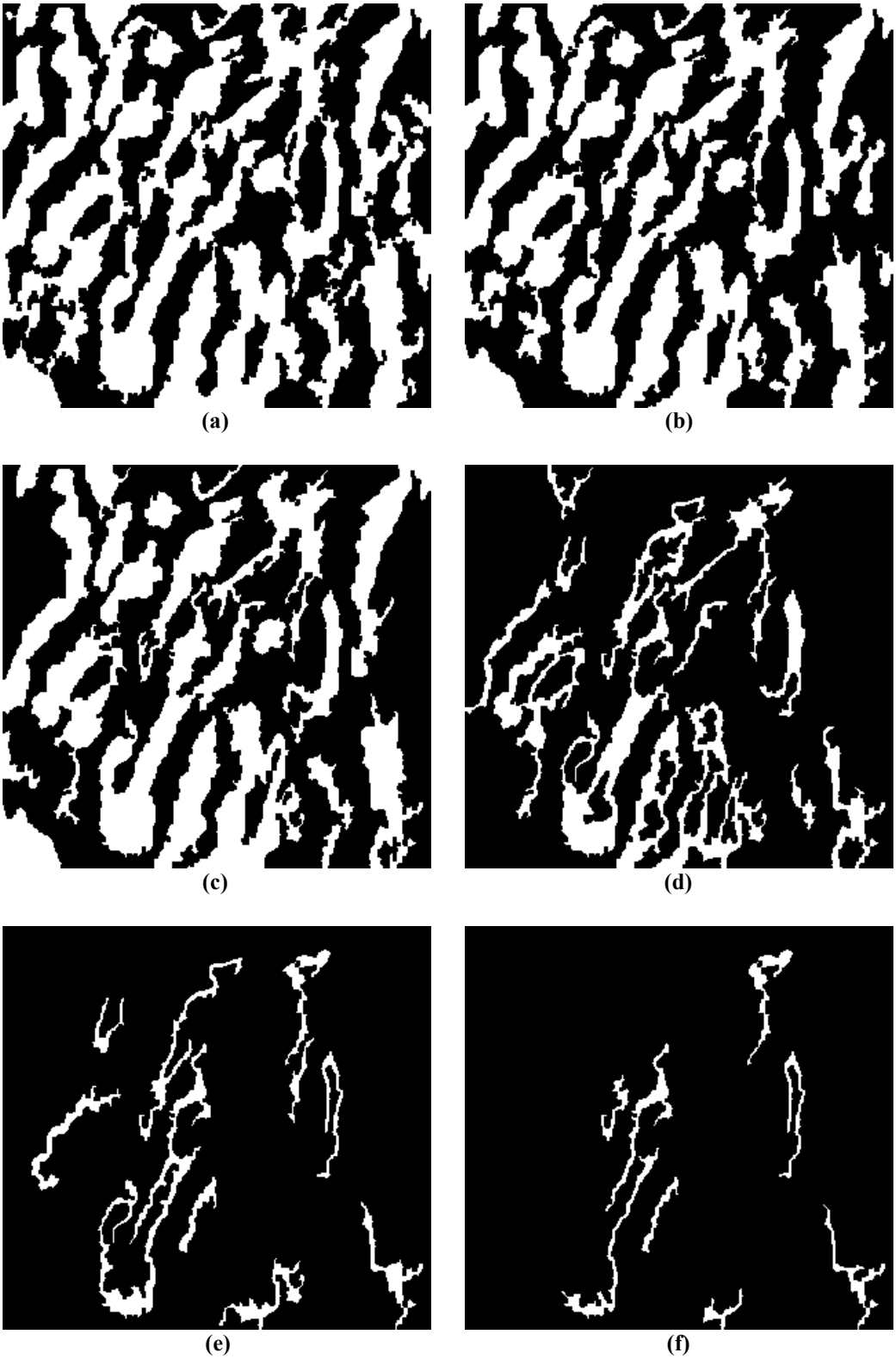

Figure 3: Mountains (the cells in white) extracted from the corresponding multiscale DEMs in Figure 2.

4. RESULTS & DISCUSSION

The computed *SSI* values of the mountain objects extracted from the original DEM (Figure 3(a)) are shown in Table 1. In general, larger mountain objects, which have better reach to the other mountains objects, have lower value of *SSI*, indicating higher significance. The spatially most significant

mountain object, with the lowest value of *SSI*, is mountain object 5 (Figure 4(a)), which is the largest mountain object and is located at the centre of the terrain.

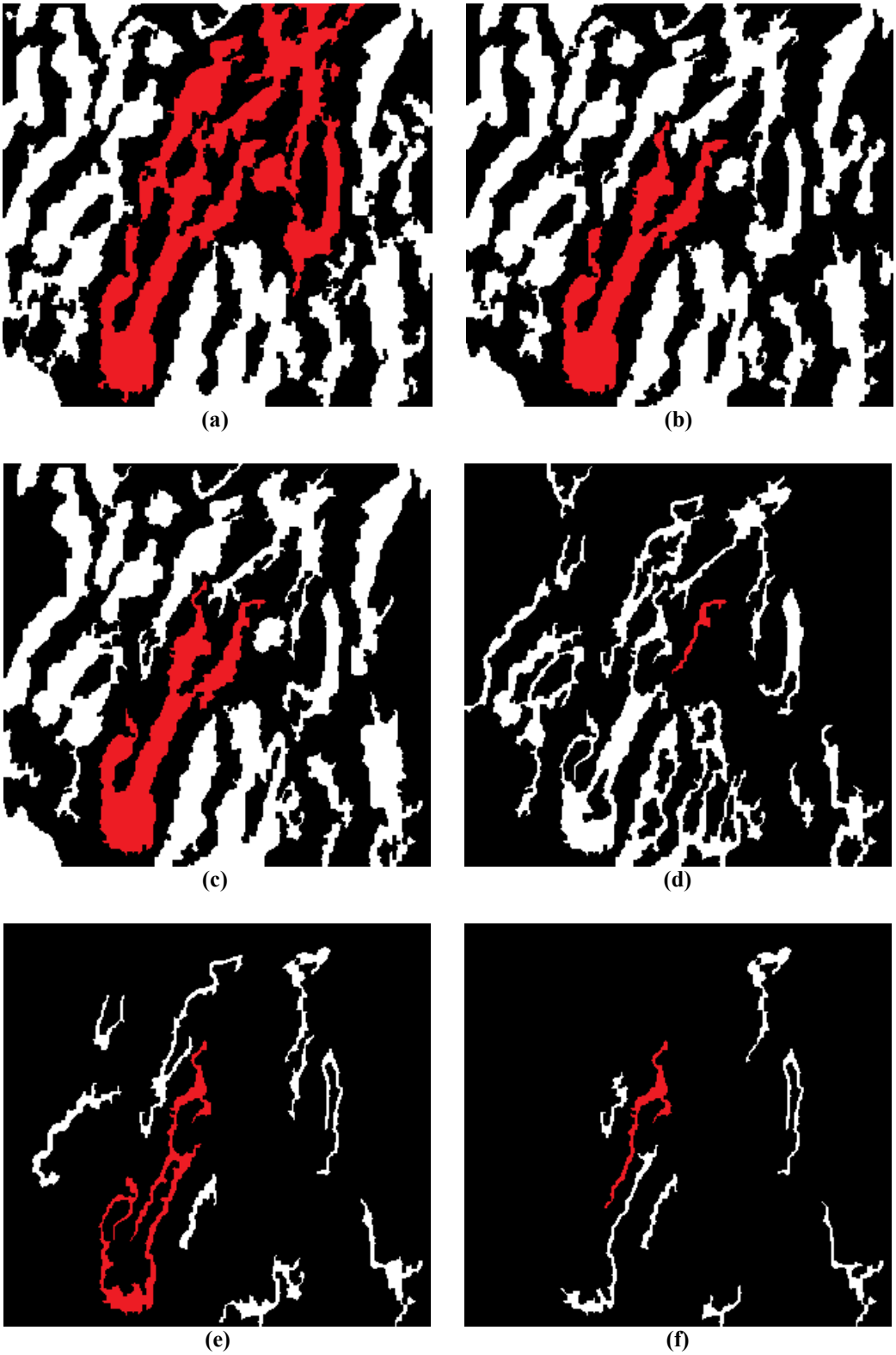

Figure 4: Spatially most significant mountain object of the mountains extracted from the corresponding multiscale DEMs in Figure 2.

Table 1: Computed *SSI* values of the mountain objects extracted from the original DEM.

Label	Area (cells)	SSI
1	1227	281
2	10422	195
3	1353	273
4	298	284
5	14232	106
6	432	246
7	6444	172
8	311	267
9	1119	221
10	219	233
11	3574	247
12	3058	252
13	494	282
14	261	289

The *SSI* values for the spatially most significant mountain objects of the multiscale DEMs (Figure 4) are shown in Table 2. As the area of the mountain objects reduce with increasing scale, the distances between the mountain objects increase, resulting in increasing values of *SSI*. At scales 2 to 7, 9 to 11 and 13 to 20, the corresponding spatially most significant mountain objects have the same values (130, 151 and 154 respectively). In these cases, the spatially most significant mountain objects are objects with corresponding locations, requiring the same minimum number of iterative dilations to reach the boundary points that are furthest out with respect to the objects. This highlights the advantages of iterative dilations in computing *SSI* values as compared to other proximity based algorithms that do not consider the geometric properties of the objects.

Table 2: Spatially most significant mountain object for each scale.

Scale	Num. of objects	Spatially most significant object	Area (cells)	SSI
1	14	5	14232	106
2	20	8	9581	130
3	21	8	5518	130
4	19	7	5350	130
5	19	7	5282	130
6	18	7	5280	130
7	18	7	5040	130
8	19	12	288	145
9	16	12	263	151
10	14	10	263	151
11	14	10	263	151
12	15	11	263	140
13	12	5	2670	154
14	10	3	2599	154
15	10	3	2183	154
16	10	2	2025	154
17	9	2	1946	154
18	8	2	1912	154
19	7	1	1402	154
20	8	3	629	154

For scales 1 to 7 and 13 to 20, smaller mountain objects located at the centre of the terrain are classified as spatially most significant. However, for scales 8 to 12, significantly smaller mountain objects located at the centre of the terrain are classified as spatially most significant. This indicates that the strategic location of a mountain object at the centre of the terrain is more important than its size in determining its reach to other mountain objects and hence, its spatial significance. For example, for scale 10 (Figure 4(d)), the strategic location of mountain object 10 allows it better reach to the other mountain objects as compared to the larger mountain objects (Table 3).

Table 3: Computed SSI values of the mountain objects extracted from the DEM of scale 10.

Label	Area (cells)	SSI
1	571	242
2	1967	218
3	266	253
4	255	217
5	3330	154
6	1298	173
7	1420	182
8	2176	172
9	1152	187
10	263	151
11	221	207
12	803	214
13	229	236
14	1048	260

The results obtained thus far are based on analysis of a mountainous terrain with rough surface profile. The analysis is further extended for the GTOPO30 DEM of Great Plains, Nebraska (bounded by latitude 39° to 43° N and longitude 98° to 101° W) with a smoother surface profile (Figure 5). The smoother surface profile of the terrain results in fewer multiscaling iterations (11) required to remove all the curvature regions. It is observed in Figure 6 and Table 4 that for scales 1 to 7, smaller mountain objects located at the centre of the terrain are classified as spatially most significant. For scales 8 to 11, with with no strategically located mountain objects at the centre of the terrain, larger mountain objects located at the corner of the terrain are classified as spatially most significant. For both cases, the corresponding spatially most significant mountain objects have the same values (165 for scales 1 to 7, and 169 for scales 8 to 11), as the objects require the same minimum dilation distances to the boundary points that are furthest out with respect to the objects.

4. CONCLUSION

In this paper, iterative morphological dilations were used to study the spatial significance of mountain objects extracted from multiscale DEMs. It was observed that as the area of the mountain objects reduce with increasing scale, the distances between the mountain objects increase, resulting in increasing values of SSI. The results obtained indicate that the strategic location of a mountain object at the centre of the terrain is more important than its size in determining its reach to other mountain objects and thus, its spatial significance.

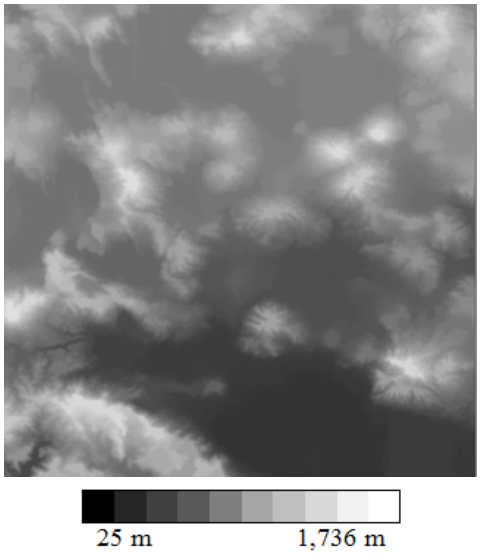

Figure 5: The GTOPO30 DEM Great Plains. The scale is approximately 1:3,900,000.

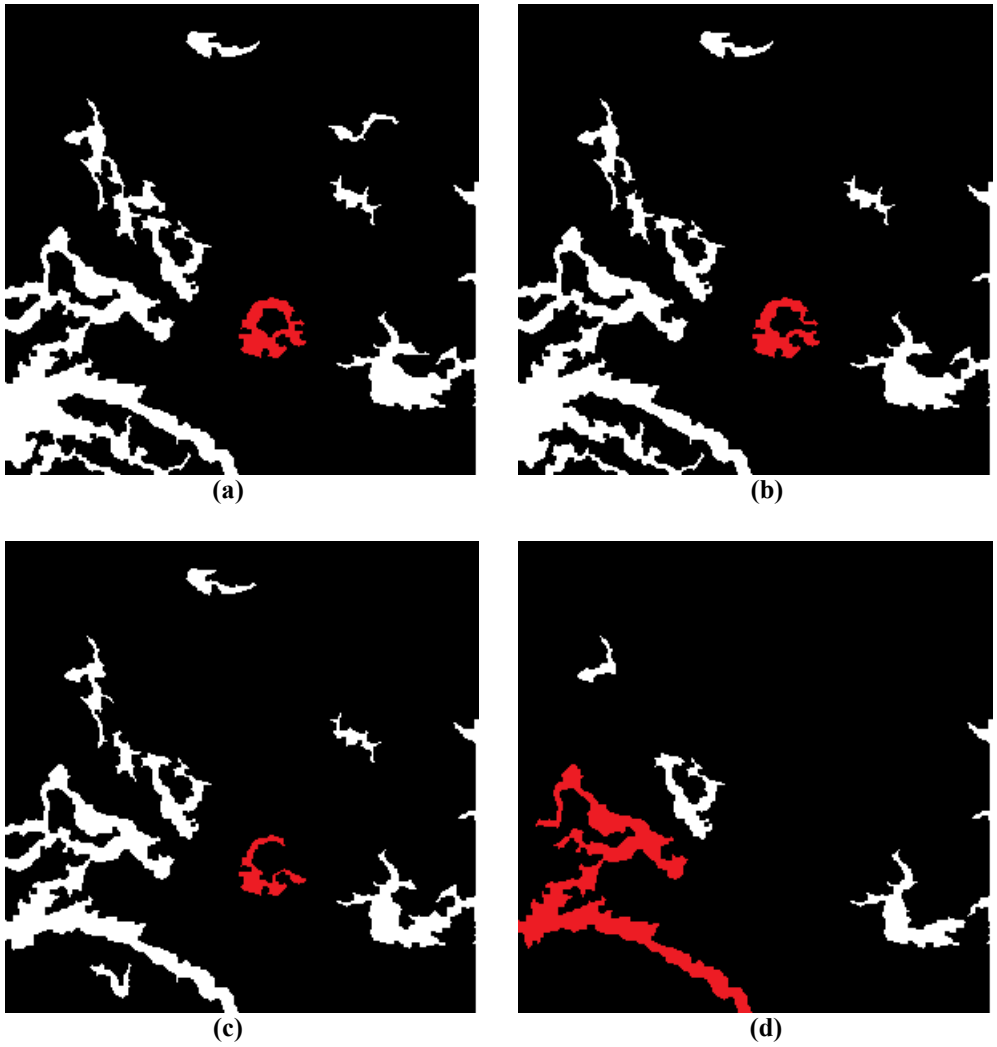

Figure 6: Spatially most significant mountain objects for the multiscale DEMs of Great Plains at scales of: (a) 1 (b) 3 (c) 5 (d) 11.

Table 4: Spatially most significant mountain objects for the multiscale DEMs of Great Plains.

Scale	Num. of objects	Spatially most significant object	Area (cells)	SSI
1	8	5	743	165
2	8	5	743	165
3	9	7	701	165
4	8	6	587	165
5	9	7	474	165
6	7	5	397	165
7	6	5	333	165
8	5	1	4269	169
9	6	1	4244	169
10	6	1	4170	169
11	5	1	3951	169

ACKNOWLEDGEMENT

The author is grateful to Assoc. Prof. Dr. Behara Seshadri Daya Sagar, Head of the Systems Science and Informatics Unit (SSIU), Indian Statistical Institute, for his suggestions that have helped strengthen this manuscript.

REFERENCES

Abdul-Rahman, H.S., Jiang, X.J. & Scott, P.J. (2013) Freeform surface filtering using the lifting wavelet transform. *Precis. Eng.*, **37**: 187-202.

Ahmad Fadzil, M.H., Dinesh, S. & Vijanth Sagayan, A. (2011). A method for computation of surface roughness of digital elevation model terrains via multiscale analysis. *Comput. Geosci.*, **37**: 177-192.

Anselin, L. (1992). *Spatial Data Analysis with GIS: An Introduction to Application in the Social Sciences*. National Center for Geographic Information and Analysis, University of California, Santa Barbara, California.

Anselin, L. (1995). Local indicators of spatial association (LISA). *Geogr. Anal.*, **27**: 93-115.

Baohua, L., Madden, L.V. & Xu, X. (2012). Spatial analysis by distance indices: an alternative local clustering index for studying spatial patterns. *Method. Ecol. Evol.*, **3**: 368-377.

Bernardin, T., Cowgill, E. S., Gold, R.D., Hamann, B., Kreylos, O. & Schmitt, A., 2008. Real-time terrain mapping. *In*: H. Hagen, ed., *Scientific Visualization: Challenges for the Future*. IEEE Computer Society Press, Los Alamitos, California, pp. 275-288.

Câmara, G. & Carvalho, M.S. (2002). *A Tutorial on Spatial Analysis of Areas*. National Institute for Space Research (INPE), São José dos Campos, Brazil.

Chainey, S.P. (2008). Identifying priority neighbourhoods using the Vulnerable Localities Index. *Policing J. Policy Prac.*, **2**: 196-209.

Chainey, S.P. (2010). *Spatial Significance Hotspot Mapping Using the NNI and Gi* Statistic*. UCL Jill Dando Institute of Crime Science, London.

Chiao, L.Y., Hsieh, C. & Chiu, T.S. (2013). Exploring spatiotemporal ecological variations by the multiscale interpolation. *Ecol. Model.*, **246**: 26-33.

Claypoole, R.L. & Baraniuk, R.G. (2000). A multiresolution wedgelet transform for image processing. *In* Unser, M.A., Aldroubi, A. & Laine, A.F. (Eds.), *Wavelet Applications in Signal and Image Processing VIII, Volume 4119 of SPIE Proceedings*. SPIE, Bellingham, Washington, pp. 253-262.

de Aguiar, A.P.D., Câmara, G., Monteiro, A.M.V., Cartaxo, R. & de Souza, M. (2003). Modelling spatial relations by generalized proximity matrices. *Geoinfo 2003*, 3-5 November 2003, São José dos Campos, Brazil.

Dinesh, S. (2006). Extraction of mountains from digital elevation models using mathematical morphology. *GIS Malaysia*, **1**: 16-19.

Ding, Y. & Fotheringham, A.S. (1992). The integration of spatial analysis and GIS. *Comput. Environ. Urban*, **16**: 3-19.

Drăguţ, L. & Eisank, C. (2011). Object representations at multiple scales from digital elevation models. *Geomorphology*, **129**: 183-189.

Drăguţ, L., Eisank, C. & Strasser, T. (2011). Local variance for multi-scale analysis in geomorphometry. *Geomorphology*, **130**: 162-172.

Feitosa, F., Câmara, G., Monteiro, A.M.V., Koschitzki, T. & Silva, M.P.S. (2007). Global and local spatial indices of urban segregation. *Int. J. Geogr. Inf. Sci.*, **21**: 299-323.

Goodchild, M.F. (2011). Scale in GIS: An overview. *Geomorphology*, **130**: 5-9.

GTOPO30 (1996). *GTOPO30: Global 30 Arc Second Elevation Data Set*. Available online at: http://edcwww.cr.usgs.gov/landdaac/gtopo30/gtopo30.html (Last access date: 1 June 2009).

Guo, S.M., Chang, W.H., Tsai, J.S.H., Zhuang, B.L. & Chen, L.C. (2008). JPEG 2000 wavelet next term filter design framework with chaos evolutionary programming. *Signal Process.*, **88**: 2542-2553.

Hayat, K, Puech, W. & Gesquère, G., 2008. Scalable 3-D terrain visualization through reversible JPEG2000-based blind data hiding. *IEEE T. Multimedia*, **10**: 1261-1276.

Howell, D. (1995). *Principles of Terrain Analysis: New Applications for Global Tectonics*. Chapman and Hall, London.

Jiang, X.Q., Blunt, L. & Stout, K.J. (2001a). Application of the lifting scheme to rough surfaces. *Precis. Eng.*, **25**: 83-89.

Jiang, X.Q., Blunt, L. & Stout, K.J. (2001b). Lifting wavelet for three-dimensional surface analysis. *Int. J. Mach. Tool. Manu.*, **41**: 2163-2169.

Lam, N., Catts, D., Quattrochi, D, Brown, D. & McMaster, R. (2004). Scale. *In*: Rechcígl, M., McMaster, R.B., Usery, E.L. (Eds.), *A Research Agenda for Geographic Information Science*. CRC Press, New York, pp. 93-128.

Li, Z. (2008). Multi-scale digital terrain modelling and analysis. In: Zhou, Q., Lees, B. & Tang, G. (Eds.), *Advances in Digital Terrain Analysis*. Springer, Berlin, pp. 59-83.

Miliaresis G. (2008). Quantification of terrain processes. *Lect. Notes Geoinform. Cartogr.* **XIV**: 13-28.

Miliaresis, G. & Argialas, D.P. (1999). Segmentation of physiographic features from Global Digital Elevation Model/GTOPO30. *Comput. Geosci.*, **25**: 715-728.

Miliaresis, G. & Argialas, D.P. (2002). Quantitative representation of mountain objects extracted from the Global Digital Elevation Model (GTOPO30). *Int. J. Remote Sens.*, **23**: 949-964.

Nonomura, K., Ono, M., Zhou, L.B., Shimizu, J. & Ojima, H. (2010). Design of digital filters for Si wafer surface profile measurement : Noise reduction by lifting scheme wavelet transform. *Adv. Mater. Res.*, **126-128**: 732-737.

Poulos, M.J., Pierce, J.L., Flores, A.N. & Benner, S.G. (2012). Hillslope asymmetry maps reveal widespread, multi-scale organization. *Geophys. Res. Lett.*, **39**: L06406.

Sagar, B.S.D. (2013). *Mathematical Morphology in Geomorphology and GISci*. CRC Press, New York.

Sagar. B.S.D., Rajesh, N., Ashok Vardhan, S. & Vardhan, P. (2013). Metric based on morphological dilation for detection of spatially significant zones. *IEEE Geosci. Remote Sens. Lett.*, **10**: 500-504.

Schölkopf, B. & Smola, A.J. (2002). *Learning with Kernels: Support Vector Machines, Regularization, Optimization and Beyond*. MIT Press, Cambridge, Massachusetts.

Silverman, B.W. (1986). *Density Estimation for Statistics and Data Analysis*. Chapman & Hall, London.

Starck, J.L. (2002). No- linear multiscale transforms. *In* Barth, T.J., Chan, T. & Haimes, R. (Eds.), *Multiscale and Multiresolution Methods: Theory and Applications*. Springer, Heidelberg, Germany, pp. 239-266.

Summerfield, M. (1996). *Global Geomorphology*. Longman, Essex.

Summerfield, M. (Ed.) (2000). *Geomorphology and Global Tectonics*. John Wiley & Sons, New York.

Summerfield, M. (2005). A tale of two scales, or two geomorphologies. *T. I. Brit. Geogr.*, **30**: 402-415.

Sweldens, W. (1996). The lifting scheme: A custom-design construction of biothorgonal wavelets. *Appl. Comput. Harmonics Anal.*, **3**: 186-200.

Sweldens, W. (1997). The lifting scheme: A construction of second generation wavelets. *J.Math. Anal.*, **29**: 511-546.

Tate, N., & Wood, J. (2001). Fractals and scale dependencies in topography. *In*: Tate, N., Atkinson, P. (Eds.), *Modelling Scale in Geographical Information Science*, Wiley, Chicester, pp. 35-51.

Wood, J. (2009). Geomorphometry in LandSerf, *In*: Hengl, T. & Reuter, H.I. (Eds.), *Developments in Soil Science, vol. 33: Geomorphometry: Concepts, Software, Applications*, Elsevier, Armsterdam, pp. 333-349.

Wu, S., Li, J. & Huang, G.H. (2008). A study on DEM-derived primary topographic attributes for hydrologic applications: Sensitivity to elevation data resolution. *Appl. Geogr.*, **28**: 210-223.

Yang, Z., Liu, H., Yang, N. & Xiao, X. (2009). Study on multiscale generalization of DEM based on lifting scheme. *In* Liu, Y. & Tang, X. (Eds.), *Proceedings of the SPIE, Volume 7492*. SPIE, Bellingham, Washington, pp. 74922E-74922E-6.

CURRENT INNOVATION PRACTICES IN MALAYSIAN GOVERNMENT AND CORPORATE ORGANISATIONS: CASE STUDIES ON STRIDE AND CELCOM AXIATA BERHAD

Khairul Manami Kamarudin[1*], Siti Rozanna Yusuf[2], Norfazzila Omar[3], Mohd Salahuddin Mohd Basri[1] & Nur Hidayah Ariffin[1]

[1] Faculty of Engineering, University Putra Malaysia (UPM), Malaysia
[2]Mechanical and Aerospace Technology Division (BTJA), Science & Technology Research Institute for Defence (STRIDE), Ministry of Defence, Malaysia
[3] Product Innovation Team (PIT), Celcom Axiata Berhad, Malaysia

[*]E-mail: manami@upm.edu.my

ABSTRACT

For government and non-government organisations to prosper, the practice and culture of innovation must be adopted. Therefore, innovation has been encouraged for each organisation by the Malaysian government since the year 2009. This paper discusses on the innovation processes in two organisations; the Science & Technology Research Institute for Defence (STRIDE), a government agency, and Celcom Axiata Berhad, a public listed company. This study is conducted based on information on innovation activities gathered from representatives from both organisations' top managements. STRIDE, being the government's R&D centre for defence & security, and Celcom, a telecommunications service provider, have unique ways of implementing innovations in their respective departments. This paper focuses on both organisations' achievements with their latest innovations, their plans for the next five to ten years, and the challenges faced in maintaining and improving their performances. Organisation strategies, job motivation and incentives, and intellectual property (IP) patents in both organisations are also discussed.

Keywords: *Innovation; organising strategies; incentives; intellectual property (IP) patents; challenges.*

1. Introduction

Creativity and sense of innovativeness separate innovative leaders such as Jeff Bezos, Steve Jobs and Marc Benioff from ordinary business leaders. They are successful not because they were born to be innovators or they were lucky, but consider innovative approaches as highly important within their companies' activities (Dyer *et al*., 2011). According to Barret (2011), Marc Benioff from *Salesforce.com*, an internet-based software provider, is one of the most innovative leaders and he was ranked first in Forbes' The World´s Most Innovative Companies in 2013 (Dyer & Gregersen, 2013).

"Innovation" literally means "*the action or process of innovating*", with the word "innovate" defined as *"make changes in something established, especially by introducing new methods, ideas, or products"* (OUP, 2014). In practising innovation with patent applications, the introduced product can be commercialised. This is different from the definition of "invention" which means "*embodiment of something new*", in that innovation carries market performance expectations, profitability, and new products or services to the society. The importance of innovation is that it helps in maintaining market competitiveness, and sustaining company revenue and income by introducing new and effective products. Innovations are also important for differentiation of own products with available products in the market, and to make consumer quality of life easier and better. In addition, consumer expectations are a driving factor for improving the efficiency and effectiveness of products, with their feedback helping in increasing the innovation process (Kamarudin, 2010).

In Malaysia, there are many successful organisations, and two of them are the Science & Technology Research Institute for Defence (STRIDE) (STRIDE, 2014), a government agency, and Celcom Axiata Berhad (Celcom, 2014), a public listed company. This paper will discuss on the innovation processes in these two organisations, focusing on the achievements of both organisations with their latest innovations, and the challenges faced in maintaining and improving their performances. In addition, organisation strategies and plans for the next five to ten years, job motivation and incentives, and intellectual property (IP) patents in the two organisations are also discussed. The study is conducted based on information gathered from representatives from the top managements of both organisations.

2. METHODOLOGY

The information gathered from STRIDE and Celcom was through interviews with representatives of the top management of the innovation department in each organisation. Dr. Mohd Yazid bin Ahmad, Director of Mechanical & Aerospace Technology Division (*Bahagian Teknologi Jentera & Aeroangkasa,* BTJA), STRIDE (Mohd Yazid, 2012), and Ms. Stephannie Chin Shiaw Ping (Senior Manager), Mr. Choke Kit Fai (Manager), Mr. Gan Yeow Jin (Assistant Manager) and Mr. Pradheep Arun a/l Narayanaswami (Executive) from Celcom's Product Innovation Team (PIT) (Chin *et al*., 2012), participated in the interview sessions. The interviews conducted focused on current innovation processes in each organisation and the challenges to catch up with global innovation. Both organisations have different innovation outputs; STRIDE provides outcomes of research findings and analyses on defence & security equipment, while Celcom produces mobile applications and digital products. However, both organisations are important in generating innovation capabilities to assist Malaysia's innovation foundation in becoming stronger and more competitive globally.

3. BACKGROUND OF ORGANISATIONS

3.1 STRIDE

STRIDE (Figure 1), which is based in Kajang, Selangor, is an agency under the Malaysian Ministry of Defence (MOD) and functions with four main objectives (STRIDE, 2014):

1) To accelerate the development of scientific, technological and human capital resources in compliance with defence requirements
2) To collaborate with industries and institutions in defence technology initiatives
3) To spearhead research and development (R&D), and innovation in the defence domain and their exploitation
4) To strengthen science and technology (S&T) support for Malaysia's defence & security requirements.

The history of STRIDE began with the establishment of the Malayan Defence Science Organisation (MDSO) in 1958. However, MSDO was not active due to lack of officers with suitable expertise. Therefore, in 1968, MOD formed a unit called the Defence Technical Centre (DTC), which was renamed in 1972 to Defence Research Centre (DRC). In view of its increasing services, ranging from technical evaluation, testing, R&D and defence investigation, it was again renamed in 1985 to the Defence Science & Technology Centre (*Pusat Sains dan Teknologi Pertahanan*, PSTP). Finally in 2001, PSTP was upgraded to the status of a government agency and renamed as STRIDE (STRIDE, 2008, 2014).

STRIDE's primary role is to lead the formulation and implementation of integrated defence S&T programmes using industrial, academic and government resources. To this end, it carries out a broad range of activities from high-level analysis to support MOD's policy and procurement decisions, to R&D, field and laboratory tests and measurements in a wide range of defence areas. STRIDE is

organised into six divisions, with each division focusing on a particular set of scientific and operation requirements (STRIDE, 2014):

1) Electronics, communications, surveillance and geospatial technologies
2) Personal protection equipment (PPE), food and rations
3) Chemical, biological, radiological and nuclear (CBRN) defence
4) Aeronautics and vehicular technologies
5) Weapons, propulsion and ballistics
6) Maritime and ship technologies.

Figure 1: STRIDE's official logo.

3.2 Celcom Axiata Berhad

Celcom Axiata Berhad (Figure 2), which is based in Kuala Lumpur, is the oldest mobile telecommunications company in Malaysia and is a member of the Axiata group of companies (formerly known as TM International, based in Malaysia). Being one of the very few companies in Malaysia to originally obtain a cellular phone license, Celcom successfully introduced mobile telephony in Malaysia, which was established in 1988 through its Automatic Radio Telephone (ART) 900 service, using first generation (1G) Extended Total Access Communications System (ETACS) (MCMC, 2012). Celcom now offers second generation (2G) Global System for Mobile Communications (GSM), third generation (3G) Universal Mobile Telecommunications System (UMTS) and High Speed Packet Access (HSPA), and fourth generation (4G) Long Term Evaluation (LTE). In addition, Celcom offers various products and services, such as business voice, business broadband, phone and devices, business email solutions, international direct dial (IDD), local and international roaming, and value added services (VAS) that are not related to short message service (SMS), multimedia message service (MMS) and data access (Chin *et al*., 2012).

Figure 2: Celcom's logo following its merger with Axiata, the largest telecommunications company in Asia.

Its brand's mission is about pleasing customers and exceeding expectations, having its own goal to empower customers with innovative solutions that gives greater control and freedom. Celcom's visions are (Celcom, 2014):

1) To build a profitable enterprise that maximises investor returns
2) To empower, develop and reward its people, and to become Malaysia's preferred employer
3) To build win-win relationships with all its business partners based on mutual trust, respect and support
4) To work on bridging the digital gap, to build the nation and to enhance its standing abroad
5) To maintain the highest levels of transparency, integrity and professionalism
6) Together with all its stakeholders, to make a premium brand; a brand that symbolises the spirit of freedom, aspiration, confidence, dynamism, timelessness, universality and globalism.

Celcom has been recognised as the best telecommunication company (TELCO) in Malaysia among other three giant TELCOs, Telekom Malaysia, Maxis and DIGI, and has been acknowledged as the best customer services provider (Napiah, 2013). As competition among TELCOs is very fierce on an almost daily basis, Celcom places innovation requirements as their top priority because they know that the impact of unique products makes the company unique compared to others (Chin *et al*., 2012). Hence, Celcom appreciates the most successful projects handled by its teams. Moving away from conventional practices of the other TELCOs, Celcom implemented the *Passion Blue* theme among its staff, which means having the passion in daily work in Celcom, as blue is its corporate colour, to inculcate innovation in their work.

4. INNOVATION PROCESSES AND ACHIEVEMENTS

4.1 STRIDE

STRIDE strives to provide technical services such as managing and conducting R&D, technical evaluation of defence procurements, conducting operational research and providing advisory services, failure analysis, testing and inspection, technical consultation and measurement, and calibration. STRIDE encourages the practice of innovation in its work routines using existing research equipment in each project carried. According to Dr. Mohd Yazid, STRIDE emphasises on three important aspects in its innovation culture; the need to innovate, competent human resources and funding.

STRIDE conducts several R&D projects, which are mostly bound by the target objectives set by its clients or end-users. The general undertaking of these projects mainly comprises of in-depth research, understanding of the innovation process and discovery of new knowledge. The "trial-and-error" approach is often used in arriving to accurate findings, while other approaches to problem solving are also practiced to give researchers the experience of discovering alternative solutions. As indicated by Dr. Mohd Yazid, experience and knowledge is the key to rapid and successful research findings. Many projects undertaken by STRIDE starts with the process of careful design, followed by model fabrication, assembly and integration, and finally, functional tests. "*With R&D, the understanding of the product is deeper, and with deep knowledge, greater invention or innovation can be created*" he said.

For example the unmanned airship system (Figure 3) developed by STRIDE researchers (Awang Sa & Yusuf, 2009) is one of many innovations developed for the Malaysian defence industry. The airship serves as a system for monitoring and surveillance of land borders and territorial waters, and for monitoring of traffic, and agricultural, forested and disaster areas. The airship, controlled by an autopilot system equipped with a Global Positioning System (GPS) navigation system and camera, can also be used as a communications repeater station for areas that are not covered by communications networks or in areas where communications networks have been destroyed due to natural disasters or by enemy forces. The process of developing the airship required the researchers to conduct in-depth research on national surveillance and monitoring before proceeding into developing a high altitude platform for satellite systems and early warning aircrafts. The project progressed to a model airship with an engine unit of 80 cc capacity and hundreds of flight test trials, which resulted to a 4 h flight with maximum height of 3,000 ft and speed of 80 km/h.

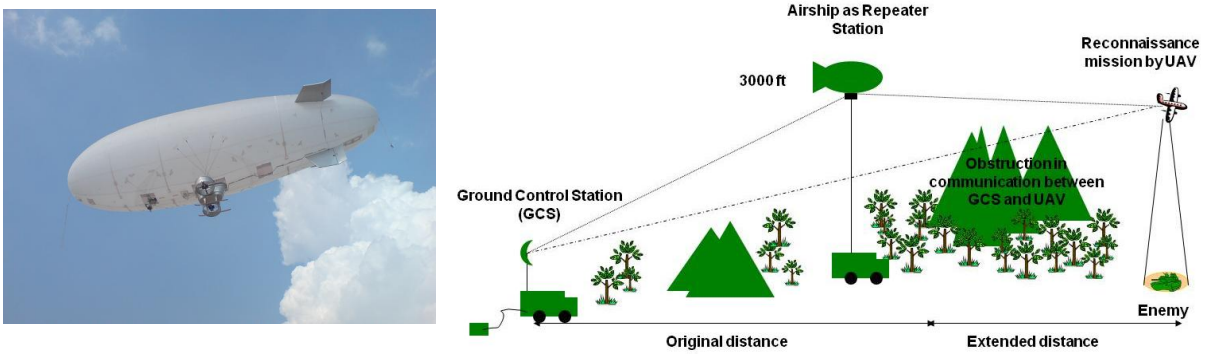

Figure 3: The unmanned airship system developed by STRIDE.
(Source: Awang Sa & Yusuf (2009))

STRIDE encourages its researchers to further their qualifications of academic studies up to the PhD level. To date, only 60% of its researchers have masters qualifications and these will be eventually upgraded to PhD. Dr. Mohd Yazid encourages his staff to bring back new ideas, knowledge and technology, and by furthering their studies, they will increase their experience and exposure in different working conditions. He hopes that the researchers will introduce positive research cultures learnt from abroad to enhance R&D activities in STRIDE. STRIDE provides offset programmes for its researchers, which are in-depth training courses for technologies related to government procurements of defence & security equipment, so that their knowledge and skills can be widened. The government's procurements of Scorpène class submarines and Eurocopter EC 725 helicopters replacing the existing Nuri (Sikorsky S-61A-4) helicopters provide good examples of this implementation (New Strait Times, 2012).

Studies have shown that research collaborations between companies and universities can increase innovativeness (Enkel *et al*., 2009). STRIDE often forges collaborations with other R&D institutes, universities and local defence industries through agreements on usage of equipment that are not available in its institution or have broken down. Through such collaborations, new research projects can be initiated, while delays for current research projects can be avoided.

4.2 Celcom

Celcom's PIT consists of 49 team members focusing on mobile applications and VAS that have high consumer usage. It strives to create products that are unique from other TELCOs by employing innovation on a daily basis. Ms. Stephannie Chin stated that PIT uses many methods in the innovation process based on company and business objectives. An example of a road map would be: first quarter of the year, innovating applications for smartphone; mid-year, midstream products; and end of year, Celcom legacy products. PIT constantly develops new mobile applications that can either be commercial, experimental or even products at incubation level.

For example, the *All About Hijab* (Figure 4) application for Android phones (Celcom, 2013) was created by PIT through its innovation process. The application introduces steps for wearing hijab in different styles and fashion. PIT already has a number of innovative ideas that have been commercialised, such as its own SMS Chat, MMS via Celcom's wireless application protocol (WAP) / web browser and online games. The WAP / web browser, also known as wireless internet, wireless web or mobile web, is a mini-browser application that navigates various services through internet (Umar, 2004). In addition, Mr. Choke Kit Fai indicated that PIT recently launched the *Facebook Packaging Usage* (Figure 5), which is a subscription on database of users to assist in simplifying the use of Facebook in mobile phones equipped with Celcom coverage.

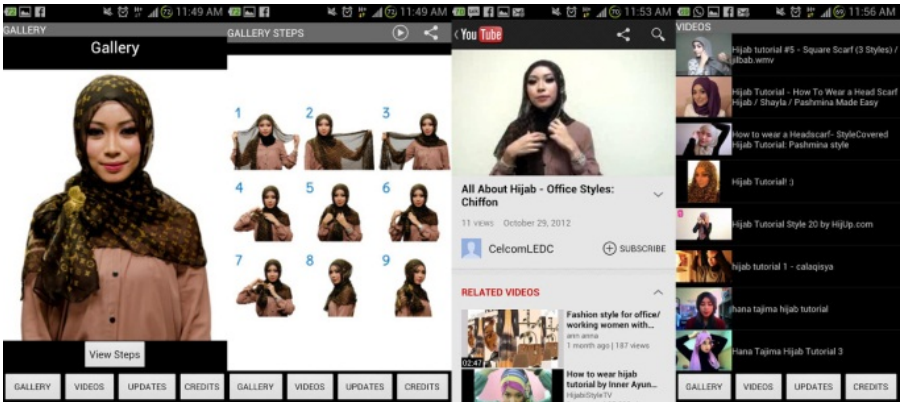

Figure 3: The *All About Hijab* Android application which was developed by Celcom's PIT.

Figure 4: Celcom's *Facebook Packaging Usage*, with SMS service.

The PIT team consider themselves as enablers with less concern on finance and costs during project completion, but focusing on the output of the project, the achievement of certain targets for return of investment (ROI) and achieving revenue target. Celcom as a whole always encourages innovation exercises among their staff with emphasis on team work. Besides completing projects, the team members also participate as invited speakers within the company and in external speaking engagements on topics related to creating mobile application and VAS.

Mr. Pradheep said that Celcom treats innovation as the most important part of the R&D process to grow a company into a more successful entity. He also stated that in PIT, any innovation process requires top management approval, and as everything regarding phone application and digital related innovation is changing rapidly in a very competitive field, fast acceptance by users is the top priority. PIT aims to come out with new ideas as frequently as possible. Since Celcom is in a very competitive industry, requests for new ideas come with increasing swiftness. While Celcom applies development troubleshooting on mobile products, PIT uses the "innovative look-back method", which refers to previous projects and applications to produce more interesting products. Salient features from previous projects are discussed among the team members. The PIT team observed that there is no set of rules for identifying the methods used, but rather uses a combination of various problem solving methods. They place great importance on team work. Underlying causes of problems are investigated at depth and cross checked with current and competitor's products. If the problems still persist, the team will refer to the top management.

5. INNOVATION STRUCTURES

5.1 Organising Strategies

STRIDE requires its researchers to undergo training for research competencies, especially in defence & security technologies. As stated in the STRIDE's fourth objective, the agency seeks to ensure that all its researchers have knowledge and competency not only in technical areas but in management as well. STRIDEs' vision for the next five to ten years is to become the main S&T service provider for defence & security forces in Malaysia. The agency hopes that its research outputs will be recognised by local and international defence & security communities. STRIDE also plans to prioritise its research focuses for further improvement and to identify its niche areas.

Celcoms' strategy is to constantly enhance their services, platforms and development of applications, and to regularly make public promotions. For example, recently, Celcom initiated the annual *Android Mobile Application Competition* for the public with the winner given a sponsored trip to Korea. Celcom continues to invite information technology (IT) faculties from local universities as well as the public to join the competition every year. Under Celcom's product innovation strategies, there is a unit called the *League Extraordinary Developer Challenge* (LEDC), which is tasked with recognising talent with the potential to increase PIT's efficiency (Chin *et al*., 2012). Via the LEDC platform, Celcom aims to develop skills from the younger generation to design, develop, commercialise and market applications. If the application is selected as a winner, the developer could potentially earn a revenue sharing contract with Celcom worth millions of ringgit. Celcom aims to be a digital company within the next five to ten years, where everything is "virtual".

5.2 Job Motivation: Incentives for Executing Innovative Ideas

STRIDE commercialises its research findings and products, giving incentives to researchers in the form of percentage of profit (royalty). STRIDE gives recognition through annual Excellence Awards (*Anugerah Kecemerlangan*) that are given to researchers with high competencies and success in innovation. It is part of Malaysian government policy to foster innovation competition in each governmental division, department or agency through *Innovation & Creativity Groups* (*Kumpulan Inovatif & Kreatif*, KIK) event. In this way, every researcher will feel appreciated for their work and thus, motivated to increase their interests. In other defence company practices, the incentive mechanism is used for delivering the best product availability requirements and research, especially in aerospace and defence organisations (Kim, 2007).

In order to encourage innovation, Celcom's PIT requires its entire staff to have at least three innovations each year for their key performance index (KPI). This requirement will simultaneously boost the staffs' competence and contribute to the end-year bonus as part of the compensation and incentives Celcom gives to its employees. Occasionally, when Celcom is looking for good mobile applications, it will open up the entire innovation department for training sessions which expose Celcoms' researchers on recent technologies and tools required for innovation on the latest mobile applications. The most innovative mobile application outcome from this activity will be rewarded with the incentive of three extra annual leaves.

5.3 Intellectual Property (IP) Patents

At present, STRIDE has IP patents for two military products, *Ufilta Hydration-Pak*, a portable water purifier (The Star, 2012) and military uniform digital camouflage (Figure 6) (David, 2013), that are pending for approval. These patent applications require compulsory publications for each project completed. STRIDE is not directly involved in the innovation of physical and tangible products, but rather focuses more on commercialisation of its research, information and ideas of new technologies,

particularly for military. The problem faced by STRIDE in patenting is the bureaucracy faced in patent documentation and costs (Mohd Yazid, 2012). STRIDE considers publications as a protection of innovation, which also strengthens the credentials for the individual researchers and the agency's reputation.

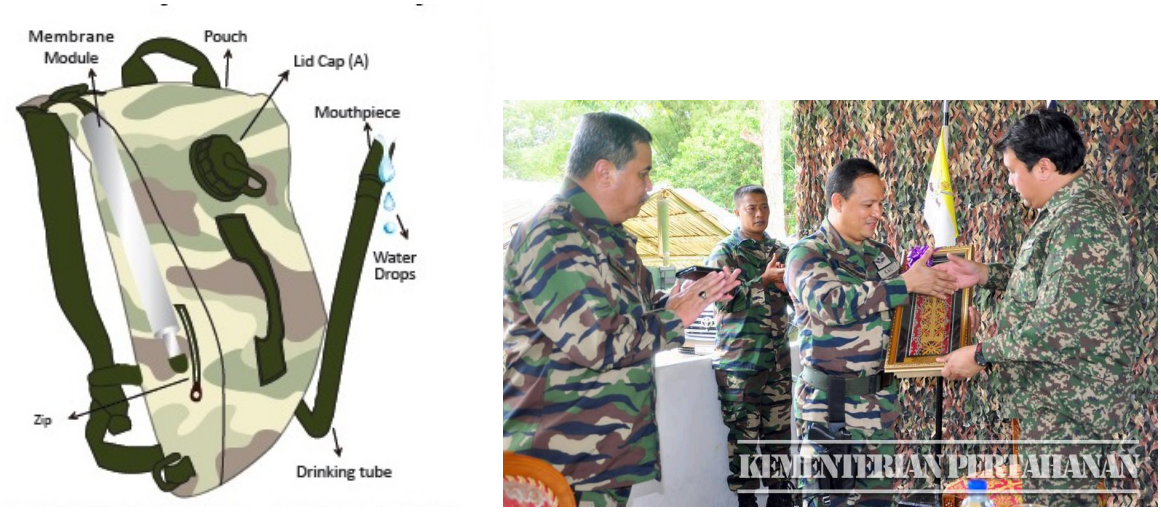

(a) **(b)**

Figure 6: STRIDE's patented products: (a) *Ufilta Hydration-Pak* (AquaFilta, 2014) (b) Military uniform digital camouflage (MOD, 2014).

Celcom applies IP rights for each of their completed innovation projects. For example, *Kolony* (Figure 7), a social networking platform using SMS, is a branded product that has been copyrighted, with the vendors involved in the project prohibited from infringing this right by dealing with other TELCOs. Celcom requires legal agreements signed between the company and vendors to safeguard the security of its products.

5.4 Innovation Challenges

In terms of challenges faced by STRIDE, the company is in need for improved human capital, skilful researchers and funding. In addition, research activities in STRIDE require specialised equipment, especially for military research, that sometimes needs higher costs for procurement. Research requirements may be subjected to interruption and delays if problems are encountered in the delivery of the equipment. STRIDE conducts collaborations with universities and other research entities for machineries and other research tools to avoid project interruption and maintain the quality of analysis result in each project they handled.

In Celcom, the challenges for the PIT are that the innovative products that they produce seldom receive immediate return from the market and in obtaining sufficient budget from the top management. That is why most of its products are more of an enhancement of previous products accepted by users, rather than creating totally new outputs which the management considers as highly risky. In the future, PIT wishes to gain access to marketing strategies which supports them to produce suitable products for customers as well as receive support from the top management for each innovative product that they design.

Figure 7: Celcom's *Kolony* offers SMS social networking services.

6. SUCCESSFUL INNOVATORS

The final question asked during the interview for each organisation's representatives was on their opinion on the type of person who could potentially be successful in the field of innovation. The question that was posed was "*Between a creative, a genius and a hardworking individual, which one will be the most successful innovator?*" All the respondents replied that the creative individual normally generates the most ideas and potentially be a successful innovator in comparison to the other two. According to Dr. Mohd Yazid, creativity can be learnt and taught. However, for the bigger picture, a successful innovator must have all these three qualities, which complement each other to produce a successful invention. Dr. Mohd Yazid indicated that innovation is not only for geniuses and highly educated people, but rather anyone can be an innovator. The key is to be passionate, never give up easily, have the drive to achieve his or her goals, and to be someone who can contribute to the society.

In aspects of management, Dr. Mohd Yazid stated that research leaders must be creative in managing their workers, and improving their staff's skills and knowledge, especially under tight budget conditions. Leaders must know how to tackle situations that have constraints and limitations. They should also know how to guide and align people based by their capabilities and specialties.

7. CONCLUSION

This paper has highlighted the importance of innovation in improving the performances of the two organisations which were involved in the study. STRIDE conducts a number of projects which require detailed research beyond the scope of most companies. These high quality researches have helped designers and engineers to constantly improve defence & security equipment. Celcom's multi-innovation tasking, mostly on mobile applications and VAS, encourages designers and engineers to come up with better products, including other digital product besides mobile services. Its customer service has been awarded with several Excellence Awards by the Customer Relationship Management

and Contact Centre Association of Malaysia due to their commitment to serve, flexibility, nationwide coverage, global coverage and the best customer service, which is what commercialisation of innovation is all about, namely to please the customers.

ACKNOWLEDGEMENT

We are grateful to Dr. Mohd Yazid bin Ahmad, Director of STRIDE's Mechanical & Aerospace Technology Division (BTJA), and Ms. Stephannie Chin Shiaw Ping (Senior Manager), Mr. Choke Kit Fai (Manager), Mr. Gan Yeow Jin (Assistant Manager) and Mr. Pradheep Arun a/l Narayanaswami (Executive) from Celcom's Product Innovation Team (PIT), for participating in the interview sessions conducted for this study. We would also like to thank Assoc. Prof. Dr. Faizal Mustapha, Department of Aerospace Engineering, Universiti Putra Malaysia (UPM), for his valuable guidance.

REFERENCES

AquaFilta (2014). *AquaFilta (M) Sdn Bhd.* Available online at: http://www.ufilta.com (Last access date: 19 February 2014).

Awang Sa, Z.A., & Yusuf, S.R. (2009). Sistem kapal udara tanpa juruterbang: Pelengkap kepada sistem pemantauan dan pengawasan negara. *PATRIOT Mag.*, **2009**: 25.

Barret, V. (2011). *Marc Benioff: Mister Disrupter.* Available online at: http://www.forbes.com/sites/victoriabarret/2011/07/20/marc-benioff-mister-disrupter (Last access date: 13 February 2013).

Celcom (2013). *All About Hijab*. Available online at: https://play.google.com/store/apps/details?id=celcom.application.hijabapplication&hl=en_GB (Last access date: 13 February 2013).

Celcom (2014). *Celcom Axiata Berhad.* Available online at: http://www.celcom.com.my (Last access date: 14 February 2014).

Chin, S., Choke, K., Gan, Y., & Pradheep, A. (2012). Interviews with the management of the Product Innovation Team (PIT), Celcom Axiata Berhad on 24 September 2012 (Interviewers: Kamarudin, K.M., Yusuf, S.R. & Omar, N.).

David, A. (2013). *Digital Camouflage for Our Men*. Available online at: http://www.nst.com.my/nation/general/digital-camouflage-for-our-men-1.357508 (Last access date: 14 February 2014).

Dyer, J., & Gregersen, H. (2013). *The World's Most Innovative Companies*. Available online at: http://www.forbes.com/innovative-companies/list (Last access date: 13 February 2014).

Dyer, J., Gregersen, H. & Christensen, C. (2011). *The Innovator's DNA: Mastering the Five Skills of Disruptive Innovators*. Harvard Business Press Books, Boston, Massachusetts.

Enkel, E., Gassmann, O. & Chesbrough, H. (2009). Open R&D and open innovation. *R&D Manage.*, **39**: 311-316.

Kamarudin, K.M. (2010). *Modeling the Green Automotive Innovations with Modern TRIZ*. Masters Thesis, Technical University of Berlin, Berlin.

(MOD) Ministry of Defence Malaysia (2014). *Ministry of Defence Malaysia.* Available online at: http://www.mod.gov.my (Last access date: 19 February 2014).

Mohd Yazid, A. (2012). Interview with the Director of the Mechanical & Aerospace Technology Division (BTJA), Science & Technology Research Institute for Defence (STRIDE), Ministry of Defence, Malaysia on 23 September 2012 (Interviewers: Kamarudin, K.M., Yusuf, S.R., Mohd Basri, M.B. & Ariffin, N.H.).

Napiah, M.Z. (2013). *Quality Control System in Telecom System Engineering Project Management Practices: An Exploratory Case Study in Celcom Axiata (Malaysia) Berhad*. Masters Thesis, Cardiff Metropolitan University, Cardiff.

New Strait Times (2012). *RMAF's Two New Copters Arrive*. Available online at: http://www.eurocopter.com.my/rmafs-two-new-copters-arrive (Last access date: 13 February 2014).

Oxford Universities Press (OUP) (2014). *Oxford Dictionaries: British and World English*. Oxford Universities Press (OUP), Oxford.

STRIDE (Science & Technology Research Institute for Defence (STRIDE) (2008). *Institut Penyelidikan Sains & Teknologi Pertahanan (STRIDE): 40 Tahun (1968-2008)*. Science & Technology Research Institute for Defence (STRIDE), Ministry of Defence, Malaysia.

STRIDE (Science & Technology Research Institute for Defence) (2014). *Science & Technology Research Institute for Defence (STRIDE).* Available online at: http://www.stride.gov.my (Last access date: 13 February 2014).

The Star. (2012). *Army to Test Portable Water Filter for Troops*. Available online at: http://www.thestar.com.my/News/Nation/2012/04/20/Army-to-test-portable-water-filter-for-troops (Last access date: 13 February 2014).

Umar, A. (2004). *Mobile Computing and Wireless Communications*. NGE Solutions Inc., New York.

CATCH OF THE NET

Natural disaster relief efforts have never really been considered as a primary mission for any military. Nonetheless, in practice, militaries play a preeminent role in disaster relief operations. In general, militaries' missions during disasters involve three kinds of support: 1) special functional skills and equipment that support specific response operations, including transportation (e.g., trucks, helicopters, boats and other off-road vehicles), military construction equipment (e.g., constructing temporary housing and restoring essential infrastructure, such as water and sanitation), search and rescue operations, surveillance and reconnaissance, and situation and damage assessment; 2) communications that can be used to augment the limited survivable local communications; 3) organised forces, such as for assisting medical teams. All these are primary military tasks, and hence, militaries are able to provide this support with little level of preparedness, and on an immediate basis. Militaries' pre-disaster activities include participating in planning, conducting training and earmarking specific types of equipment for support operations, which is a commitment that will ensure that individuals and units receive adequate training, resources and recognition for their disaster response role. The following are relatively interesting and useful websites on the role of militaries in natural disaster relief:

1) **Stockholm International Peace Research Institute (SIPRI): The Effectiveness of Foreign Military Assets in Natural Disaster Response**
   http://books.sipri.org/files/misc/FMA/SIPRI08FMA.pdf

2) **RAND Corporation: The Army's Role in Domestic Disaster Support: An Assessment of Policy Choices**
   http://www.rand.org/content/dam/rand/pubs/monograph_reports/2006/MR303.pdf

3) **National Institute for Defense Studies (NIDS): The Military's Role in Disaster Relief Operations: A Japanese Perspective**
   http://www.nids.go.jp/english/event/symposium/pdf/2011/e_06.pdf

4) **Brookings Institution: Future Directions in Civil-Military Responses to Natural Disasters**
   http://www.brookings.edu/research/papers/2012/05/civ-mil-disasters-ferris
   Reports on the advantages, limitations and implications of using military assets as part of the response to natural disasters.

5) **Public Broadcasting Service (PBS): Use of the Military in Humanitarian Relief**
   http://www.pbs.org/wgbh/pages/frontline/shows/cuny/laptop/humanrelief.html
   Provides a history of military involvement in natural disaster relief.

6) **United Nations (UN) Office for the Coordination of Humanitarian Affairs (OCHA): Guidelines on the Use of Foreign Military and Civil Defence Assets in Disaster Relief**
   https://docs.unocha.org/sites/dms/Documents/Oslo%20Guidelines%20ENGLISH%20(November%202007).pdf

7) **UK Ministry of Defence: Disaster Relief Operations**
   https://www.gov.uk/government/uploads/system/uploads/attachment_data/file/43340/jdp3522nded.pdf

8) **Swiss Armed Forces: Military Disaster Relief**
   http://www.vtg.admin.ch/internet/vtg/en/home/themen/katahi.html

9) **Office of US Foreign Disaster Relief: Field Operations Guide For Disaster Assessment and Response**
   https://scms.usaid.gov/sites/default/files/documents/1866/fog_v4.pdf
   Guidelines on the use of military assets in natural disaster relief.